UNIVERSIDAD MICHOACANA DE SAN NICOLÁS DE HIDALGO

INSTITUTO DE INVESTIGACIÓN EN METALURGIA Y MATERIALES

Consolidation of Municipal Solid Waste Incineration Fly Ash and Immobilization of Heavy metals through Alkaline activation system

Tesis para obtener Doctorado en ciencias en metalurgia y ciencias de los materiales

PRESENTA:
M.C. Xiang Tian

ASESOR:
Dr. Feng Rao Wu

COASESOR:
Dr. Shaoxian Song Hu

Morelia, Michoacán, México, Julio, 2021

Acknowledgement

The financial supports from the Consejo Nacional de Ciencia y Tecnología (CONACyT) of Mexico under the grant No. 270186, the Natural Science Foundation of Hubei Province of China under the grant No. 2016CFA013 and No. 51974093, and the Wuhan Science and Technology Bureau of China under the project No. 2016070204020156 are gratefully acknowledged. I would like to thank CONACyT for granting the scholarship NO. 896492 during my PhD study. I appreciate Universidad Michoacana de San Nicolás de Hidalgo (UMSNH) and the Instituto de Investigacion en Metalurgia y Materials (IIMM) providing an enjoyable study and working environment.

Next, I would like to express my sincere gratitude to my advisor Dr. Feng Rao Wu for the continuous support of my Ph.D study and related research, for his patience, motivation, and immense knowledge. His guidance helped me in all the time of research and writing of the thesis. I also want to give my great gratitude to my co-supervisor, Dr. Shaoxian Song. His fund of knowledge and serious attitude in work are worthy of my learning. And he always steers me in the right direction both in my research work and my life.

Besides my advisor, I would like to thank the rest of my thesis committee: Dr. Carlos Leon Patiño, Dr. Noemi Ortiz, Dr. Ricardo Morales Estrella, and Dr. Yanmei Li, for their insightful comments and encouragement, but also for the hard question which incented me to widen my research from various perspectives. I also want to thank all my friends in IIMM, M.C. Qian Wan, M.C. Zhili Li, M.C. Xing Li, M.C. Carlos Arreola, M.C. María del Carmen Ramírez López and Ing. Alma Gallegos. Thanks for your help and support in my work and life. Thanks to all my friends at Wuhan University of Technology.

I would like to thank my family: my parents, my sister for supporting me spiritually throughout my PhD study. Without their support and encouragement, I would not concentrate on my study and research work.

Xiang Tian

Content

Index of Figures

Index of Tables

Abstract

Hazardous heavy metals in municipal solid waste incineration (MSWI) fly ash are a threat to the environment and eco-systems. Alkaline activation was considered as a potential method in the waste management field. In this thesis work, the solidification/stabilization of MSWI fly ash were investigated through the alkaline activation reaction. First, the effects of metallic aluminum on the expansion and microstructure of alkali-activated MSWI fly ash-based pastes were investigated. Then, effects of aluminum dosage on gel formation and heavy metals immobilization in alkali-activated MSWI fly ash were given. After that, the influence of waste glass on the immobilization of heavy metals originated from MSWI fly ash was studied. Finally, co-disposal of MSWI fly ash and spent caustic was investigated.

In these experiments, the compressive strength was performed to assess the consolidation effect, and heavy metals concentration measurement was used to get qualitative the immobilization effect of heavy metals. Then alkali-activated MSWI fly ash-based pastes were characterized by scanning electron microscopy (SEM), x-ray diffraction (XRD), Fourier transform infrared spectroscopy (FTIR), X-ray photoelectron spectroscopy (XPS) and ^{29}Si nuclear magnetic resonance (NMR) spectra for the microstructure and immobilization mechanisms of heavy metals. Total organics carbon (TOC) was measured to access the organics immobilization effect.

Through studying the effects of metallic aluminum on the expansion and microstructure of alkali-activated MSWI fly ash-based pastes, it is concluded that MSWI fly ash could be consolidated through alkaline activation when using a small amount of aluminosilicate additives to adjust the reactive silica and aluminum ratios. The expansion in alkali-activated MSWI fly ash-based pastes could be eliminated using an optimized preparation process, with which the compressive strength of the pastes increased. Through studying the aluminum dosage on gel formation and heavy metals immobilization in alkali-activated MSWI fly ash, it is found that 1) small amount of aluminum addition increased compressive strength and improved the immobilization of heavy metals; 2) the addition of aluminum dosage converted soluble chloride salt into Friedel's salt, subsequently, improve the immobilization of heavy metals. By investigating the influence of waste glass on the immobilization of heavy metals originated from MSWI fly ash, it is concluded that waste glass addition effectively reinforced the consolidation of MSWI fly ash and immobilized the heavy

metals. As 40% addition of waste glass, the compressive strength reached a maximum of 3.55 MPa. The immobilization efficiency of Cr increased with the addition of waste glass, while that of Cu, Pb, Zn and Cd is dependent on the eluant final pH, which decreased with the decrease of eluant final pH. The main immobilization mechanisms include physical encapsulation, alkaline environment formation and the generation of insoluble compounds. Through studying co-disposal MSWI fly ash and spent caustic, it was found that the sulfate in spent caustic favored the ettringite formation in spent caustic-activated pastes. Compared with NaOH-activated pastes, spent caustic-activated pastes formed less $Q^4(4Al)$, leading to the compressive strength of spent caustic-activated pastes was higher than that of NaOH-activated pastes. However, the spent caustic-activated pastes exhibited a weaker immobilization performance for Cu, Pb, Zn and Cd, and a better performance for Cr (VI), comparing to NaOH-activated pastes. The presence of organics and the formation of ettringite in spent caustic-activated pastes made the immobilization of Cr(VI) more feasible. For the immobilization of organics, the spent caustic-activated pastes were of a medium performance.

Keywords: MSWI fly ash; Alkaline activation reaction; Microstructure; ^{29}Si NMR spectra, Waste glass; spent caustic

Resumen

Los metales pesados peligrosos presentes en las cenizas volantes de la incineración de residuos sólidos urbanos (RSU) representan una amenaza para el medio ambiente y los ecosistemas. La activación alcalina se consideró un método potencial en el campo de la gestión de residuos. En este trabajo de tesis, se investigó la solidificación/estabilización de las cenizas volantes de RSU mediante la reacción de activación alcalina. En primer lugar, se investigaron los efectos del aluminio metálico en la expansión y microestructura de las pastas a base de cenizas volantes de RSU activadas con álcali. A continuación, se analizó los efectos de la dosis de aluminio sobre la formación de gel y la inmovilización de metales pesados en las cenizas volantes de RSU activadas con álcali. A continuación, se estudió la influencia del vidrio reciclado en la inmovilización de los metales pesados procedentes de las cenizas volantes de RSU. Por último, se investigó la co-eliminación de las cenizas volantes de RSU y la sosa cáustica gastada.

Durante la experimentación, se determinó la resistencia a la compresión para evaluar el efecto de consolidación, y se utilizó la medición de la concentración de metales pesados para obtener el efecto cualitativo de inmovilización de los metales pesados. A continuación, las pastas a base de cenizas volantes activadas con álcali se caracterizaron mediante microscopía electrónica de barrido (MEB), difracción de rayos X (DRX), espectroscopia de infrarrojos por transformada de Fourier (FTIR, por sus siglas en ingles), espectroscopia de fotoelectrones de rayos X (XPS, por sus siglas en ingles) y espectros de resonancia magnética nuclear (Espectroscopía RMN) de 29Si para la microestructura y los mecanismos de inmovilización de los metales pesados. Se midió el carbono orgánico total (COT) para determinar al efecto de inmovilización de los orgánicos.

Mediante el estudio de los efectos del aluminio metálico en la expansión y microestructura de las pastas a base de cenizas volantes de RSU activadas con álcali, se concluyó que las cenizas volantes de RSU podrían consolidarse mediante activación alcalina cuando se utiliza una pequeña cantidad de aditivos de aluminosilicato para ajustar las proporciones de sílice reactiva y aluminio. La expansión en las pastas a base de cenizas volantes de RSU activadas con álcali podía eliminarse utilizando un proceso de preparación optimizado, con lo que aumentaba la resistencia a la compresión de las pastas. Comparando las diferentes dosis de aluminio en la formación de gel y la inmovilización de metales pesados en las cenizas volantes de RSU activadas con álcali, se

encuentra que 1) Una pequeña cantidad de adición de aluminio aumentó la resistencia a la compresión y mejoró la inmovilización de los metales pesados; 2) La adición de la dosis de aluminio convirtió la sal de cloruro soluble en sal de Friedel, posteriormente, mejoró la inmovilización de los metales pesados. Al investigar la influencia del vidrio reciclado en la inmovilización de los metales pesados procedentes de las cenizas volantes de RSU, se concluye que la adición de vidrio reciclado reforzó eficazmente la consolidación de las cenizas volantes de RSU e inmovilizó los metales pesados. Con un 40% de adición de vidrio de desecho, la resistencia a la compresión alcanzó un máximo de 3,55 MPa. La eficiencia de inmovilización del Cr aumentó con la adición de vidrio de desecho, mientras que la del Cu, Pb, Zn y Cd depende del pH final del eluyente, la cuál disminuyó con la disminución del pH final del eluyente. Los principales mecanismos de inmovilización incluyen la encapsulación física, la formación de un entorno alcalino y la generación de compuestos insolubles. Mediante el estudio de las cenizas volantes de RSU y la sosa cáustica gastada, se descubrió que el sulfato de la sosa cáustica gastada favorecía la formación de etringita en las pastas activadas con sosa cáustica gastada. En comparación con las pastas activadas con NaOH, las pastas activadas con sosa cáustica gastada formaban menos $Q^4(4Al)$, lo que hacía que la resistencia a la compresión de las pastas activadas con sosa cáustica gastada fuera mayor que la de las pastas activadas con NaOH. Sin embargo, las pastas activadas con sosa cáustica gastada mostraron un menor rendimiento de inmovilización para el Cu, Pb, Zn y Cd, y un mejor rendimiento de inmovilización para el Cr (VI), en comparación con las pastas activadas con NaOH. La presencia de sustancias orgánicas y la formación de ettringita en las pastas activadas con sosa cáustica gastada hicieron más factible la inmovilización de Cr(VI). Para la inmovilización de orgánicos, las pastas activadas con cáustica gastada tuvieron un rendimiento medio.

Palabras clave: Cenizas volantes de RSU; Reacción de activación alcalina; Microestructura; Espectros de RMN de 29Si, Vidrio reciclado; Cáustico usado

Introduction

With the urbanization and the development of industry and economy, municipal solid waste is growly generated. In the treatment of municipal solid waste, landfill is mainly used. However, vast areas occupation, toxic bacteria and viruses remain, and underground water pollution in landfill area prompt to seek other methods for the treatment of municipal solid waste. Waste-to-energy technology is becoming a more preferred method for the disposal of municipal solid waste (Luo et al., 2019; Mroueh et al., 2001; Phua et al., 2019; Sarmiento et al., 2019), due to its advantages of mass and volume, recycles thermal energy, and disinfects toxic bacteria and viruses (Du et al., 2019; Tian et al., 2020b; Y. Wang et al., 2018; Xin-gang et al., 2016). In the incineration process, municipal solid waste incineration (MSWI) fly ash was produced. It contains a large amount of heavy metals (e.g., Pb and Cr) and toxic organics (e.g., PCDD). When exposed to landfill conditions, it would pose environmental threats due to its leaching behavior of heavy metals and toxic organic matter (Nowak et al., 2012). Therefore, it has been defined as hazardous waste (Zhan et al., 2018).

Alkaline activation is the generic term that is applied to the reaction of a solid aluminosilicate (termed the “precursor”) under alkaline conditions (induced by the “alkaline activator”) to produce a hardened binder with combined phases of hydrous alkali-aluminosilicate (N-A-S-H) and calcium silicate hydrate (CSH). Alkali-activated materials could be designed to have superior properties compared to binders prepared from Ordinary Portland Cements (OPC), namely better resistance to acids and sulfate (Bakharev, 2005), better heat resistance (Sarker et al., 2014; Sarker and Mcbeath, 2015), lower drying shrinkage and creep (Sagoe-Crentsil et al., 2013), and higher strength (Bakri et al., 2013). It is proved that many materials containing silica and aluminum can be alkali-activated (Li et al., 2010).

Alkali-activated materials have found a variety of applications, particularly since the 1970s, such as agricultural, industrial, residential, transportation (e.g., railway ties), mining, various high-volume applications, oil well cements, and water stop or sealing applications. As discussed, one of the major newer applications expected to play an increasingly important role is in waste management, including nuclear waste management and immobilization of toxic metals.

In the current thesis work, we investigated the consolidation of MSWI fly ash using alkaline activation reaction，and immobilization of its heavy metals through the produced gel.

Justification

In MSWI fly ash, the content of heavy metals is generally 10-100 times higher than the background value of the soil. In addition, the MSWI fly ash is powdery, and it has a strong mobility, so it is easily washed away by the water and spreads the pollutants (Audry et al., 2004; Bolan et al., 2014; Conesa et al., 2010). According to the United States Environmental Protection Agency (USEPA), the maximum concentration of contaminants for toxicity characteristic leaching procedure is summarized in Table 1. These contaminations are known to have adverse effects on individual biological recipients and populations (Bolan et al., 2014; Komárek et al., 2013). Therefore, the safe disposal of MSWI fly ash is an essential environmental protection task. This disposal mainly involves the consolidation of MSWI fly ash and the immobilization of toxic components in it.

Table 1. Maximum concentration of contaminants for toxicity characteristic leaching procedure

USEPA hazardous waste code	Contaminants	Regulated level (ppm)
D004	arsenic (As)	5.0
D005	barium (Ba)	100.0
D006	cadmium (Cd)	1.0
D007	chromium (Cr)	5.0
D008	lead (Pb)	5.0
D009	mercury (Hg)	0.2
D010	selenium (Se)	1.0
D011	silver (Ag)	5.0

Hypothesis

In the present thesis, we hypothesize that MSWI fly ash can be consolidated through applying appropriate regimes in the alkaline activation process, and the heavy metals can be immobilized in the formed alkali-activated cementitious binders based on MSWI fly ash. Several reasons would support the solidification/stabilization of MSWI fly ash through alkaline activation based on the reaction parameters. 1) MSWI fly ash is calcium oxide and aluminosilicates, which are suitable raw materials for alkaline activation; 2) minerals in MSWI fly ash are highly activated by the incineration process; 3) MSWI fly ash contains high alkalinity, which could be partly activator; 4) Alkaline activation materials have high compressive strength and the formation of alkaline surroundings with high acid resistance and durability, which could retain heavy metals in the form of hydroxide; and 5) the three-dimensional microstructure of Alkaline activation materials is beneficial to micro-encapsulate heavy metals.

General Objective

We attempt to consolidate the MSWI fly ash and to immobilize its heavy metals through the alkaline activation process, as well as to obtain a further understanding of the mechanisms.

Particular objectives

1) To collect and characterize MSWI fly ash samples.

2) To study the preparation regimes and processes in the preparation of alkali-activated MSWI fly ash-based paste.

3) To characterize the microstructures of the prepared alkali-activated MSWI fly ash-based paste.

4) To study the effect of the dosage of silicon and aluminum on the solidification/stabilization of MSWI fly ash-based paste.

5) To study the mechanisms for the consolidation of MSWI fly ash and immobilization of heavy metals through the alkaline activation process.

6) To find a waste-derived alkaline activator for the co-disposal of MSWI fly ash.

CHAPTER 1.

Literature Review

1.1. Origin of MSWI fly ash

According to the *National Bureau of Statistics of China (2020),* more than 242 million tons of municipal solid waste were collected in 2019, which surging increase compared to the 157 million tons in 2009. It is estimated that more than 300 million tons of municipal solid waste will be collected in 2030 (Lu et al., 2017). How to dispose of millions of tons of municipal solid waste is becoming the biggest issue for environmental managers (Kanhar et al., 2020); alternatively, municipal solid waste disposal is expected to make developments in improved landfill bioreactors, composting and thermal processes. Amongst these, incineration is widely accepted because it dramatically reduces the mass and volume, recycles thermal energy, and disinfects toxic bacteria and viruses (Du et al., 2019; Y. Wang et al., 2018; Xin-gang et al., 2016). Because of its advantages, the amounts of waste incineration increased from 20 million tons in 2011 to 101 million tons in 2018 in China (*National Bureau of Statistics of China, 2019*).

In an incineration plant, there is the combustion chamber where the waste is burnt for volume reduction, the boiler system to recover energy, and the air pollution control system to reduce emissions. The air pollution control system removes fine particulates (with devices such as the electrostatic precipitator, fabric filter, or cyclone) and regulates harmful gases (with devices such as dry lime scrubbing or wet lime scrubbing) (Phua et al., 2019). According to the International Ash Working Group (IAWG), MSWI fly ash is defined as the ash that is discharged from the combustion chamber without the addition of any type of sorbents, such as the ash from a superheater, economizer and air preheater. However, in the study of municipal solid waste incineration (MSWI), fly ash is referred to the air pollution control (APC) residues that include the ash trapped by electrostatic precipitators and bag filters. It is estimated that the amount of MSWI fly ash produced accounts for approximately 3–10% of incineration waste (Yao et al., 2014). The MSWI fly ash possesses a higher amount of heavy metal concentrations than that of bottom ash, which is resulted from the chemical partitioning of heavy metals accelerated by the temperature and the presence of chlorine, originated from the types of wastes incinerated (food, PVC, etc.) (Wang et al., 2019). Therefore, various countries, such as the USA, France, Canada, Japan, Italy, Germany, Sweden, etc., have introduced policies for the proper control and management of MSWI fly ash.

1.2. Properties of MSWI fly ash

The properties of MSWI fly ash were influenced by some factors such as the source of waste incinerator design, combustion method, combustion conditions, and type of air pollution control system. Therefore, the properties of MWSI fly ash will be quite complicated. Therefore, it is necessary to understand the properties of the MSWI fly ash itself before disposal or recycling of the MSWI fly ash.

1.2.1. Physical properties of MSWI fly ash

Physical properties such as particle size distribution, permeability, moisture content, and density generally affect heavy metal leaching and determine the environmental impacts after disposal. The particle size distribution, which is estimated by sieving, is one of the most important physical properties as MSWI fly ash with smaller particle size tends to retain a higher concentration of heavy metals (Shi and Kan, 2009; S. Wan et al., 2018) due to the larger surface area for condensation of volatile heavy metals.

The particle size of MSWI fly ash is on the micron scale. Size is influenced by the municipal solid waste feedstock and location that the particulates are collected, and it also is largely dependent on operating conditions of the incinerator, such as flue gas velocity and temperature in the heat recovery system (boiler). As we can see from Table 1.2.1, the average size in terms of % volume passing D_{50} of MSWI fly ash is between 10–166.41 um. Other information such as the D_{10} and D_{90} indicating the smallest 10% and largest 10% fraction can also be used to illustrate the size distribution. Besides, among the different types of MSWI fly ash, the more downstream the point of the collection is, the smaller the particle sizes are, as the larger fly ash particles are captured by the upstream systems (boiler, economizer).

Table 1.2.1. The particle size distribution of MSWI fly ash

Volume particle size passing (%)			References
D_{10}	D_{50}	D_{90}	
2.15	10.02	31.03	(H. Li et al., 2015)
5	30.34	77	(Mangialardi, 2001)

0.2	55	300	(De Boom and Degrez, 2012)
13.32	70.72	2.56	(Florea et al., 2016)
12.05	40	72	(Karlfeldt and Steenari, 2007)
104	166.41	332.08	(Lin et al., 2018)

1.2.2. Chemical components of MSWI fly ash

Table 1.2.2. The Chemical components of MSWI fly ash

Major elements (%)									References
SiO_2	Al_2O_3	Fe_2O_3	CaO	Na_2O	K_2O	MgO	Cl	SO_3	
15.4	7.2	3.6	28.8	6.5	4.3	-	19.6	8.7	(Zheng et al., 2011)
4.22	1.33	2.03	49.6	2.54	5.17	1.66	12.48	6.15	(X. Liu et al., 2018)
3.37	1.69	1.04	39.43	2.88	2.65	1.02	16.32	2.94	(Diaz-Loya et al.,
15.4	7.2	3.6	28.8	6.5	4.3	2.2	19.6	8.7	(Zheng et al., 2010)
16.4	4.7	5.9	31.5	-	-	6.9	14.5	6.3	(Li et al., 2014)
Heavy metals (ppm)									
Pb	Cd	Cr	Cu	Zn	Ni	Rb	Sr		
826	103	1369	2817	3692	78	-	-		(Zheng et al., 2011)
339	-	22	160	1994	-	-	-		(X. Liu et al., 2018)
826	103	1785	2817	3692	-	-	-		(Zheng et al., 2010)
1232	66	70	553	5060	-	-	-		(Li et al., 2014)
1030	-	210	710	8800		44	200		(Assi et al., 2020)

The chemical components of MSWI fly ash were classified as major elements and heavy metals. The major elements were characterized by X-ray fluorescence (XRF) and given in the form of

oxide. The heavy metals were usually determined through digesting the sample and then was measured by an inductively coupled plasma spectrometer (ICP). Table 1.2.2 lists the composition of MSWI fly ash in several countries and regions. It can be seen that MSWI fly ash is a CaO-SiO_2-Al_2O_3-SO_3-Cl based system that is rich in the elements of calcium and chlorine and relatively have scarcity in silicon and aluminum. For air pollution control (scrubber unit), lime is added to the gas stream to neutralize the acidic gases such as HCl to form $CaCl_2$. This leads to MSWI fly ash contains high contents of calcium and chlorine. Except for these major elements, there also are many kinds of heavy metals, such as lead (Pb), zinc (Zn), copper (Cu), chromium (Cr), cadmium (Cd), arsenic (As), and selenium (Se). Even though their contents are relatively low, they have been studied extensively due to their high toxicity.

Other than inorganic elements, MSWI fly ash also contains toxic organic pollutants. Chlorinated organic compounds, such as chlorobenzene, polychlorinated biphenyls (PCBs), polychlorinated dibenzodioxins (PCDDs), and polychlorinated dibenzofurans (PCDFs), have been detected (Tabata et al., 2013). The presence of various forms of organic and inorganic chlorides results in the formation of PCDDs and PCDFs during the cooling process of the flue gas.

1.2.3. Mineralogy of MSWI fly ash

Table 1.2.3. The mineralogy of MSWI fly ash

Mineralogy	References
Calcium chloride hydroxide (CaClOH), halite (NaCl), sylvite (KCl), anhydrite ($CaSO_4$), calcite ($CaCO_3$), and quartz (SiO_2)	(Zheng et al., 2011)
Calcium chloride hydroxide (CaClOH), sylvite (KCl), anhydrite ($CaSO_4$), quartz (SiO_2), and halite (NaCl)	(Zheng et al., 2010)
Halite (NaCl), sylvite (KCl), quartz (SiO_2), calcite ($CaCO_3$), and anhydrite ($CaSO_4$)	(Li et al., 2014)
Halite (NaCl), sylvite (KCl), Calcium chloride hydroxide (CaClOH), anhydrite ($CaSO_4$), calcite ($CaCO_3$), and calcium oxide (CaO)	(Liu et al., 2021)
quartz (SiO_2), mullite ($Al_6Si_2O_{13}$), calcium oxide (CaO), and corundum (Al_2O_3)	(Guo and Zhang, 2020)
Calcium chloride hydroxide (CaClOH), sodium chloride (NaCl), sylvite (KCl), calcite ($CaCO_3$), anhydrite ($CaSO_4$), and $Ca(OH)_2$.	(Assi et al., 2020)

The mineralogy of MSWI fly ash was studied by X-ray diffraction (XRD). XRD analysis measures the intensity of different crystal peaks from each unique compound to estimate relative amounts within the sample. However, MSWI fly ash contains many different phases, which can cause overlapping and difficulties in identifying the phases. This problem is usually overcome by using software programs to simplify the matching process. As can be seen in Table 1.2.3, the main mineral phases in MSWI fly ash contain Calcium chloride hydroxide (CaClOH), halite (NaCl), sylvite (KCl), anhydrite ($CaSO_4$), calcite ($CaCO_3$), a certain kind of MSWI fly ash contains a minor amount of quartz (SiO_2).

1.2.4. Leaching behavior

MSWI fly ash is often disposed of in landfills (Lo and Liao, 2007). It has been reported that MSWI ash may be recycled for the production of cement and concrete, road pavement, glasses and ceramics, agricultural nutrients, stabilizing agents, adsorbents, and zeolites ((Dabo et al., 2009; Ferreira et al., 2003). However, leaching of harmful elements, such as soluble heavy metals and toxic organic compounds (e.g., dioxins and furans), is the main concern for MSWI ash disposal and recycling (Baun and Christensen, 2004; Gao et al., 2017; Yin et al., 2018).

The leaching characteristics are influenced by several factors, including pH, liquid to solid (L/S) ratio, ash properties, weathering and aging, leaching methods, contact time, and investigation scale (Dou et al., 2017; Phoungthong et al., 2016). Static batch tests and dynamic column tests have been used to evaluate the leaching of MSWI ash (Di Gianfilippo et al., 2016b). Column leaching tests provide more reliable information because the percolation-based data are obtained from a flow-through pattern similar to field conditions (Meza et al., 2010).

The pH is the most important physical property of MSWI fly ash as this affected the leaching of heavy metals in it when it was exposed to the solution. On the other hand, MSWI fly ash contains a significant amount of alkaline substances. Normally, it could establish an alkaline pH of around 11 to 12 in water, which exhibited a high buffering capacity against acidification called acid neutralization capacity (ANC) (Dou et al., 2017). Moreover, the leaching of trace elements is highly pH-dependent. In particular, the solubility of heavy metals is sensitive to pH. However, the degree of sensitivity differs among different metal species (Quina et al., 2009). Most metal species (e.g.,

Ca, Cu, Mn, Zn, Cd, and Pb) follow a cationic leaching pattern, and the concentrations of leached elements decrease with increasing solution pH (Figure 1.2.1). In comparison, the maximum leaching of Al and As is observed at extremely acidic (pH~2) and alkaline (pH ~12) conditions, assigned to an amphoteric leaching pattern. Se and Ba show an oxyanionic leaching pattern and the highest concentrations are reached at a very alkaline condition (pH>11) (Y. Zhang et al., 2016). According to previous studies, the pH-dependent leaching of elements, except As, Se, Ag, and Cr, is controlled by the dissolution of common minerals from MSWI fly ash (Di Gianfilippo et al., 2016a) or by the precipitation of their hydroxides, carbonate, and sulfate solids (Cetin et al., 2012). Sorption-controlled leaching mechanisms are proposed for As, Se, and Ag, while Cr leaching is likely controlled by $BaCrO_4$(s) minerals (Komonweeraket et al., 2015).

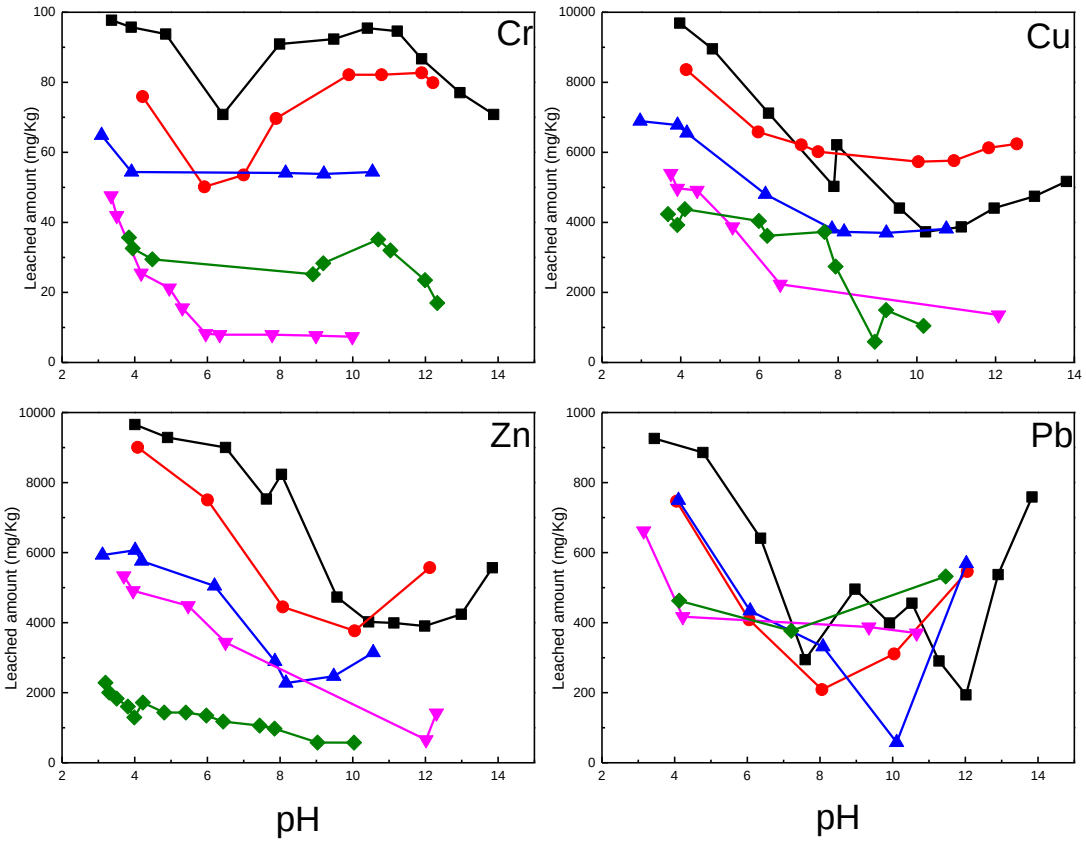

Figure 1.2.1. Typical pH-dependent leaching behavior of Cr, Cu, Zn and Pb from different MSWI fly ash (Luo et al., 2019)

1.3. Methods to dispose of MSWI fly ash

Due to MSWI fly ash containing high chloride and toxic metals, it is necessary to be treated before its disposal into landfill. *The National Hazardous Waste List* clearly designates that MSWI fly ash must be stabilized before landfill. Therefore, various treatment techniques are exercised to eliminate the hazardous and toxic content in MSWI fly ash. The characteristics of MSWI fly ash may serve as a key tool to choose the best option for treatment (Zou et al., 2013). At present, there are lots of studies carried out on the stabilization/removal of heavy metals from MSWI fly ash. The treatment techniques can be classified as (1) separation processes, (2) thermal processes, and (3) solidification/stabilization (S/S) processes. This section summarizes the treatment techniques of fly ash developed in recent years. The treatment methods and principles of treatment of MSWI fly ash are discussed below in Figure 1.3.1.

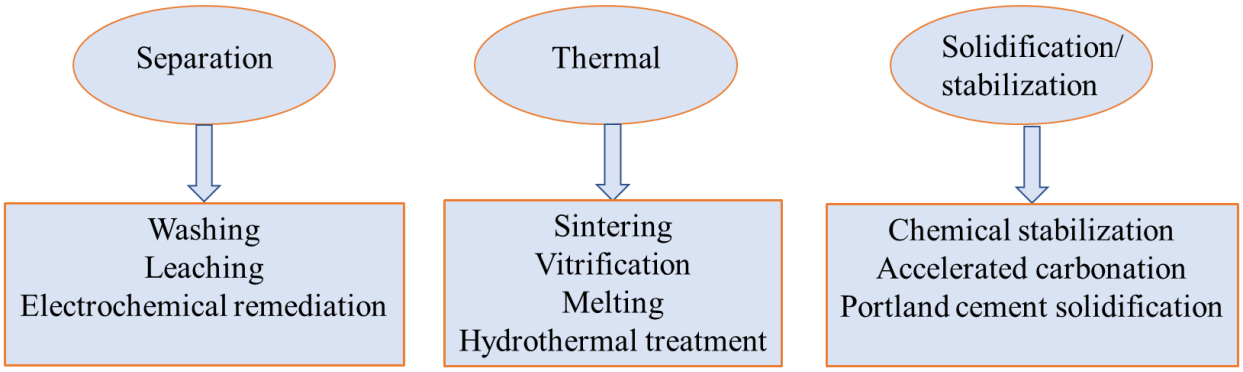

Figure 1.3.1. the treatment methods of MSWI fly ash

1.3.1. Separation process

Separation methods are mainly making use of the different chemical and physical properties in the ash components to separate them using water washing, leaching, and electrochemical remediation. The main goal of these methods is to improve the quality and homogeneity of the product for further treatment or utilization, but some methods can also extract valuable metals (De Boom and Degrez, 2015).

1.3.1.1. Washing processes

Washing processes are the most commonly applied pre-treatments of MSWI fly ash and have been extensively investigated. MSWI fly ash contains a high amount of salt, which is detrimental to the

stability and quality of final products (Chen et al., 2017). Therefore, washing processes are usually a pretreatment method to remove these salt before the MSWI fly ash is consolidated. Washing pre-treatment efficiency is dependent on the liquid to solid (L/S) ratio and on the number of washing steps, especially for chloride extraction (L. Wang et al., 2010b). Generally, the washing process could remove 90~95% of the chlorides at a properly L/S ratio and duration (Chen et al., 2016). The L/S ratio of 25 with a 15-min duration was recommended by Mangialardi (2001), while Wang et al. (2009) used only an L/S ratio of 2 with a 1-h duration to reduce the amount of effluent. It has been reported that multi-step washing pre-treatment allowed better chlorides removal even at a low L/S ratio (Mangialardi et al., 1999). In fact, due to the repetition of washing steps, it was possible to increase the volume of water, which enhanced the removal of chlorides; the extraction of chlorides was improved with greater volumes of water (Chen et al., 2017).

The extraction efficiency and leaching of undesirable metals are highly dependent on the pH of the MSWI fly ash, the L/S ratio, and the metal of concern. Due to MSWI fly ash contains large amount of alkaline substances, its pH higher than 12 when it exposed to water, resulting in the amphoteric metals (Pb, Zn and Cr) to be leached out. Funari et al. (2017) investigated the recovery of heavy metals after the washing process. They concluded that the results are highly dependent on the particle size of the raw MSWI fly ash. Another study towards washing is to develop agitation equipment and recirculation of wastewater in various sequential washing steps to reduce the amount of wastewater generated (Chimenos et al., 2005).

1.3.1.2. Leaching

The objective of leaching is to extract heavy metals from MSWI fly ash under an aggressive leaching environment. After that, the heavy metals were recovered from the leachate. The extraction efficiency of heavy metals is dependent on the kind of extraction solvent, pH and liquid-to-solid ratio. In a leaching solution, an increase in pH may hinder the leachability of heavy metals because of the formation of insoluble hydroxides. Some researchers compared the efficiencies of EDTA, $HClO_4$, HCl, NH_4Cl, NH_4NO_3, and various organic acids with usually used mineral acids and water (Fedje et al., 2010; Okada et al., 2007). They found that strong mineral acids were effective in the leaching of heavy metals compared to organic acids. In particular, Cu and Pb were effectively removed by using EDTA, whereas NH_4NO_3 was seen as effective for Cu. Usually, the

recovery efficiency is higher in acid leaching than alkaline leaching. Due to MSWI fly ash is of high acid neutralization capacity (ANC), acid leaching is not economically feasible because it would consume large amounts of acid used (Okada et al., 2007). Such a result highlighted the economically suitable applicability of different options compared to the acid leaching, such as the alkaline and the ammonia/chloride processes (Okada et al., 2007). Moreover, despite the lower extraction efficiency compared to the acid leaching, the alkaline leaching displayed a better efficacy for selective element recovery (Nagib and Inoue, 2000).

Bioleaching is considered perspective because it is more economical and environmentally-sustainable alternative to the chemical leaching treatment (Xu et al., 2014). It has been reported that the extraction efficiency of bioleaching is comparable to the chemical leaching with the use of organic acids biologically produced by Aspergillus niger fungi (Bosshard et al., 1996; Wu and Ting, 2006). Similarly, the use of sulfur-oxidizing and iron-oxidizing bacteria mixed cultures provided an elevated bioleaching efficiency towards several heavy metals, overcoming the limitations arising from the use of the pure cultures, in separate or mixed applications (Ishigaki et al., 2005).

1.3.1.3. Electrochemical remediation

Electrodialytic remediation is a technique that combines electrodialysis with electromigration of ions for the removal of heavy metals from MSWI fly ash. The basic principle of the electrodialytic remediation technique involves the suspension of MSWI fly ash in a solution placed in electrodialytic cells. An electric current is then applied across the cells, which enables the metal ions to migrate towards the electrodes based on their charge (Kanhar et al., 2020).

The advantage of this method is that no additional chemicals are required and no residues are generated. Jensen et al. (2015) have investigated the potential of electrodialysis on three different types of MSWI fly ash. However, the removal efficiency of heavy metals was generally low when the metal concentration becomes low. The operational parameters may help to achieve somehow better results; like with low pH, higher amounts of heavy metals can be removed. Also, removal of heavy metals was shown to be dependent on the current, density and the type of incineration residue rather than the type of electrodialytic cells (Ottosen et al., 2016). (Viader et al., 2017) have tried electrodialytic separation assisted by cationic membranes and achieved good removal efficiencies for Cr, Cu, Ni, Pb, and Zn. In another study, pretreatment steps (water washing and sieving) were

used to improve the electrodialytic process (Chen et al., 2018). Furthermore, research studies should be carried out to minimize time consumption, lowering the demand for continuous energy (Kanhar et al., 2020).

1.3.2. Thermal treatment

The thermal treatments are aimed to acquire stabilization in the residue, which is resistant to leaching and creating a residue for utilization. Thermal treatment thus ensures the maximum detoxification of residue. In contrast to this, Mangialardi et al. (1999) reported the threat by the presence of alkali chlorides, sulfates and volatile compounds during the thermal treatments. Therefore, these processes involve high temperatures, which increases the cost but creates a possibility for the removal of pollutants and toxic materials (Margallo et al., 2015). Wang et al. (2010a) reported an option to dodge heavy metal volatilization, achieving immobilization in a specific atmosphere, use of additives, temperature and pretreatment. As thermal treatment undergoes an air control system, Haiying et al. (2010) reported to take measures for cooling methods because it may influence the characteristics and leaching behavior of residues. The major thermal treatments are grouped as sintering, vitrification, melting and hydrothermal treatment.

1.3.2.1. Sintering

Sintering is the coalescence and densification of powdered substances into larger particles at elevated temperatures below their melting point. This process usually takes place at temperatures between 900 and 1100 °C. Sintering involves heating the MSWI fly ash to the point at which particle bonding occurs and chemical phases in the MSWI fly ash reorganize; then the solid phase transformation and recrystallization occurs, which results in a product with lower porosity and with higher density and strength. The sintered product with lower porosity tends to eliminate the chances of leachability from the final product.

Several studies have been performed to investigate the effects of sintering on MSWI fly ash (Fedje et al., 2010; Mizutani et al., 1996). According to R. Li et al. (2015), the sintered heavy metals (Zn, Cr, Pb, and Cu) were mainly present in an oxidized form. Except for Pb, the leaching concentrations of most of the heavy metals were within the limits of the national standard. No significant increase was seen in the leaching concentrations of heavy metals even after 30 days of aging of sintered products. The operational conditions, such as sintering time and treatment temperature, may have

an influence on the solidification of heavy metals. Therefore, to establish an overall pollution toxicity index (OPTI), a study was conducted by Chou et al. (2009) for the evaluation of heavy metal pollution. According to experimental results, higher sintering temperature led to more volatilization of heavy metals, and the lowest value for the overall pollution toxicity index (OPTI) was at 1040 °C. Wang et al. (2008) concluded that higher integrated control efficiency conditions of heavy metals were achieved at lower temperatures and shorter times. Some suggested various pretreatments such as water washing, ball milling, sieving and pelletizing of the MSWI fly ash (Wang et al., 1998). These pretreatments are comparable to traditional ceramic processing as the glass-ceramics produced by the sintering process often undergo pre-melting (Boccaccini et al., 2000). The study on untreated fly ash by Mangialardi (2001) proved ineffective for the production of concrete aggregates because of the adverse chemical characteristics of these MSWI fly ashes in terms of chloride, sulfate, and vitrifying oxide contents. Contrastingly, to counter the presence of soluble salts, water-washing treatment can enhance the chemical properties of sintered products, which, according to Wey et al. (2006), satisfies the basic requirements for concrete aggregates. Water washing treatment is not only effective for the removal of metal chlorides but also serves as an effective tool for reducing the sintering temperature and treatment time. Although water washing lowers the power consumption during the sintering, it would require further treatment for wastewater generated.

Co-sintering with various additives such as bottom ash and slag to achieve the optimal proportion of CaO and SiO_2 ratio for better mechanical properties has been demonstrated (Hu et al., 2016). It is also found that Ca aluminosilicate formed during co-sintering is capable of suppressing ash agglomeration and favoring metal chloride recovery via volatilization.

1.3.2.2. Vitrification

Vitrification is the melting of ash residues with other glass-forming additives to produce a homogenous liquid phase between 1100 and 1500 °C, followed by rapid cooling to form a rigid and amorphous glassy matrix without crystallization (Quina et al., 2008a). Vitrified products are generally more consistent and chemically stable due to the incorporation of heavy metals into the glass matrix to form a homogenous solid phase and also the encapsulation effects provided by the outermost glassy layer (Ghouleh and Shao, 2018). Although vitrification is a technically feasible

solution, the high energy consumption during the process increases the treatment cost and this has limited its potential due to economic issues. Therefore, the research has focused on using other additives such as biomass (Alhadj-Mallah et al., 2015) or make use of co-treatment with other wastes (Huber et al., 2016) to reduce the energy demand and make this process more economically viable. However, due to the heterogeneous nature of MSWI fly ash, the quality of the final product is affected, and the subsequent utilization can be limited.

1.3.2.3. Melting

Melting process operates at a similar temperature as vitrification, but the main difference is that during melting, no additives are added. Also, the final product formed is homogenous and contains various major crystalline phases. As compared to vitrification, melting is preferable as no additives are required and there is no need for rapid cooling of the final product. Melting systems are reported to be used on a commercial scale to treat MSWI fly ash especially in Japan where disposal at landfills is costly (Ecke et al., 2000). According to Sakai and Hiraoka (2000), the two main systems are (i) fuel-burning melting system and (ii) electric melting system. The fuel-burning melting involves fuel oil, coke and gas. In this regard, a detailed study is presented by Sakai and Hiraoka (2000), which summarizes the properties of fuel burning and electric melting furnaces and systems. The volatilization of heavy metals during melting processes were studied by several researchers (Okada and Tomikawa, 2012; Tian et al., 2012; X. Wang et al., 2017; Yue et al., 2019; Zhao et al., 2010). The low volatile heavy metals are transformed and solidified in the dense lattice structure of melted slag, thereby reducing their leaching rate. However, the easily and semi-volatile heavy metals in MSWI fly ash exist in the secondary fly ash during the melting process. The volatilization of these heavy metals is related to the high content of Cl in the raw fly ash. According to Okada and Tomikawa (2012), the volatilization of Cl in MSWI fly ash melting furnace is directly related to the molar ratio of Cl/(Na + K) in the raw fly ash sample. A higher Cl/(Na + K) molar ratio promoted the volatilization of Cl, leading to the detection of more $PbCl_2$ in the secondary fly ash. Similarly, Yue et al. (2019) shows that low volatile heavy metals (Cr, Ni) were better solidified in the melting slag. In contrast, the easily and semi-volatile heavy metals such as Hg, Cd, Pb, and Zn are challenging to stabilize. Plasma is currently an area of electric melting. The high-energy-density and high-temperature of a plasma flame can promote the melting reactions and reduce the residence time of MSWI fly ash. Related research has shown, after plasma melting treatment, the volume

reduction of MSWI fly ash (Q. Wang et al., 2010; Zhao et al., 2010). The volatilization and leaching characteristics of heavy metals before and after plasma melting determined that most heavy metals sealed in vitreous slag are Cr, and Ni, which are low volatile heavy metals (Čarnogurská et al., 2015; Ma et al., 2017; Q. Wang et al., 2010; Zhao et al., 2010). In comparison, Cd and Pb exhibit a strong volatile property. The leaching of other heavy metals in melting slag such as Zn and Cu is significantly lower than that of the original MSWI fly ash, which proves that vitreous slag can seal the heavy metals from MSWI fly ash.

1.3.2.4. Hydrothermal treatment

Hydrothermal process is a form of thermochemical of subcritical or supercritical water at relatively low temperature with the advantage of self-generated pressure. In recent years, investigations of hydrothermal treatment on MSWI fly ash have become more popular due to the destruction of organic contaminants and improved stability of heavy metal leaching (Hu et al., 2015). In general, reaction catalysts (such as ferric compounds) can be added during the treatment to enhance the contaminant decomposition. The hydrothermal process with ferric compounds carried out on water-washed MSWI fly ash increased leaching of heavy metal leaching and slightly improved the degradation of polychlorinated dibenzo-dioxins (PCDDs) and dibenzo-furans (PCDFs). This outcome could be ascribed to the formation of magnetite (Fe_3O_4) in the hydrothermally treated washed MSWI fly ash, which functioned as a catalyst during the decomposition of PCDDs/PCDFs (Hu et al., 2012). Bayuseno et al. (2009) reported contrasting information, stating that hydrothermal treatment decreased the efficiency of metal leaching from washed MSWI fly ash due to the incorporation of the metals into low soluble tobermorite -11 A° formed during the hydrothermal step. However, Hu et al. (2015) achieved a more efficient solution to decrease metals leaching by applying an acid leaching pre-treatment of MSWI fly ash by the hydrothermal process compared to water-washed MSWI fly ash. Additionally, possible acid post-treatment could also further improve metals separation and recovery since their enhanced exposure due to MSWI fly ash aggregated particles disintegration occurring during the hydrothermal process (Hu et al., 2015).

1.3.3. Solidification/stabilization (S/S) processes

Stabilization/solidification (S/S) are widely employed processes for MSWI fly ash. S/S processes tend to deal with waste residues whose properties (physical, chemical and mechanical) favor

reducing the leachability of contaminants from waste (Sabbas et al., 2003). The S/S indicates the processes, which involve additives or binders to either physically or chemically immobilize the hazardous content in waste (Lam et al., 2010). The goal of the stabilization process is to decrease the toxicity and solubility of contaminants to make it less soluble and less toxic with or without solidification. Contrastingly, in solidification in order to lessen the leachability and to immobilize contaminants, binders such as cement are usually added. This process reduces the mobility of contaminants in the treated material through encapsulation. The approach to S/S includes chemical stabilization, accelerated carbonation, and Portland cement solidification.

1.3.3.1. Chemical stabilization

Chemical stabilization makes use of chemical additives to produce thermodynamically favored solid phases in order to reduce the total availability for leaching. This treatment method consists of (1) dissolution of the waste residues, (2) addition of chemicals for stabilization and pH adjustment, and (3) filtration to separate the high salt filtrate from the stabilized residues. The technology is quite established, and various additives such as soluble phosphates, sulfides, and activated carbon have been used at full scale (Nzihou and Sharrock, 2002). Eighmy et al. (1997) demonstrated that 1.2 mol of H_3PO_4 per kg MSWI fly ash with an L/S ratio of 0.4 could reduce Pb leaching by 99.5%, while the pH of the final product was not affected by the H_3PO_4 added due to high alkalinity. Quina et al. (2010) suggested that H_3PO_4 could affect the neutralizing capacity since both Zn and Pb were stabilized, and there was increased leaching of Cr (VI). Recently, H. Wang et al. (2017) have utilized phosphate and other chelate agents to stabilize MSWI fly ash, while the leaching effect was examined using citric acid. Other additives such as ferrous sulfate, colloidal silica, Bayer red mud, and alumina oxides have also been investigated with good immobilizing potential (Hu, 2005; Liu et al., 2018; Park, 2009). In general, MSWI fly ash is commonly treated via chemical stabilization due to the high alkalinity and high acid-neutralizing capacity.

1.3.3.2. Accelerated carbonation

Carbonation is a natural weathering process due to the dissolution of CO_2 in water, which lowers the pH and eventually results in the formation of calcite and other new minerals capable of entrapping heavy metals. Ecke (2003) has reported decreased leaching of MSWI fly ash at 2 orders of magnitude for amphoteric metals such as Zn and Pb after carbonation but also highlighted the

increased release of other metals such as Cd, Cr, Ni, and Sb. Li et al. (2007) studied the effect of the L/S ratio between 0.1 and 0.8 using accelerated carbonation and suggested the optimum L/S ratio is 0.3. The main factors affecting the rate of carbonation are diffusivity and reactivity of carbon dioxide, and these can be controlled by adjusting the pH, L/S ratio, humidity, temperature, and pressure (Mccarthy et al., 2017). Gerven et al. (2004) reported that supercritical carbonation could enhance/accelerate the aging characteristics of solidified products. It has been reported that using supercritical carbonated cement product to study the heavy metals' leaching characteristics and found that supercritical carbonation promoted the leaching of Cu and Pb (Zha et al., 2019). Furthermore, not all heavy metals can be fixed through solidification, such as Hg. The study of Du et al. (2018) showed that Hg released by the solidified products reaches 8.51 ng/g–18.48 ng/g, resembling that of raw fly ash. Additionally, the increase in temperature and water content also promoted the release of Hg. According to Quina et al. (2008), this process has a drawback, which makes it ineffective for the treatment of soluble salts, and in return, long-standing leaching will bring an environmental issue. During this process, a significant increase in the volume of waste may occur, which may affect shipping and landfill costs (Margallo et al., 2015).

1.3.3.3. Portland cement solidification

The addition of inorganic binders such as Portland cement for S/S has been in practice for a long time in several parts of the world. Numerous research studies have shown that cement solidification can fix the heavy metals (Conner and Hoeffner, 1998; Valls and Vazquez, 2002; Zhang et al., 2009). The enhanced properties of the final product, such as lower hydraulic conductivity and lower porosity, limit the leachability of the heavy metals by reducing contact, while the increase in structural strength and durability ensures long-term stability and structural integrity (Bie et al., 2015). In addition, the formation of a crystalline structure during the pozzolanic reaction is capable of incorporating heavy metals into the matrix to provide potential long-term immobilization. However, heavy metals in cement-solidified products are not stable in the long term and also the exposed environment may increase the leaching ability of heavy metals. The introduction of a new stabilization technique by Derie (1996) is shown to be capable of destroying the toxic content, reducing the heavy metal reactivity, and solidifying the hazardous waste beyond the leaching limit. This four-stage technique involves eliminating alkali chlorides by solidification, the addition of phosphoric acid, calcination, and solidification with cement. The combined treatments, such as

washing-immobilization treatments, can remove noteworthy quantities of sulfate and mainly chloride from MSWI fly ash. This treatment would encourage the development of the hydrate phase, which will change the heavy metals into less reactive forms. Afterward, the water remained as waste after washing treatment could be treated as explained by Mangialardi et al. (1999). This treatment can not only help to treat the MSWI fly ash and stabilize it in cement with any issue of heavy metals leaching but can also reduce the cost to make this treatment economical.

On the other hand, S/S using a binder results in an increase in the mass of the secondary waste which has to be disposed of. A new trend to resolve the increase in the mass of the secondary product is to use the combination of MSWI fly ash, and solidifying agents to increase the proportion of waste-to-binder ratio (Wang et al., 2015).

1.4. S/S MSWI fly ash through alkaline activation reaction

Alkaline activation reaction exhibited high prospect in waste management field and was extensively studied. In the alkaline activation reaction, alkaline solution activates aluminosilicates in waste to produce a monolithic matrix with enough strength by the formation of cementitious gel (Liu et al., 2021). Alkaline activation materials are considered as an eco-friendly alternative for OPC (Haider et al., 2014). They exhibited superior acid resistance comparing to matrices prepared from OPC (Ye et al., 2016a), which allows them to retain heavy metals in matrices when exposed to the landfill environment. As for the S/S of MSWI fly ash, researchers conducted some work but limited. Some critical problems need to be further investigated using an alkaline activation reaction to treat MSWI fly ash.

1.4.1. Expansion in alkali-activated MSWI fly ash-based matrix

Commonly, metallic aluminum that originates from aluminum foils and nails (Joseph et al., 2017) usually remains in MSWI fly ash after the incineration process, in which the incineration temperature is generally between 800℃ and 1000℃, and the residence time of calcined solid waste in the furnace is generally 1-1.5 s. The short residence time and the newly formed oxides on the metal surface resulting in metallic aluminum can not be effectively oxidized and remains in the MSWI fly ash. Most of the non-oxidized metal blocks are separated into the bottom ash after passing through the combustion furnace, and the finer metal particles are collected together with the flue gas through the bag filter to form fly ash. When it reacts with alkalis in alkaline activation

process, hydrogen gas (H2) releases, as noted in equations [1.1] and [1.2]. The emission of H_2 results in porous structure in the alkali-activated MSWI fly ash-based pastes, leading to low compressive strength and durability. For example, in OPC solidified MSWI fly ash-based pastes, it was found that the pastes expanded 25% in 10 h (Aubert et al., 2006). Therefore, pretreatments such as washing and heating were explored to remove the metallic aluminum before alkaline activation, but they are costly in industrial applications (Saikia et al., 2015; Tang et al., 2016). Therefore, the expansion in alkali-activated MSWI fly ash-based matrix should be eliminated to increase the encapsulation capacity and durability of the matrix.

$$Al + 2OH^- + H_2O \rightarrow [AlO(OH)_2]^- + H_2 \uparrow \quad [1.4.1]$$

$$2Al + 2OH^- + 6H_2O \rightarrow 2[Al(OH)_4]^-_{aq} + 3H_2 \uparrow \quad [1.4.2]$$

1.4.2. Additives

Usually, the composition of the MSWI fly ash is a CaO-SiO_2-Al_2O_3-SO_3-Cl based system that is rich in the elements of calcium, chloride and sulfur, and relatively have scarcity in silicon and aluminum. Except for CaO, few compositions are congruent with the activation of the alkaline reactions. The characteristic of MSWI fly ash that is deficient in silicon and aluminum components necessitates extra aluminosilicate addition in alkaline activation reaction. Some researchers used metakaolin (Cyr et al., 2012; Lancellotti et al., 2010), coal fly ash (Diaz-Loya et al., 2012; Galiano et al., 2011), and silica fume (Li et al., 2014) as additives in the S/S of MSWI fly ash through alkaline activation technology. For example, Li et al. (2014) studied the feasibility and effectiveness of the silica fume on the immobilization of heavy metal waste in the MSWI fly ash. They found that heavy metals leaching could be significantly reduced by only 10% of silica fume used. Diaz-Loya et al. (2012) used 80% MSWI fly ash and 20% coal fly ash were alkali-activated by sodium hydroxide and sodium silicate, producing pastes with compressive strength higher than 15.8 MPa. The S/S process for heavy metals in MSWI fly ash should meet the few requirements on the priority basis, namely, strong fixing ability, structural stability of the solidified paste with considerable strength, and low volume-added rate (Zheng et al., 2010). Therefore, a low amount of active silicon is necessary to be added to the process.

1.4.3. Alkaline activator

In studying alkaline activation materials (AAMs), the environmental impact remains an open debate in the life cycle assessment. Generally, AAMs consist of a high concentration of alkaline activator (i.e., sodium hydroxide and silicate) and aluminosilicate raw materials (Liu et al., 2021). The CO_2 footprint reduction of AAMs is less than expected if considering the transport of the raw materials, the energy required to prepare the alkaline activators, and the high temperature used to achieve comparables strength (Ouellet-Plamondon and Habert, 2015). However, these cannot overcome the critical advantage that alkaline activation can be a way to manage solid waste due to alkali-activated binders have high acid resistance durability and the immobilization ability for heavy metals (X. Liu et al., 2018). It has been reported that the compacted three-dimension tetrahedral aluminosilicate structure formed in AAMs could protect the matrix from attacking by chloride ions (Albitar et al., 2017; Kwan et al., 2018) and favor the heavy metals immobilization (Liu et al., 2021; Tian et al., 2020b; Zhu et al., 2019a). In the alkaline activation process, the commonly used traditional alkaline activators are sodium hydroxide and silicate (Diaz-Loya et al., 2012; Zhan et al., 2018), which relates to the high cost, and thus dramatically reduces the economic advantage (Ouellet-Plamondon and Habert, 2015; J. Wang et al., 2018). Therefore, the most recent studies are trying to use waste-derived activators for the sustainable development of the alkaline activation field (Ahmed et al., 2018; Moraes et al., 2018).

1.4.4. Immobilization mechanism of heavy metals

Currently, alkaline activation is reported as an effective S/S process in the treatment of MSWI fly ash (Li et al., 2014; Zheng et al., 2010). In such treatment, hazardous heavy metals are stabilized through the formation of heavy metal compounds (Q. Wan et al., 2018), physical encapsulation (Phair and Deventer, 2001; Wan et al., 2019b), the formation of alkaline surroundings (Zhan et al., 2018) and the formation of the gel structure of the pastes (Q. Wan et al., 2018; Zhan et al., 2018). For example, Li et al. (2014) studied the feasibility and effectiveness of the silica fume on the immobilization of heavy metal waste in the MSWI fly ash. They found that heavy metals can be immobilized through physical entrapment and chemical incorporation of precipitates. Zhan et al. (2018) reported the S/S process for MSWI fly ash with electrolytic manganese residue. They

concluded that the stabilization mechanism of the heavy metals in the S/S matrix is likely due to the alkaline conditions and encapsulation ability created by alkaline activation reaction.

CHAPTER 2.

Experimental

2.1. Research line

Research line of the work is presented schematically in Figure 2.1. As it shows, in Chapter 1, the literature concerning the characteristics and treatment method for MSWI fly ash were reviewed. Chapter 2 presents the experimental of the thesis work. Chapter 3 shows the results and discussion. In Chapter 3.1, the effects of metallic aluminum on the expansion and microstructure of alkali-activated MSWI fly ash-based pastes were investigated. The metallic aluminum in MSWI fly ash caused expansion of alkali-activated MSWI fly ash-based pastes due to the generation of hydrogen gas. An optimum synthesis process was employed to mitigate the expansion, improve the formation of geopolymer gel and enhance the compressive strength of pastes. Chapter 3.2 showed the effects of aluminum dosage on gel formation and heavy metals immobilization in alkali-activated MSWI fly ash. It was found that moderate aluminum addition increased the compressive strength of pastes. The addition of aluminum converted soluble chloride salt into Friedel's salt and subsequently improved the immobilization of heavy metals. A small amount of aluminum can improve immobilization dominantly because of the effective encapsulation ability of the pastes. Chapter 3.3 determined the influence of waste glass on the immobilization of heavy metals originated from MSWI fly ash. It was found that waste glass addition effectively reinforced the consolidation of MSWI fly ash and immobilized the heavy metals. As 40% addition of waste glass, the compressive strength reached a maximum of 3.55 MPa. The immobilization efficiency of Cr increased with the addition of waste glass, while that of Cu, Pb, Zn and Cd is dependent on the eluant final pH, which decreased with the decrease of eluant final pH. The main immobilization mechanisms include physical encapsulation, alkaline environment formation, and the generation of insoluble compounds. Chapter 3.4 studied co-disposal of spent caustic and MSWI fly ash through alkaline activation system. It was found that the sulfate in spent caustic favored the ettringite formation in spent caustic-activated pastes, and a large number of organics presented in spent caustic-activated pastes. Compared with NaOH-activated pastes, spent caustic-activated pastes formed less $Q^4(4Al)$, leading to the compressive strength of spent caustic-activated pastes was higher than that of NaOH-activated pastes. The spent caustic-activated pastes exhibited a weaker immobilization performance for Cu, Pb, Zn and Cd, and better performance for Cr (VI), comparing to NaOH-activated pastes. The presence of organics and the formation of ettringite in spent caustic-activated

pastes made the immobilization of Cr(VI) more feasible. For the immobilization of organics, the spent caustic-activated pastes were of a medium performance.

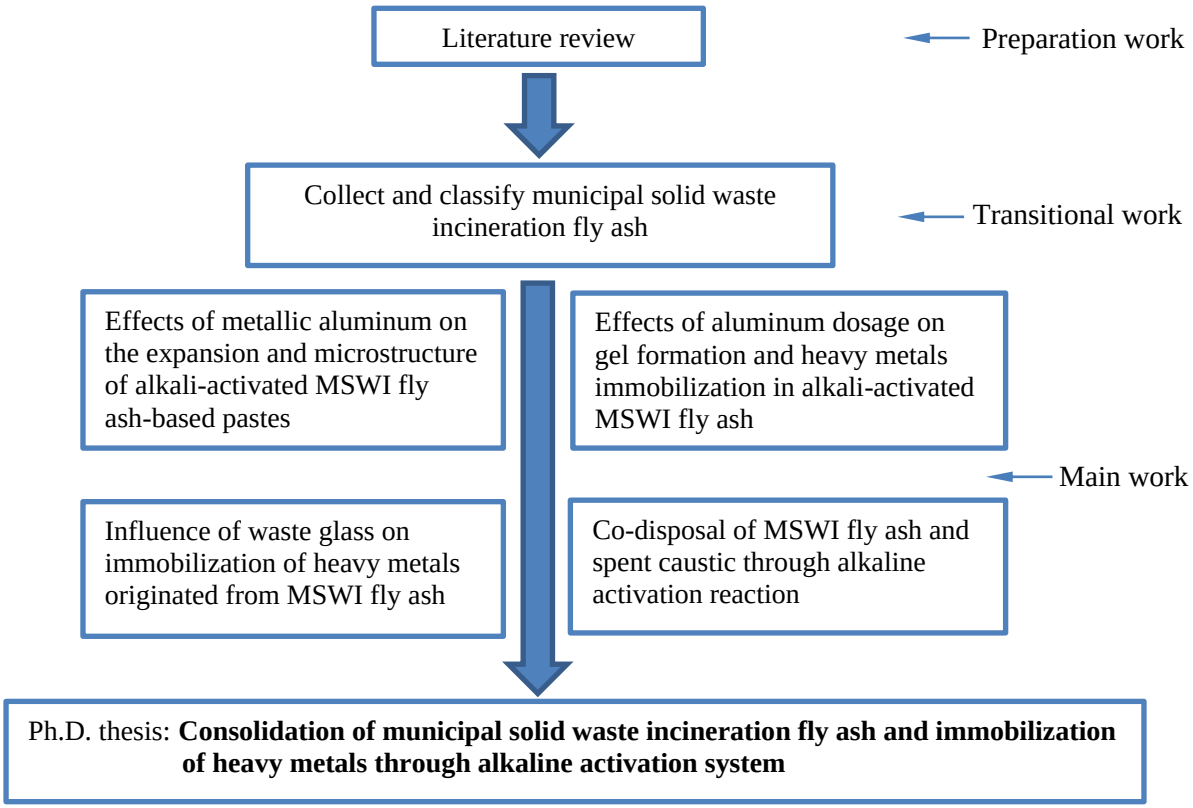

Figure 2.1. Schematic presentation of the research line

2.2. Materials

2.2.1. MSWI fly ash

The properties of MSWI fly ash varied in different parts because it was influenced by some factors such as the different living habits in different regions, source of waste incinerator design, combustion method, combustion conditions, and type of air pollution control system. Therefore, we collected three types of MSWI fly ash from different regions in China (Shenzhen, Wuhan, Chongqing). The chemical components of MSWI fly ash were classified as major elements and heavy metals. The mineralogy characterization of MSWI fly ash was characterized by X-ray diffraction (XRD, Empyrean). The major elements were characterized by X-ray fluorescence (XRF, Zetium) and given in the form of oxide. The heavy metals were determined through digesting the samples using a combination of HNO_3+ $HClO_4$+ HF acids and then was measured by an inductively coupled plasma spectrometer (ICP, Prodigy 7, China).

Figure 2.2.1 gives the XRD pattern of MSWI fly ash from Shenzhen. It contained mainly calcite ($CaCO_3$), halite (NaCl), sylvite (KCl) and Anhydrite ($CaSO_4$), with a small quantity of quartz (SiO_2). Table 2.2.1 showed the chemical compositions of the MSWI fly ash from Shenzhen. The main components CaO, Cl^- and SO_3 were 40.66%, 16.08% and 4.48% of the mass, respectively. Heavy metals were characterized at 640 ppm Cu, 910 ppm Pb, 130 ppm Cr, 127 ppm Cd, and 2930 ppm Zn (Table 2.2.2).

Figure 2.2.2 gives the mineralogy characterizations of MSWI fly ash from Wuhan. The major crystalline phases in MSWI fly ash consist of portlandite ($Ca(OH)_2$), halite (NaCl), calcite ($CaCO_3$), sylvite (KCl), and calcium chloride hydroxide (CaClOH). Table 2.2.3 gives the major chemical compositions of MSWI fly ash from Wuhan. It predominantly contains CaO, Cl, Na_2O, and a minor SiO_2 and Al_2O_3. Heavy metals were characterized at 375 ppm Cu, 1048 ppm Pb, 155 ppm Cr, 195 ppm Cd, and 2813 ppm Zn (Table 2.2.4).

Figure 2.2.3 depicts the X-ray diffraction pattern of MSWI fly ash from Chongqing. The major crystalline phases in MSWI fly ash consisted of portlandite ($Ca(OH)_2$), calcium chloride hydroxide (CaClOH), halite (NaCl), anhydrite ($CaSO_4$), calcite ($CaCO_3$) and sylvite (KCl). Table 2.2.5 gives the chemical elements of MSWI fly ash from Chongqing. The essential elements in MSWI fly ash

were Ca, Cl, Na and S. Heavy metals were characterized at 358 ppm Cu, 911 ppm Pb, 420 ppm Cr, 146 ppm Cd, and 4501 ppm Zn (Table 2.2.6).

In sum, these three types of MSWI fly ash are from different parts. However, there are some common properties. Ca-bearing crystal phases such as $CaCO_3$ and $Ca(OH)_2$, as well as halite (NaCl) always exist in MSWI fly ash. Calcium and chloride are the most elements. This is because in the waste incineration process, plastic and rubber combustion produce plenty of acidic gases (e.g., HCl, SO_2, and HF). They flow with the gas stream from the combustion chamber to the air pollution control system and are captured by the added hydrated lime to neutralize them. This process causes substantial calcium and chloride contained in MSWI fly ash. The heavy metals Zn and Pb are most existing in the MSWI fly ash. This is because Pb and Zn are usually considered as volatile metals, and so considerable concentrations may be found in MSWI fly ash (Quina et al., 2009).

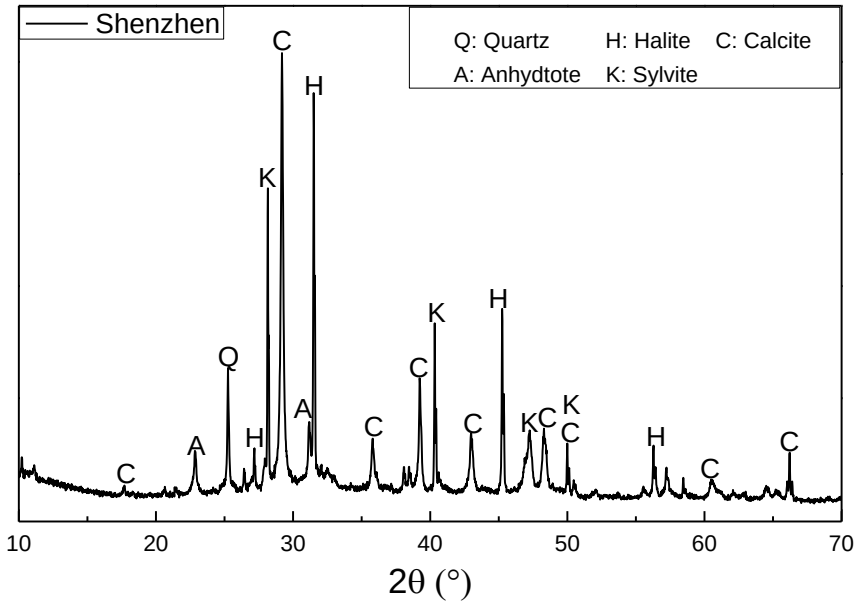

Figure 2.2.1. XRD pattern of MSWI fly ash from Shenzhen

Table 2.2.1. Chemical composition of the MSWI fly ash from Shenzhen (%)

Components	CaO	SiO_2	Al_2O_3	Cl^-	SO_3	Na_2O	K_2O
Contents	40.66	3.011	0.78	16.08	4.483	6.11	3.79

Table 2.2.2. Heavy metals in MSWI fly ash from Shenzhen (ppm)

Heavy	Pb	Cu	Cd	Zn	Cr
Contents	910	640	127	2930	130

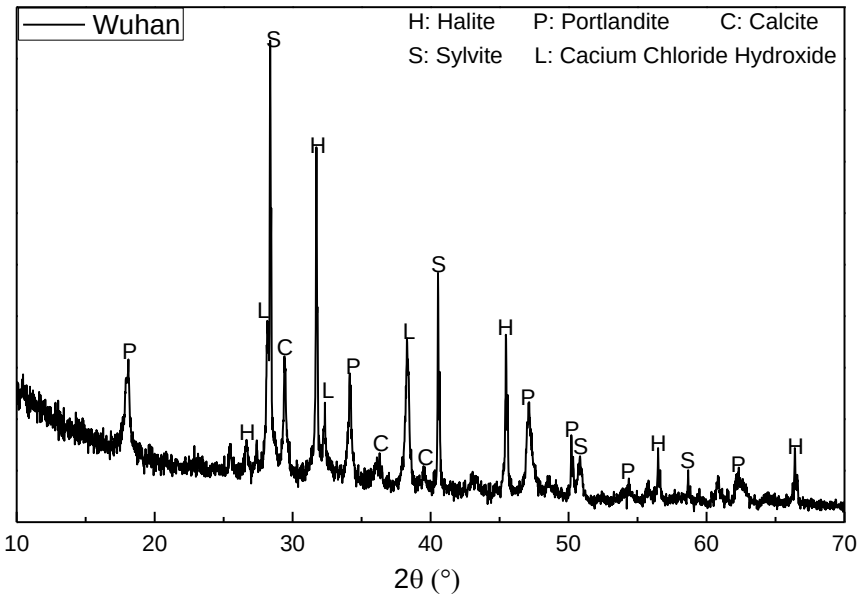

Figure 2.2.2. XRD pattern of MSWI fly ash from Wuhan

Table 2.2.3. Chemical composition of the MSWI fly ash from Wuhan (%)

Components	SiO_2	Al_2O_3	CaO	SO_3	Cl	Na_2O	K_2O	MgO
Contents	1.72	0.37	29.88	4.39	21.93	9.11	5.68	1.15

Table 2.2.4. Heavy metals in MSWI fly ash from Wuhan (ppm)

Heavy	Pb	Cu	Cd	Zn	Cr
Contents	1048	375	195	2813	155

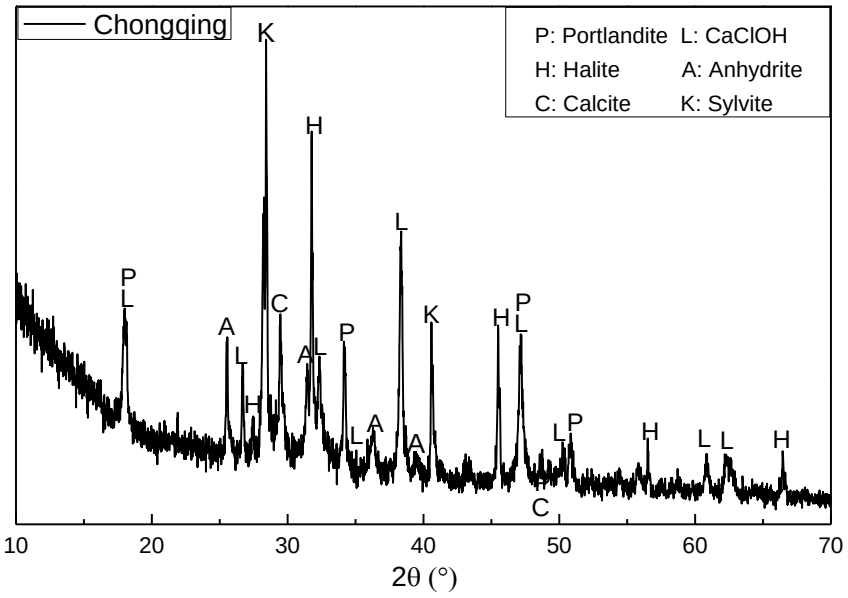

Figure 2.2.3. XRD pattern of MSWI fly ash from Chongqing

Table 2.2.5. Chemical composition of the MSWI fly ash from Chongqing (%)

Components	CaO	SiO_2	Al_2O_3	Na_2O	K_2O	SO_3	Cl
Contents	29.16	3.07	0.90	6.04	3.37	5.55	15.40

Table 2.2.6. Heavy metals in MSWI fly ash from Chongqing (ppm)

Heavy	Pb	Cu	Cd	Zn	Cr
Contents	911	358	146	4501	420

2.2.2. Aluminosilicate additives

In MSWI fly ash, Si and Al are rarely presented (Phua et al., 2019; Yin et al., 2018). Therefore, reactive aluminosilicate additives should be incorporated to consolidate them through alkaline activation reaction well. In this thesis work, we choose several different aluminosilicate additives containing coal fly ash (CFA), metakaolin, silica fume, blast furnace slag (BFS) and waste glass

(WA). Their mineralogy characterization was conducted by X-ray diffraction (XRD, Empyrean) and composition analysis was carried out by X-ray fluorescence ((XRF, Zetium)

Figure 2.2.4 gives the XRD pattern of CFA. The crystal phase in coal fly ash consisted of quartz (SiO_2), berlinite ($AlPO_4$) and anhydrote ($CaSO_4$). Table 2.2.7 gives the chemical composition of coal fly ash. The main components in coal fly ash are SiO_2 (49.9%) and Al_2O_3 (28.3%).

Figure 2.2.5 shows the XRD pattern of metakaolin. Metakaolin was prepared by the calcination of kaolinite at 600 °C in the air for 6 h. After calcination, the kaolinite dehydrated and turned into amorphous phase, which is indicated by a halo peak 2θ of 15-30°, and remained crystal phase muscovite ($Al_2Si_3AlO_{10}(OH)_2$) and quartz (SiO_2). Table 2.2.8 gives the chemical composition of metakaolin. It contained 59.48% SiO_2 and 35.13% Al_2O_3, respectively.

Figure 2.2.6 gives the XRD pattern of silica fume. It showed a hump peak at 2θ of 15-30°, which indicated a major amorphous phase. The main component in silica fume is SiO_2 of 98%.

Figure 2.2.7 shows the XRD pattern of BFS. BFS consists of the main amorphous phase indicated by a broad peak of 2θ between 25 to 35º, and a small crystal calcium silicate ($Ca_8Si_5O_{13}$). Table 2.2.9 showed the chemical composition of BFS. The essential constitutions in BFS are CaO (38.5%), SiO_2 (30.57%), and Al_2O_3 (15.09%).

Figure 2.2.8 depicted the XRD pattern of WA. WA was predominantly composed of an amorphous phase indicated by a halo peak of 2θ between 15º to 30º. Table 2.2.10 showed the chemical composition of WA. The essential elements in waste glass were Si, Na and Ca.

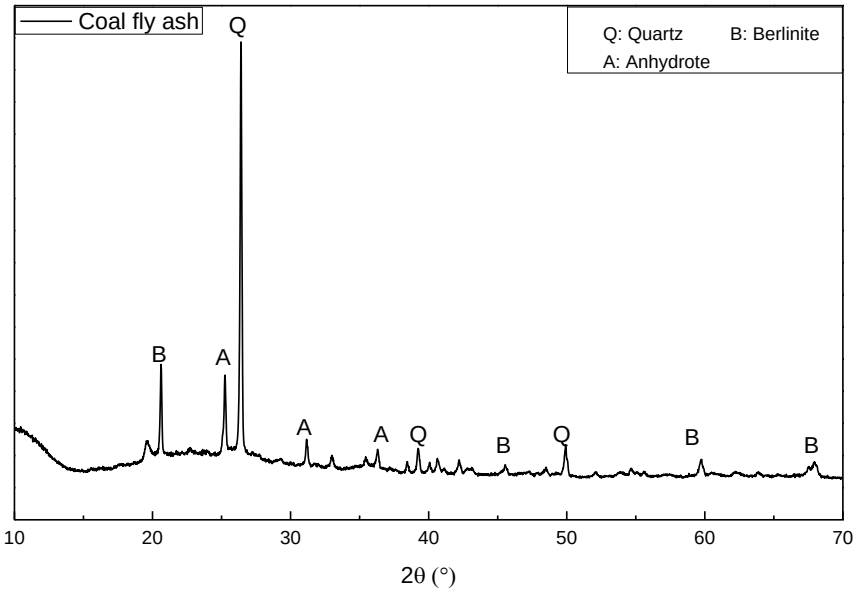

Figure 2.2.4. XRD pattern of Coal fly ash

Table 2.2.7. Chemical composition of coal fly ash (%)

Components	SiO_2	Al_2O_3	CaO	Fe_2O_3	SO_3	P_2O_5	K_2O
Contents	49.90	28.30	8.51	5.48	2.02	1.18	1.41

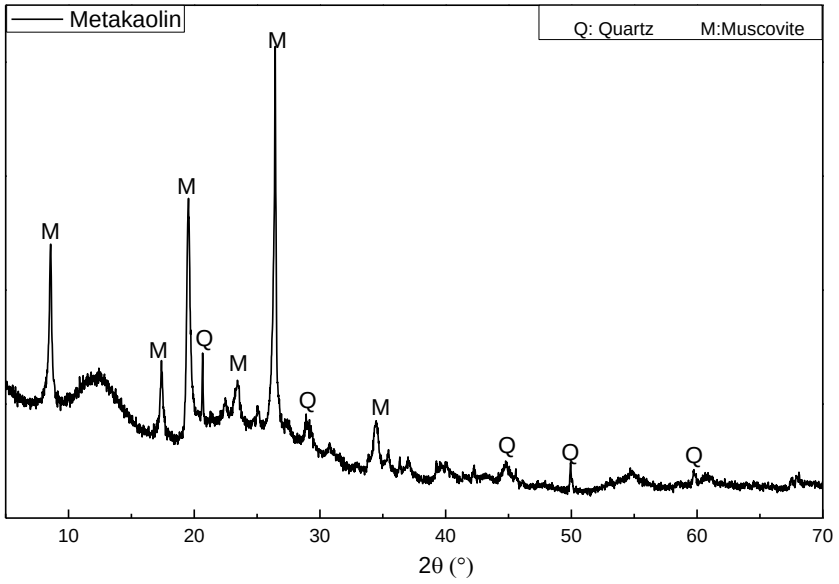

Figure 2.2.6. XRD pattern of metakaolin

Table 2.2.8. Chemical composition of metakaolin (%)

Components	SiO2	Al_2O_3	Na_2O	K_2O	Fe_2O_3
Contents	59.48	35.13	0.08	2.56	0.97

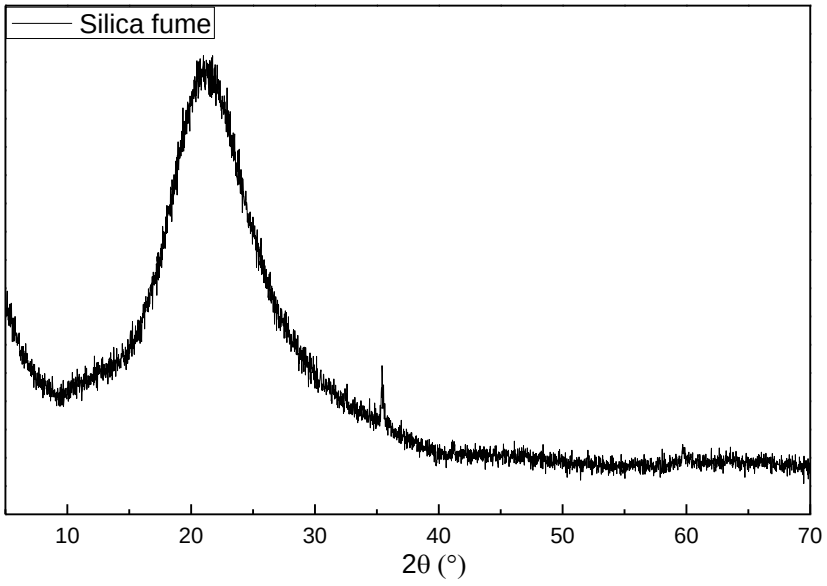

Figure 2.2.6. XRD pattern of silica fume

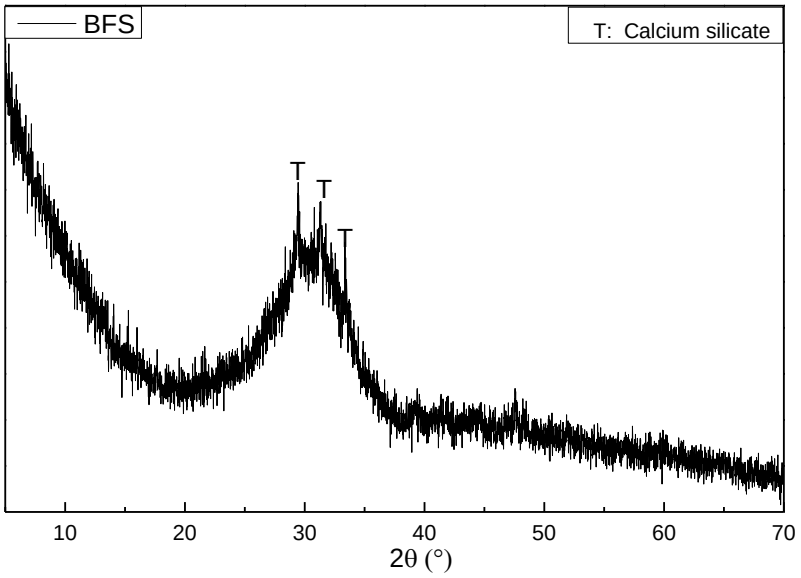

Figure 2.2.7. XRD pattern of BFS

Table 2.2.9. Chemical composition of BFS (%)

Components	CaO	SiO_2	Al_2O_3	MgO	SO_3	Cl	Na_2O	K_2O
Contents	38.55	30.57	15.09	9.56	2.54	0.05	0.50	0.37

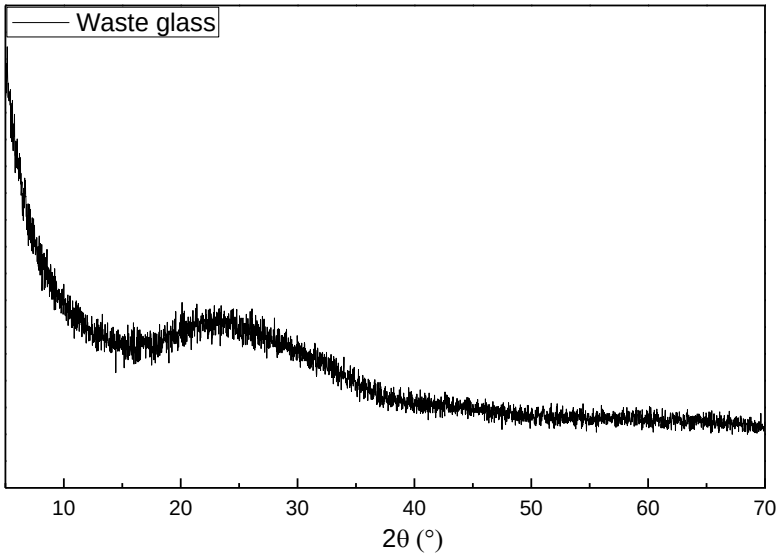

Figure 2.2.8. XRD pattern of waste glass

Table 2.2.10. Chemical composition of waste glass (%)

Components	SiO_2	CaO	Na_2O	Al_2O_3	K_2O	SO_3	Cl
Contents	70.62	8.65	14.4	0.86	0.51	0.60	0.06

2.2.3. Alkaline activators

Sodium hydroxide (NaOH) and sodium silicate (Na_2SiO_3) with reagent grade ACS were used as alkaline activators in the alkaline activation process. In the life cycle assessment for alkaline activation reaction, the utilization of hydroxide and silicate contributes the highest CO_2 footprint in most life cycle categories (Tian et al., 2020e), and is also associated with high cost (J. Wang et al., 2018). Therefore, we attempted to seek a waste-derived alkaline activator for sustainable development and achieve co-disposal. Spent caustic is an industrial byproduct during petrochemical production, which is of high alkalinity (pH > 12) due to it contains a high content of NaOH (5-12 wt%) and $NaCO_3$ (1-10 wt%) (Ntagia et al., 2019; Yuan et al., 2020). It has been reported that the mixture of sodium hydroxide (NaOH) and carbonate (Na_2CO_3) effectively alkali-activated blast furnace slag (BFS) (Jiao et al., 2019, 2018). Considering spent caustic abundance in sodium hydroxide and carbonate, we hypothesized that it could be employed as an emerging alkaline activator in alkaline activation fields. The inorganic composition and organics in spent caustic measured by inductively coupled plasma spectrometer (ICP, Prodigy 7, China) and gas chromatography-mass spectrometry (GC/MS, Q Exactive Plus-Easy - nLC 1000/Q), respectively. The alkalinity of the spent caustic was measured with the HCl titration model (Metrohm 907 Titrando, Switzerland). In brief, 20 mL spent caustic was titrated with 1M HCl until pH=7. The alkalinity was calculated with Eq. [2.2.1].

$$C_{\mathrm{SC}}V_{\mathrm{SC}} = C_{HCl}V_{HCl} \qquad [2.2.1]$$

where C_{SC} is the alkaline concentration of spent caustic, mol/L; V_{SC} is the volume of spent caustic, L; C_{HCl} is the concentration of HCl, mol/L; V_{HCl} is the volume of HCl, L.

Table 2.2.11 shows the inorganic composition in spent caustic. The dominant elements in spent caustic are sodium (Na) and sulfur (S). This is attributed to soda caustic was applied to absorb H_2S

gas in the refinery process (Alipour and Azari, 2020). Characterized by ion chromatography, sulfur exists mainly in the form of sulfate in the spent caustic (did not show here). The organics in spent caustic are shown in Figure 2.2.9. As can be seen, massive organics appeared in spent caustic. This is consistent with Ellis (1998).

Table 2.2.11. Inorganic composition in spent caustic (mg/L)

Components	Na	S	B	K	Mn	Si	Al
Concentration	141180 ± 4427	15940 ± 1241	1660 ± 239	1170 + 53	430 ± 52	65 ± 32	90 ± 21

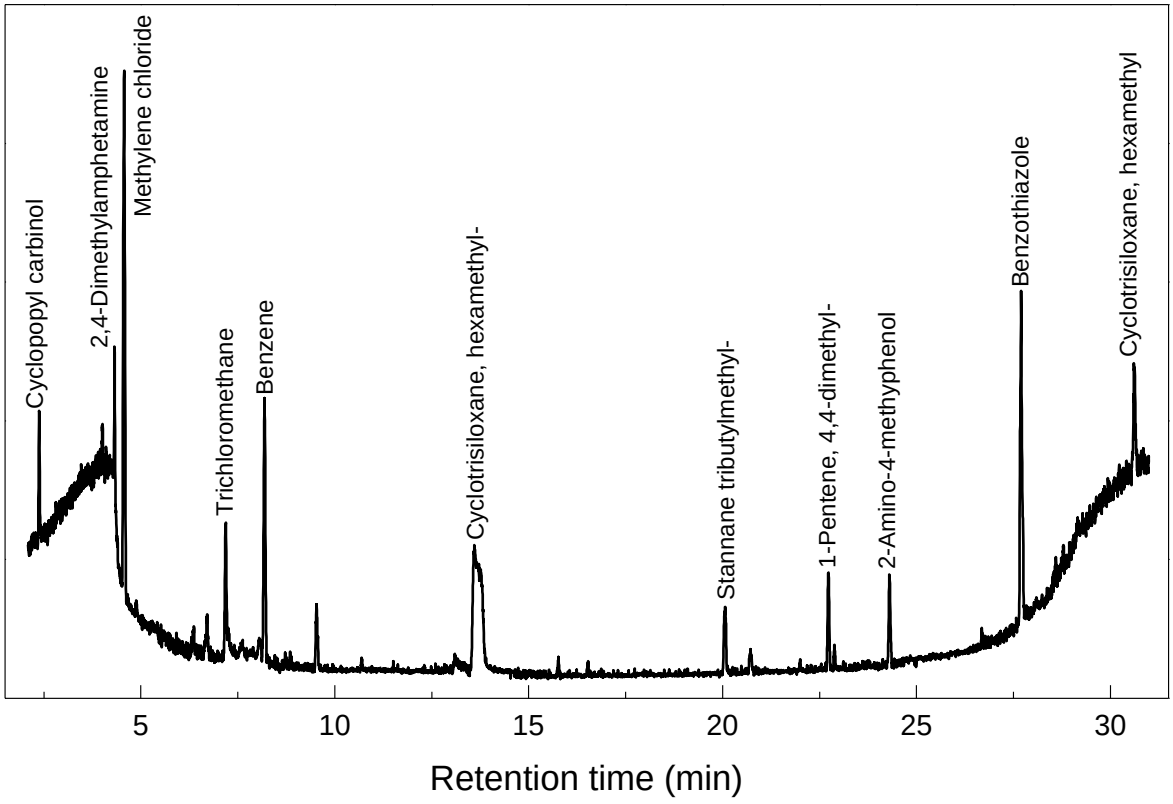

Figure 2.2.9. GC/MS analysis of spent caustic

Figure 2.2.10 shows the alkalinity titration of spent caustic. The pH value of spent caustic is increased in the initial three hours. This may be because spent caustic contains substantial content of organics that causes it to present a thick solution and hinders the contact of free hydrogen ions

with the detector. With the titration process proceeding, the added HCl solution dilutes the spent caustic and promotes the mobility of ions, leading to a slight increase in pH from 10.3 to 12.0. Then, the pH value decreased gradually until the pH around 11. After that, the pH decreases sharply to 7. The final titration volume of 1 M HCl solution reached 88.32 mL when pH value reached 7. Based on Eq. (2.2.1), the alkalinity of the spent caustic is equivalent to 4.416M NaOH solution. However, the pH value of spent caustic rarely exceeds 12. Based on the component of spent caustic in table 3, it is reasonable to conclude that the major component in spent caustic is Na_2CO_3. This data well agree with the study that the dominant compositions are NaOH and Na_2CO_3 in spent caustic (Yuan et al., 2020).

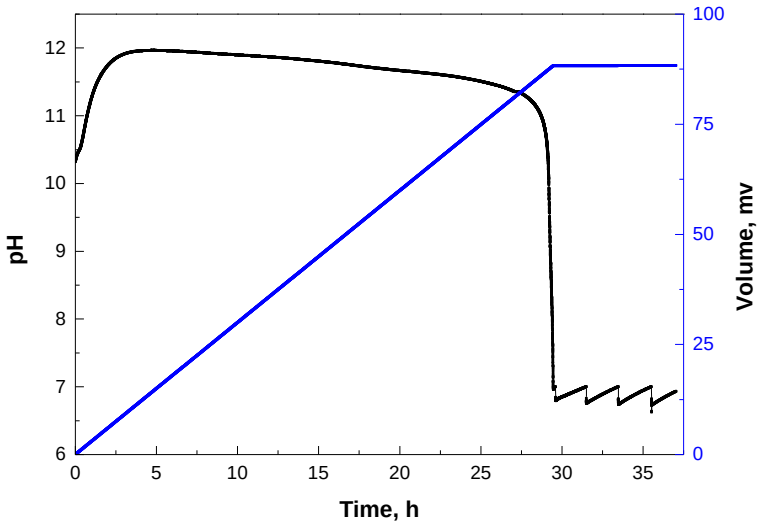

Figure 2.2.10. Alkaline titration of spent caustic

2.3. Synthesis

In studying the optimization of the synthesis process to remove the expansion, the MSWI fly ash was collected from Shenzhen. Table 2.3.1 gave the preparation regime of the alkali-activated MSWI fly ash-based pastes through baseline and optimized processes. In a typical baseline synthesis, 0.5 mol NaOH and 0.5 mol Na_2SiO_3 were dissolved in 10 mol H_2O to prepare the alkaline activator solution. Then, the solution was mixed with the raw materials of MSWI fly ash and CFA. The mixture was poured into a cubic steel mold (50 mm × 50 mm × 50 mm) and vibrated on a

vibration table for 3 min to liberate the gas bubbles. After that, the mold was sealed for the curing process, in which it was first cured at 60 °C for 6 h and subsequently cured at room temperature for 7 d. The variables in the baseline syntheses were the contents of CFA in the raw materials, namely 10% to 50% for specimens No. 1-5 and 100% for specimen No. 6. In the optimized syntheses, MSWI fly ash was first mixed with the NaOH solution for 24 h, then, the CFA and Na_2SiO_3 were added. After that, the mixture was molded, vibrated and cured by using the same conditions as in baseline syntheses to obtain the pastes. In order to study the effect of NaOH, 0.6-0.8 mol NaOH (specimens No. 7-9) were used in the optimized syntheses.

Table 2.3.1. Preparation regime of the alkali-activated MSWI fly ash-based pastes through baseline and optimized processes

No.	Process	MSWI fly ash	CFA	NaOH	Na_2SiO_3	H_2O
1	Baseline and optimized	90%	10%	0.5mol	0.5mol	10mol
2		80%	20%			
3		70%	30%			
4		60%	40%			
5		50%	50%			
6	baseline	0	100%			
7	optimized	90%	10%	0.6mol		
8				0.7mol		
9				0.8mol		

In investigating the effects of aluminum dosage on gel formation and heave metals immobilization, the MSWI fly ash was collected from Shenzhen. Table 2.3.2 showed the composition of the preparation of the alkali-activated MSWI fly ash-based pastes. In order to prevent the expansion of the pastes caused by metallic aluminum contained the MSWI fly ash, it was first dissolved in a given NaOH solution and then stirred for 24 h. The silica fume was added and the mixture was molded in the following dimension: 30 mm × 30 mm × 30 mm. The mold was vibrated on a vibration board for 3 min to liberate the bubbles. Subsequently, it was sealed for the curing process

and first cured at 60℃ for 6 h and continued at room temperature for 7 days. During the synthesis process, a total of 220 g raw materials, 0.6 mol NaOH and 10 mol water were used. The variable proportion of silica fume to metakaolin was used.

In studying the influence of waste glass on the immobilization effect of heavy metals, the MSWI fly ash was collected from Chongqing. Table 2.3.3 gives the synthesis formula of alkali-activated MSWI fly ash-based pastes. In the synthesis process, a pre-stirring method was used to eliminate the expansion of pastes caused by metallic aluminum in MSWI fly ash in the alkaline activation process, as described in 2.3.1. A total of 222 g of raw materials containing MSWI fly ash and WA were used throughout the study. The alkaline activator was prepared using 1 mol NaOH dissolved in 6.5 mol H_2O, and was allowed to cool down to room temperature before use it. For the synthesis of No. 1-6, the variation was the ratio of MSWI fly ash to WA. The alkaline activator was firstly mixed with MSWI fly ash, stirring for 24 h, followed by the WA addition, stirring for 10 minutes. Then, the mixture was molded in cubic steel (50 mm × 50 mm × 50 mm) and sealed for the curing process, in which it was firstly cured at 50 ℃ for 5 h and continued at ambient temperature for 7d. To investigate the heavy metals immobilization mechanism, $Cd(NO_3)_2$ and $Pb(NO_3)_2$ was added with the ratio of 2% to the total mass of raw materials (222g), respectively (No. 7 and 8).

Table 2.3.2. The composition of the prepared alkali-activated MSWI fly ash-based pastes

MSWI fly ash (wt%)	Silica fume (wt%)	Metakaolin (wt%)	NaOH	Si/Al	Na/Al
80%	20%	0	0.6 mol	29.78	28.55
	15%	5%		13.25	7.52
	10%	10%		3.72	4.33
	5%	15%		2.34	3.04
	0	20%		1.59	2.34

Table 2.3.3. The synthesis formula of alkali-activated MSWI fly ash-based pastes

No.	MSWI fly ash	Waste glass	NaOH	Water	$Cd(NO_3)_2$	$Pb(NO_3)_2$
1	90%	10%	1 mol	6.5 mol	0	0
2	80%	20%				
3	70%	30%				
4	60%	40%				
5	50%	50%				
6	40%	60%				
7	60%	40%			2%	
8	60%	40%				2%

In investigating the co-disposal of MSWI fly ash and spent caustic, the MSWI fly ash was collected from Wuhan. Table 2.3.4 gives the synthesis regime of alkali-activated MSWI fly ash pastes. In the synthesis process, a total of 180 g of raw materials containing MSWI fly ash and BFS were used. Spent caustic was employed as an alkaline activator, and NaOH solution with comparable alkalinity with spent caustic (4.416M) was employed as a control alkaline activator. To meet the workability, 90 mL for both alkaline activators was employed throughout the synthesis process. In the synthesis of alkali-activated pastes, BFS was selected to adjust silicon and aluminum content. The synthesis procedure details as follows: The alkaline activator was mixed with MSWI fly ash and BFS, stirring for 10 min. The mixture was then molded in cubic steel (50 mm × 50 mm × 50 mm) and vibrated until liberating the gas bubbles. After that, the mold was sealed and cured at room temperature for 28 d. In subsequent expression, two abbreviates, “X-spent caustic-pastes” and “X-NaOH-pastes,” were used, where X denotes the content of BFS, and “spent caustic” and “NaOH” denote alkaline activator used. For example, “30-spent caustic-pastes” denotes alkali-activated MSWI fly ash-based pastes synthesized with 30 wt% BFS and spent caustic as the alkaline activator.

Table 2.3.4. Synthesis regime of alkali-activated MSWI fly ash pastes

Matrices	MSWI fly ash	BFS	Spent caustic	NaOH solution (4.416M)
30-spent caustic-pastes	70%	30%	90ml	
40-spent caustic- pastes	60%	40%		
50-spent caustic- pastes	50%	50%		
30-NaOH- pastes	70%	30%		90ml
40-NaOH- pastes	60%	40%		
50-NaOH- pastes	50%	50%		

2.4. Characterizations

In studying the optimization of the synthesis process to remove the expansion, the alkali-activated MSWI fly ash-based pastes were characterized by scanning electron microscopy (SEM, JEOL JSM-5610LV) for the morphology, by X-ray diffraction (XRD, Bruker D8) and Fourier transform infrared spectroscopy (FTIR, Nexus JSM-5610) for the microstructure, and by the mechanical tester (Hangzhou Xingo Technology, EHC-1300) for the compressive strength. Pastes were grounded and dried to prepare specimens for FTIR measurements, in which 1 mg specimens mixed with 200 mg potassium bromide (KBr), and the mixture then was pressed into a disk. For XRD measurements, the specimens were milled less than 75 μm. Block specimens (size less than 1cm × 2cm × 1cm) for SEM analysis were coated copper before dried. In measurements of the compressive strength, three pastes prepared with the same regime were tested and the average value was presented. In order to understand the chemical reactions in the optimized synthesizing process, its first step was repeated using the same dosages of MSWI fly ash and NaOH. Then, the release of gas was characterized by gas chromatography analysis. Gas chromatography was performed at room temperature of column, with molecular sieve (5A, 13X) as stationary phase, argon as a carrier gas and thermal conductivity detector (TCD). The expansion of the pastes was measured by the hydrostatic balance method (Lura and Jensen, 2007). The detail was shown as follows:

Figure 2.4.1 showed the hydrostatic weighing set-up for volumetric measurement. Based on the expansion characteristics of the alkali-activated MSWI fly ash-based pastes, the volumetric change of pastes after 24 h after mixing was measured by the hydrostatic balance method, whose theory are shown as follows.

According to the Archimedes principle, an object immersed in liquid (or gas) is subjected to upward buoyancy, and the magnitude of the buoyancy is equal to the gravity of the liquid discharged by the object.

$$F = G = \rho g V \qquad [2.4.1]$$

Where F (N) is the buoyancy of the object; G (N) is the weight of the liquid discharged; V (cm^3) is the volume of the liquid discharged by the object, i.e., the volume occupied by the object; ρ (g/cm^3) is the density of the liquid.

The buoyancy of the sample is the difference between the weight of the sample (m_0) and the reading of the balance when the sample (m_i) was placed in water.

$$F = G = \rho(m_0 - m_i)g \qquad [2.4.2]$$

When liquid is water (ρ=1g/cm^3):

$$V = m_0 - m_i \qquad [2.4.3]$$

The initial volume of the specimen is $V_0 = m_0 - m_1$, and after 24 hours, the volume of the sample specimen is $V_i = m_0 - m_i$, and the volume expansion ratio is:

$$W_i = \frac{V_i - V_0}{V_0} \times 100\% = \frac{(m_0 - m_i) - (m_0 - m_1)}{m_0 - m_1} \times 100\% = \frac{m_1 - m_i}{m_0 - m_1} \times 100\% \qquad [2.4.4]$$

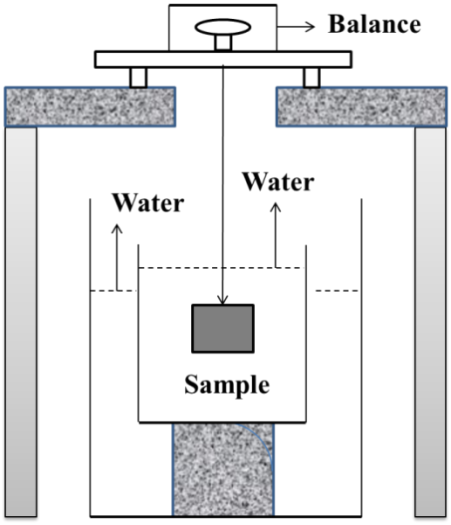

Figure 2.4.1. Hydrostatic weighing set-up for volumetric measurement

In investigating the effects of aluminum dosage on gel formation and heave metals immobilization, the alkali-activated MSWI fly ash-based pastes were characterized by the X-ray diffraction (XRD, Empyrean, Netherlands) technique to determine the existing phase and phase transformation. Pastes were grounded less than 75 mm to prepare specimens for XRD measurements, in which $CuKa_1$ radiation and a scanning rate of 0.1°/s from 5 to 80º of 2θ was used. The scanning electron microscope (SEM, /JEM-2100F, China) was used to observe the morphology of the prepared pastes. ^{29}Si NMR spectra of the pastes were obtained by using an NMR spectroscopy (Bruker AVANCE III, China). Powdered paste specimens were packed into 7 mm ZrO_2 rotors. Spectra were acquired at spinning speeds of 5 kHz with peak positions referenced to an external standard of tetramethylsilane (TMS) and recorded with 5 seconds delay time. The excitation pulse for ^{29}Si was 6 μs with a recycle time of 5 seconds. The pastes were subjected to the compressive strength test by the mechanical tester. The observed compressive strength was reported as the average result of three specimens with a variation of not more than 10%. The leaching test was conducted to examine the leaching of heavy metals from MSWI fly ash according to Toxicity Characteristic Leaching Procedure (TCLP) tests (Q. Wan et al., 2018). The extraction liquid was prepared by dissolving 5.7 mL of acetic acid in 1 L of deionized water. The pastes were grounded into powder form with a size of less than 48 μm. In a polyethylene container, the extraction liquid and the powder were

mixed at a L/S ratio of 20:1, followed by stirring for 20 h. Then, the leachate was separated by centrifugation and filtration. And, the concentration of heavy metals in the leachate was determined by an inductively coupled plasma spectrometer (ICP, Prodigy 7, China). In order to illustrate the bond state of the different metallic ion to balance negative charge related to Al(III) in N-A-S-H gel, molecular modeling and simulation were used to calculate the binding energy related to the charge-balanced ion. The N-A-S-H structure was built through the Amorphous Cell module in Materials Studio software (Wan et al., 2017c). Figure 2.4.2 showed the model of N-A-S-H gel with different charge-balanced ions, where each Si or Al atom had 4 bonded oxygen neighbors. The model was geometrically optimized using density functional theory (DFT). For energy calculation, all the first-principles calculations of this subject were based on the DMol^3 package in Materials Studio by employing the plane-wave pseudopotential method (Kupwade-patil et al., 2013). The self-consistent field (SCF) convergence condition was set to 1.0×10^{-5} eV. The tolerance offset was less than 0.004 Å and the force on each atom was less than 0.01 eV/Å. The binding energy relative to charge-balanced ion was calculated as follows:

$$E_{\text{charge-bananced ion}} = E_{\text{atom}} + E_{\text{oligomer-atom}} - E_{\text{oligomer}} \qquad [2.4.5]$$

Where, E_{atom} was the binding energy relative to one charge-balanced atom. $E_{oligomer\text{-}atom}$ was the total energy of oligomer gel without charge-balanced ion and $E_{oligomer}$ was the total energy of oligomer after incorporating charge-balanced ion.

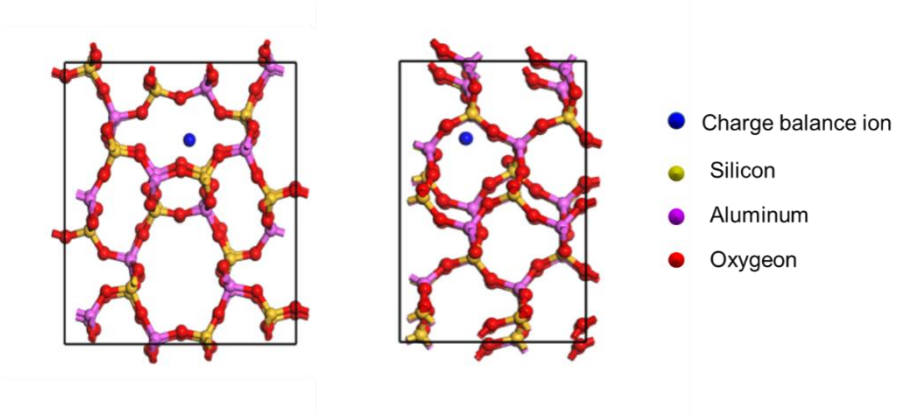

Figure 2.4.2. The model of N-A-S-H gel along with the incorporation of different charge-balanced ion including Na, Pb, Cd, Cu, and Zn

In studying the influence of waste glass on the immobilization effect of heavy metals, the compressive strength of alkali-activated MSWI fly ash pastes was determined by the mechanical tester (EHC-1300, China). The microstructure of pastes was characterized by X-ray diffraction (XRD, Empyrean, Netherlands), scanning electron microscope (SEM, /JEM-2100F, China) and nuclear magnetic resonance spectroscopy (NMR, Bruker AVANCE III, China). The leaching of heavy metals in pastes was assessed by the Chinese Ministry of Environmental Protection Standard HJ/T 300–2007 (Yi et al., 2019), in which 17.25 mL acetic acid was dissolved in 1l distilled water as extraction solution; then the pastes powder with the size under 48 μm was mixed with extraction solution at a ratio of 1:20; followed by stirring 20 h; after that, the eluates were filtered through 0.45 μm filter membranes, and then the concentration of heavy metals was determined by ICP. The immobilization efficiency of heavy metals was calculated by Eq. [2.4.6]. The backscattered electron (BSE/EDS) microscopy and X-ray photoelectron spectroscopy (XPS) were carried out to explore the immobilization form of heavy metals.

$$Immobilization\ efficiency\ (\%) = (C_r - C_l)/C_r * 100 \qquad [2.4.6]$$

where C_r is the amount of heavy metals leached out from raw MSWI fly ash. C_l is the amount of heavy metals leached out from pastes specimen.

In investigating the co-disposal of MSWI fly ash and spent caustic, the alkali-activated MSWI fly ash-based pastes were characterized by X-ray diffraction (XRD, Empyrean, Netherlands) technique, in which pastes were grounded less than 75 mm to prepare specimens for XRD measurements, and $CuKa_1$ radiation and a scanning rate of 0.1°/s from 5 to 70º of 2θ was used. In Fourier transform infrared spectroscopy (FTIR, Nexus JSM-5610) measurement, 1 mg specimens mixed with 200 mg potassium bromide (KBr). and the mixture then was pressed into disk. ^{29}Si NMR spectra of pastes were obtained by using an NMR spectroscopy (Bruker AVANCE III, China). Powdered paste specimens were packed into 7 mm ZrO_2 rotors. Spectra were acquired at spinning speeds of 5 kHz with peak positions referenced to an external standard of tetramethylsilane (TMS) and recorded with 5 seconds delay time. The excitation pulse for ^{29}Si was 6 μs with a recycle time of 5 seconds. The scanning electron microscope (SEM, /JEM-2100F, China) was used to observe the morphology of pastes. The pastes were subjected to the compressive strength test by the mechanical

tester. The compressive strength was reported as the average result of three specimens with a variation of not more than 10%. The immobilization effect of heavy metals in the pastes was assessed by Chinese Ministry of Environmental Protection Standard HJ/T 300–2007 (Ye et al., 2016a; Zhan et al., 2018). This standard is far more aggressive than the toxicity characteristic leaching procedure (TCLP) set by the United States Environmental Protection Agency (USEPA). In the former, the extraction liquid was prepared using 1 L distilled water and 17.25 mL acetic acid, whereas, in the latter, only 5.7 mL acetic acid was used. Considering the MSWI fly ash and its solidified matrices are of high alkalinity, we chose the former leaching standard. Firstly, the pastes were milled into powder with a sized under 48 μm. Then the powder mixed with extraction liquid with a solid to liquid ratio of 1:20, followed by stirring for 20 h. After that, the eluates were filtered through 0.45 μm filter membranes, and then the concentration of heavy metals was determined by ICP. The Cr (VI) concentration in eluates was measured by UV-vis spectrophotometer (UV-Orion AquaMate 8000, USA). When calculating the immobilization efficiency, the inert fraction of heavy metals did not be considered. The immobilization efficiency of each heavy metal is calculated using Eq. [2.4.7]:

$$\text{Immobilization efficiency (\%)} = (1 - \frac{C_L}{C_M} \times \frac{m_T}{m_M}) * 100 \qquad [2.4.7]$$

where C_L is the leaching concentration of heavy metals in pastes, mg/L; C_M is the leaching concentration of heavy metals in raw MSWI fly ash, mg/L; m_T is the mass of pastes, g; m_M is the mass of MSWI fly ash contained in paste, g.

BCR chemical speciation analysis is an effective method to determine the chemical speciation，through which we can understand whether heavy metals are harmful to the environment. The extraction procedure was shown in Table 2.4.1. The water-soluble and exchangeable fractions are easily leaching in a natural environment; Reducible and oxidizable fractions are available in reducing and oxidizing environment, respectively; and the residual fraction is unavailable for leaching (Chandler et al., 1997).

Table 2.4.1. BCR chemical speciation analysis of heavy metals

Stage	Fraction	Reagents/1g sample	Shaking time and temperature
1	Water-soluble	40 ml H_2O (pH=4.8)	16 h at 25 ℃
2	Exchangeable	40 ml 0.1 M CH_3COOH	16 h at 25 ℃
3	Reducible	40 ml 0.1M $HONH_3Cl$	16 h at 25 ℃
4	Oxidizable	10 ml 30% H_2O_2	1 h at 85 ℃
5	Residual	20 ml HF (evaporation)	8h at 90 ℃

The spent caustic contains large amounts of organics, and the pastes synthesized with spent caustic would be landfilled underground. Therefore the environmental influence of organics should be considered. The Chinese Ministry of Environmental Protection Standard HJ/T 300–2007, which was also applied to the identification of leaching toxicity of organics in solid waste and its reuse products. The test procedures are the same as in the measurement of heavy metals. However, to prevent the volatilization of organics, all the procedures were conducted in a zero-headspace extraction vessel (ZHE), the specific operation was described as in Karamalidis and Voudrias (2007). The qualitative analysis of organics in spent caustic and eluate of paste was conducted by gas chromatography-mass spectrometry (GC/MS, Q Exactive Plus – nLC 1000/Q). The quantified analysis was conducted by measuring the total organic carbon (TOC), in which the TOC of the extraction liquid, spent caustic, raw MSWI fly eluate and spent caustic-pastes eluate were measured. The TOC of raw MSWI fly ash eluate and spent caustic-pastes eluate consist of two parts: (1)TOC of extraction liquid, and (2) TOC contributed by MSWI fly ash and pastes. Therefore, the TOC of MSWI fly ash eluate contributed by MSWI fly ash and spent-caustic pastes eluant contributed by pastes are calculated using Eqs. [2.4.8] and [2.4.9], respectively. The immobilization efficiency of organics is calculated using Eq. [2.4.10].

$$TOC_{MS} = TOC_{EMS} - TOC_{EX} \quad [2.4.8]$$

$$TOC_{MT} = TOC_{EMT} - TOC_{EX} \quad [2.4.9]$$

$$\text{Immobilization efficiency (\%)} = \left(1 - \frac{40TOC_{MT}}{40aTOC_{MS}+TOC_{SC}}\right) * 100 \quad [2.4.10]$$

where TOC_{MS} and TOC_{MT} are the TOC of MSWI fly eluant contributed by MSWI fly ash and of spent-caustic pastes eluant contributed by pastes, respectively, mg/L; TOC_{EMS}, TOC_{EMT}, TOC_{EX} and TOC_{SC} are the TOC of MSWI fly ash eluate, spent caustic-pastes eluate, extraction liquid and spent caustic, respectively, mg/L; a is the mass fraction of MSWI fly ash in paste.

CHAPTER 3.

Results and Discussion

3.1. The optimization of synthesis process to remove the expansion

Figure 3.1.1 presents the photographs of pastes synthesized with the baseline and optimized processes. The pastes synthesized with the baseline process show rough surface, cracks and faultage, but the pastes synthesized with the optimized process show smoother surface and more compact structure. The paste synthesized without MSWI fly ash but with the baseline process also shows smooth surface and compact structure. In addition, the paste synthesized with the optimized process but with high contents of MSWI fly ash (90%) shows some expansion. These results suggest that alkaline activation of the MSWI fly ash leads to the expansion and a loose structure of the pastes, which can be mitigated by using the optimized synthesizing process.

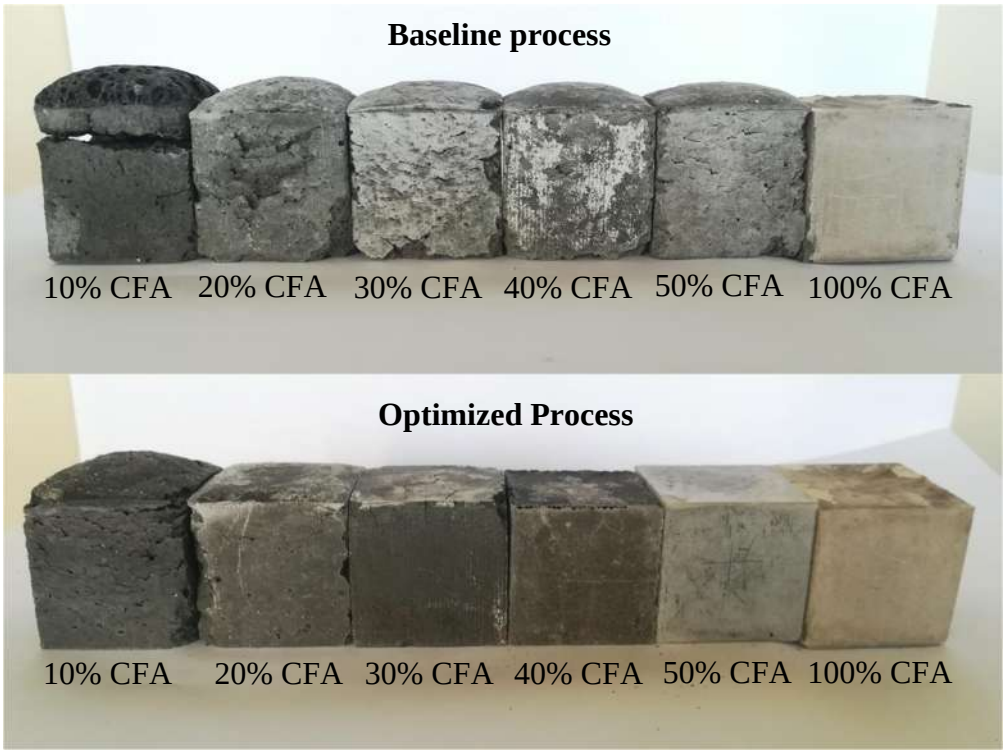

Figure 3.1.1. Photo of the pastes synthesized with the baseline and optimized processes

Figure 3.1.2 shows the expansion ratio of the alkali-activated MSWI fly ash-based pastes. With the addition of MSWI fly ash, the pastes expanded. The expansion ratios of the pastes synthesized with the baseline process increased steadily from 8.9% to 13.9% as the content of MSWI fly ash is

increased from 50% to 90%, respectively. However, the expansion ratios of the pastes synthesized with the optimized process were 0.2%, 0.2%, 0.3%, 3% and 9% as the content of MSWI fly ash is increased from 50 to 90%, respectively. This indicates that after optimizing the synthesis process, the expansion of the pastes is significantly mitigated, and little expansion is produced with MSWI fly ash additions below 70%.

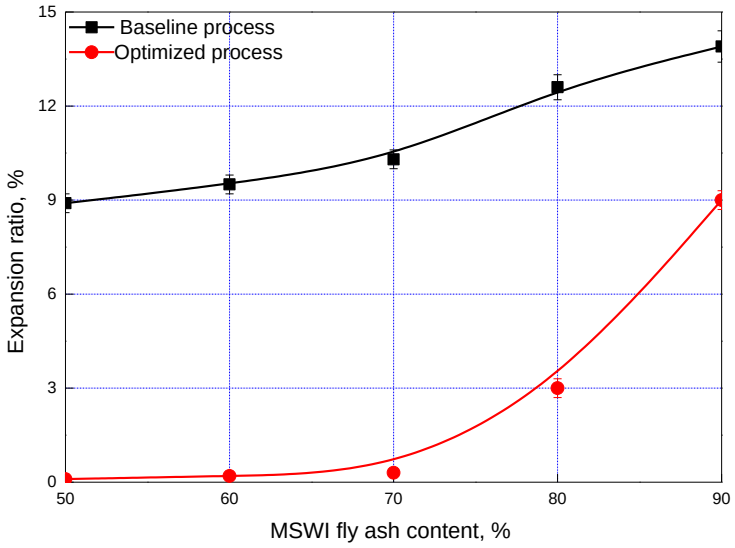

Figure 3.1.2. Expansion ratios of the alkali-activated MSWI fly ash-based pastes

Figure 3.1.3 shows the SEM images of the pastes synthesized with 70% of MSWI fly ash with the baseline and optimized processes. Pores and cracks are observed in the paste synthesized with the baseline process, while the paste synthesized with the optimized process shows homogeneous and compact structure.

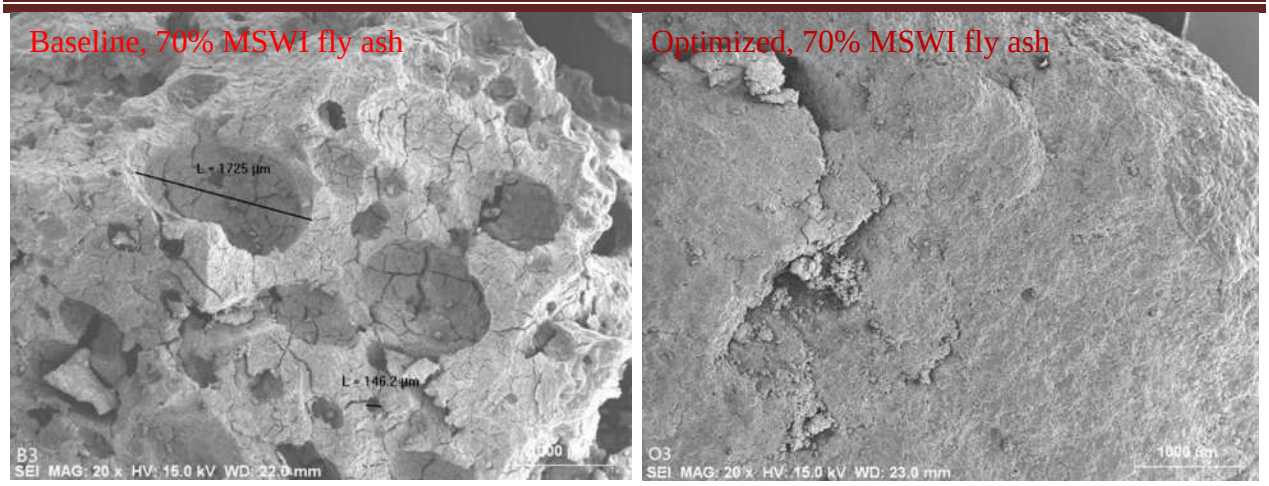

Figure 3.1.3. SEM images of the pastes synthesized with the baseline and optimized processes

Figure 3.1.4 gives the compressive strength of the pastes synthesized with varying contents of MSWI fly ash and CFA (No. 1-5). Without the addition of CFA, the MSWI fly ash was difficult to be solidified with the both processes. With the addition of CFA from 10% to 50%, the compressive strength of the pastes increased from 0.3 MPa to 1.96 MPa with the baseline process, while it increased from 1.47 MPa to 10.51 MPa with the optimized process. These results suggest that 1) the addition of CFA with main components of SiO_2 and Al_2O_3 greatly improves the solidification reactions; 2) the solidification of MSWI fly ash through alkaline activation is significantly improved after optimizing the synthesis process to prevent expansion.

The alkali-activated MSWI fly ash-based pastes synthesized differently give not only different physical properties in morphology, porous structure and mechanical strength, but also are different in the microstructures. Figure 3.1.5 presents the XRD patterns of the pastes synthesized differently, in which those of the raw MSWI fly ash and CFA are included as references. As CFA content is increased in the raw materials in both processes, CSH gel and/or geopolymer gel ($2\theta=29.3°$) are observed, indicating that alkaline activation takes place. As increasing CFA in the raw materials in both synthesizing processes, the pastes show the higher intensity of quartz (SiO_2) that comes from the added CFA. Using the same ratios of MSWI fly ash to CFA in the raw materials, the pastes synthesized through the optimized process show higher intensity in quartz (SiO_2) and anhydrite ($CaSO_4$) compared with those synthesized through the baseline process. This might be attributed

to the consumption of NaOH in the separated reaction with raw materials, resulting in lower alkalis remained for the alkaline activation.

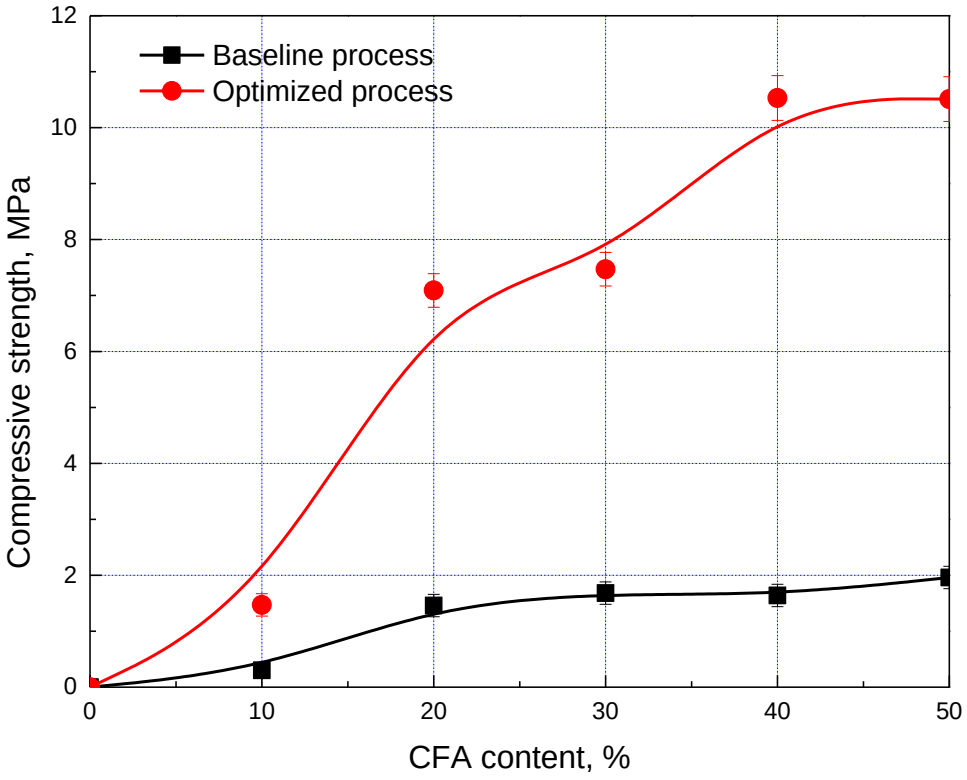

Figure 3.1.4. Compressive strength of the pastes synthesized differently as a function of CFA additions

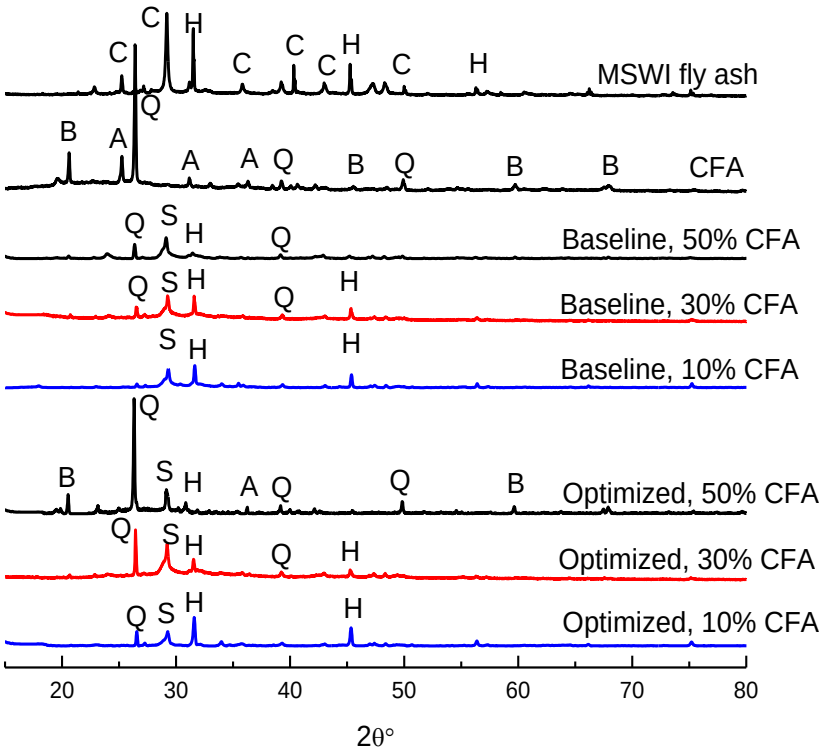

Figure 3.1.5. XRD patterns of the raw materials and the pastes synthesized differently. Q: quartz, A: anhydrite, C: calcite, B: berlinite, H: halite, S: CSH

Figure 3.1.6 presents the FTIR spectra of the pastes synthesized differently. The adsorption peak at 1640 cm^- and 1410 cm^- are attributed to the H-OH bonds of free water, and asymmetric stretching of O-C-O bonds in CO_3^{2-} groups, respectively, corresponding to the adsorbed water and carbonation during the curing process (Tang et al., 2016; Zhao et al., 2020). The peaks at 1120 cm^- and 650 cm^- are attributed to the stretching vibrations of $SO4^{2-}$ in $CaSO_4$ (Miller and Wilkins, 1952), which comes from the MSWI fly ash. The peak at 455 cm^- is attributed to the O-Si-O stretching vibration in quartz that comes from raw MSWI fly ash and CFA (Yi et al., 2019). The peak around 1000 cm^- is assigned to the asymmetric stretching vibration of Si-O-T of the geopolymer gel, where T is tetrahedral Si or Al (Wan et al., 2017b; W. Wang et al., 2018). Its intensity increases as the CFA content is increased in the raw materials, indicating some SiO_2 and Al_2O_3 in the CFA are converted into geopolymer gel. Compared with the baseline synthesis, the spectra of the pastes synthesized with the optimized process show higher intensity in geopolymer gel. This suggests that

expansion in the pastes (Figure 3.1.1 and 3.1.2) weakens the geopolymer gel formation, leading to lower compressive strength (Figure 3.1.4).

Based on previous discussions, it is revealed that the optimization of the synthesizing process through reacting the raw materials with NaOH before the addition of CFA and Na_2SiO_3 leads to the mitigation of expansion, geopolymer gel formation and high compressive strength of the pastes. Therefore, release of gas during the NaOH activation was hypothesized, and the released gas was collected and subjected to a chromatogram analysis, which is given in Fig 3.1.7. Compared to the standard gas mixture in the atmosphere (N_2, O_2 and CO_2), H_2 was observed in the chromatogram. The H_2 might be released by NaOH activation of metallic aluminum in the MSWI fly ash as noted in equations [1.4.1] and [1.4.2], which is in agreement with the results of other studies (Xuan and Poon, 2018).

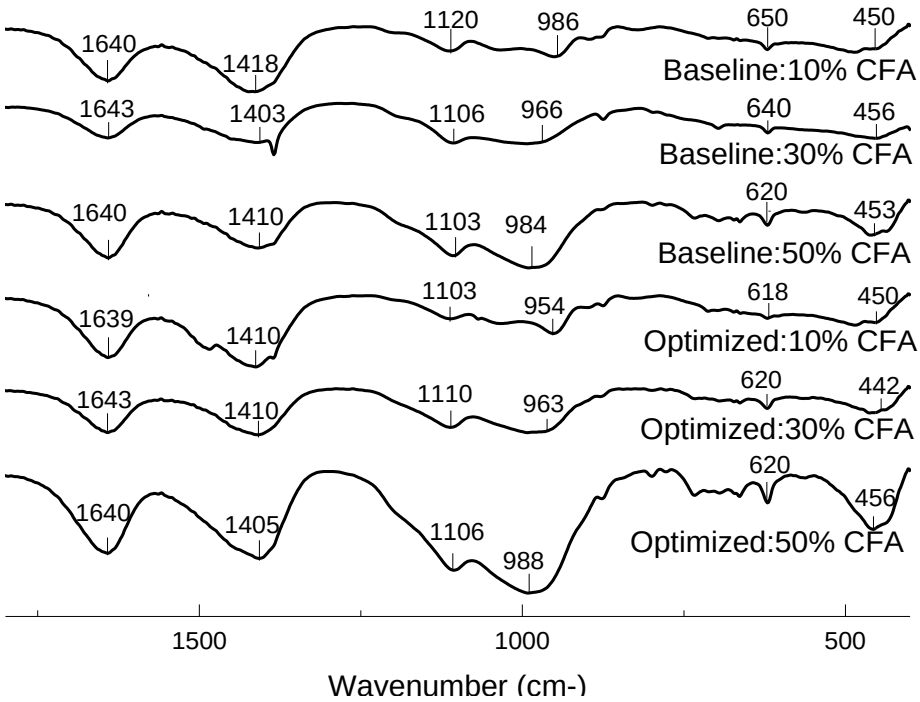

Figure 3.1.6. FTIR spectra of the MSWI fly ash-based pastes synthesized differently

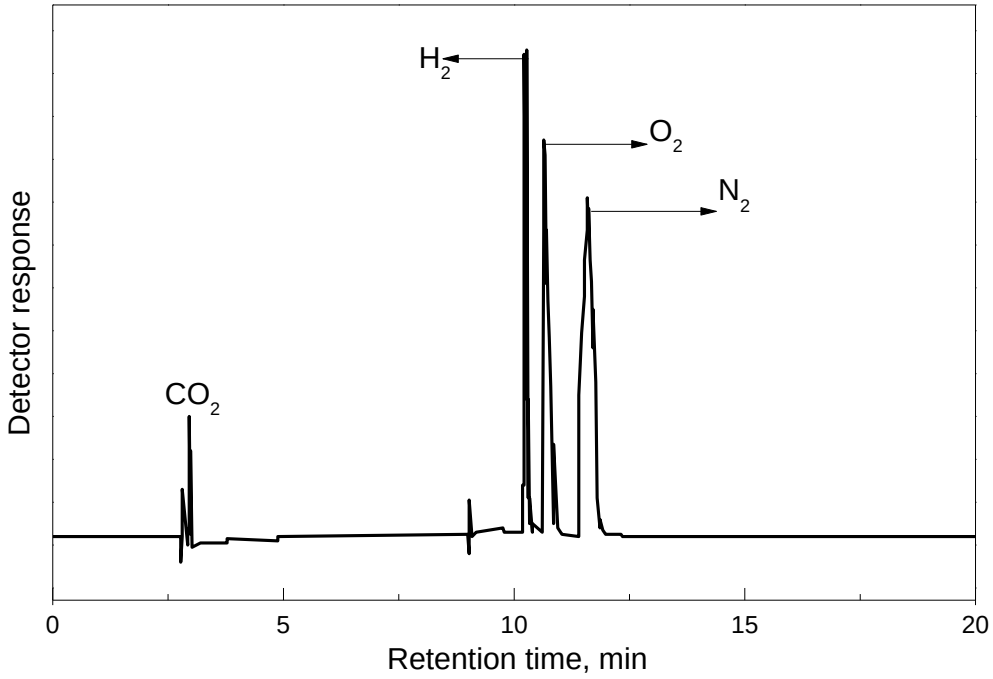

Figure 3.1.7. Chromatogram of the collected gas in NaOH activation

Furthermore, the dosage of NaOH on the hydrolysis of metallic aluminum and the formation of alkali-activated MSWI fly ash-based pastes are further examined. Figure 3.1.8 shows the pastes synthesized with 90% MSWI fly ash and 10% CFA with the optimized process as a function of NaOH dosage. As the NaOH dosage is increased from 0.5 mol to 0.8 mol, the expansion of the pastes decreased from 9% to 0.2%, and the pastes became more compact and smoother. For this raw material, a dosage of 0.7 mol NaOH was sufficient for the hydrolysis of the included metallic aluminum since the expansion in the paste decreased to the minimum of 0.2%. Therefore, according to the metallic aluminum in the raw materials, an appropriate dosage of NaOH should be tested for the hydrolysis and alkaline activation process to take place.

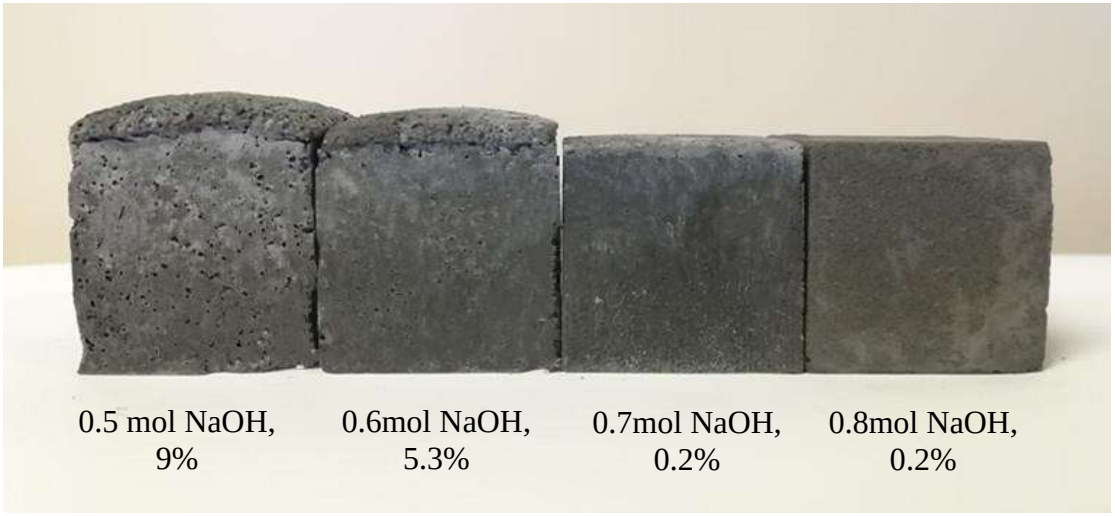

Figure 3.1.8. Photographs showing the expansion of the pastes synthesized with the optimized process as a function of NaOH dosage

3.2. The effects of aluminum dosage on gel formation and heavy metals immobilization

3.2.1. Compressive strength of pastes

Figure 3.2.1 shows the compressive strength of the alkali-activated MSWI fly ash-based pastes as a function of the proportion of metakaolin that was gradually substituted in the silica fume. The synthesized paste with a 5% metakaolin exhibited a slightly higher compressive strength (10.94 MPa) compared to pristine silica fume. However, with an increasing proportion of metakaolin from 5 % to 20 %, the compressive strength showed a sudden reduction from 10.94 to 2.15 MPa. In reference to the calculated Si/Al in Table 2.3.2, it depicted that a high-silicon source causes the increased compressive strength of alkali-activated MSWI fly ash-based pastes. In addition, a small amount of aluminum increases the compressive strength of pastes, and excess addition leads to a successive decrement of compressive strength. Thus, the exhibited result is well consistent with the earlier study based on the impact of varying aluminum in the synthesis process. A moderate addition of aluminum in the synthesis process improves the compressive strength, while resulted products exhibited low strength by incorporation of the excessive aluminum in the paste at a low SiO_2/Al_2O_3 ratio (Kouamo et al., 2012). It has been reported that a geopolymer synthesized with a ratio “2” of Si/Al possesses the optimum mechanical properties (Wan et al., 2017c). The

investigated compressive strength of the alkali-activated MSWI fly ash-based pastes is not in a similar trend with the previous research. This may be due to the component in MSWI fly ash affected the formed gel and related explanation can be discussed in-depth on the basis of XRD and ^{29}Si NMR analysis.

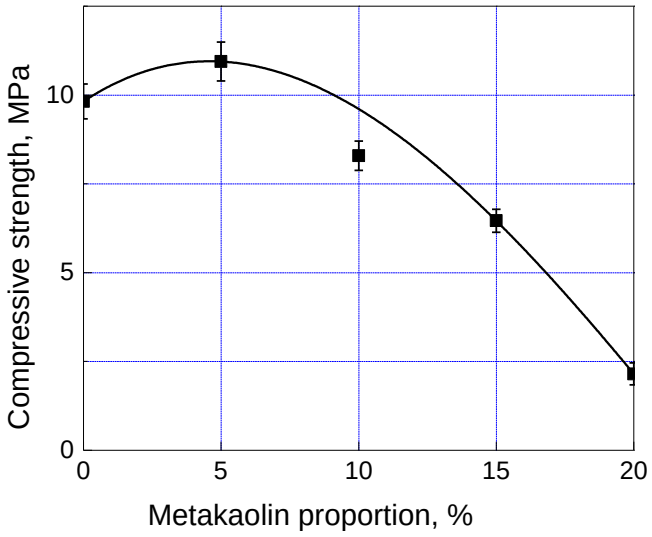

Figure 3.2.1. Compressive strength of the alkali-activated MSWI fly ash-based pastes as a function of the metakaolin proportion

3.2.2. Microstructure characterizations

Figure 3.2.2 shows the XRD patterns of the alkali-activated MSWI fly ash-based pastes synthesized with varying proportions of metakaolin. It can be seen that the major crystal phases in all the synthesized pastes are calcite ($CaCO_3$) and sodium chloride (NaCl). It suggested that calcite originated from MSWI fly ash keeps inert in the alkaline activation reaction. NaCl was formed due to a large amount of Cl^- from MSWI fly ash reacted with the added NaOH as an alkaline activator. In the alkaline activation system, Na^+ mainly exists as a charge-balanced ion that balances the negative charge caused by Al (III) substitution of Si (IV) (Wan et al., 2017c). However, in the current system due to a large amount of Cl^-, Na^+ was partially converted to NaCl. With the addition of metakaolin from 0% to 20%, the intensity of peaks at 2θ of 26.5° and 19.6° was increased, which is assigned to quartz and muscovite phase, respectively. The intensity of the strongest diffraction peak of NaCl (2θ=31.5º) was decreased gradually as compared to the adjacent calcite peak (2θ=29.2º) in the synthesized paste with increasing metakaolin fraction from 5% to 20%. There is

no Friedel's salt generated for the 5% metakaolin. This indicates that aluminum from metakaolin was completely incorporated in the tetrahedral backbone of gel (C-(A)-S-H and N-A-S-H), compensating the shortening of the backbone i.e., chain length caused by reactive silicon decreases. Thus, the increased compressive strength is attributed to the modification of gel by aluminum. With increasing metakaolin from 10% to 20%, more and more Friedel's salt was generated and to some extent consumes the aluminum source for alkaline activation reaction. This causes less amount of gel in pastes. Accordingly, the compressive strength constantly decreased as pastes synthesized with metakaolin from 10% to 20%.

$$4Ca^{2+} + 6OH^{-} + 2Cl^{-} + Al_2O_3 + 7H_2O \rightarrow 3CaO \cdot Al_2O_3 \cdot CaCl_2 \cdot 10H_2O \quad [3.2.1]$$

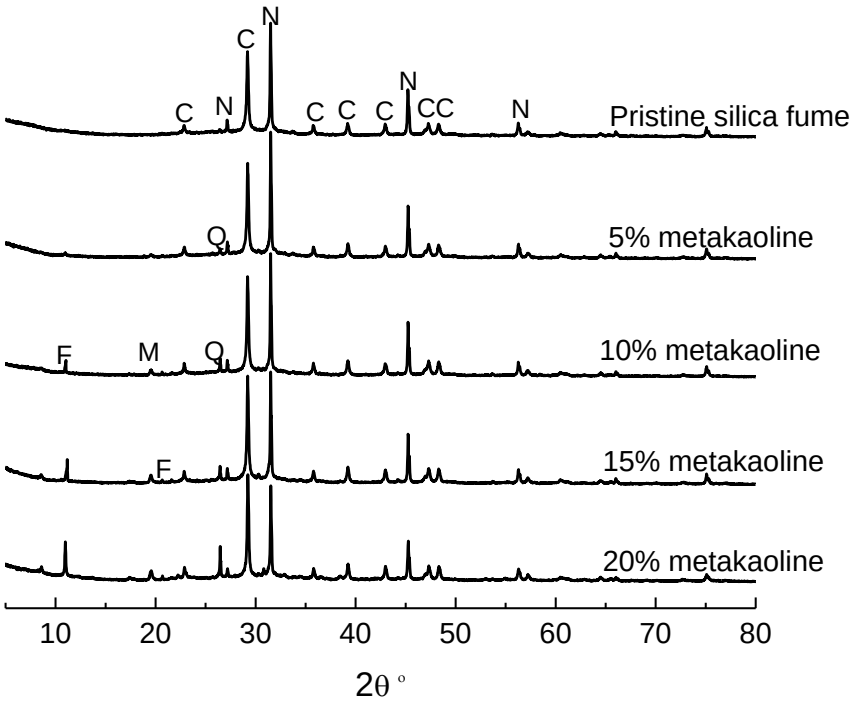

Figure 3.2.2. XRD patterns of the alkali-activated MSWI fly ash-based pastes with varying proportions of metakaolin. Here notation C: Calcite, N: NaCl, Q: quartz, M: Muscovite, F: Friedel's salt

NMR spectroscopy is commonly employed to investigate the molecular structure and short-range ordering in alkali-activated binders (Duxson et al., 2005). In the alkali-activating $(Na, K)_2O$-CaO-Al_2O_3-SiO_2-H_2O system, the major products of C-(A)-S-H and N-A-S-H gel were in coexistence

with binders (Santiago Alonso and Palomo, 2001; Criado et al., 2007). The scarcity of the spectral resolution for silicon in these binders was overcome by adopting Gaussian peak deconvolution to separate and quantify Q^n (m Al) species ($0 \leqslant m \leqslant n \leqslant 4$, m, n = integer). Where Q is a silicate tetrahedron, m is the number of tetrahedral silicon substituted by tetrahedral aluminum and n is the number of oxygen which bridge to the adjacent tetrahedra. The deconvolution of the overlapped peaks was carried out using Gaussian line shapes for quantification. Binder structures of C-(A)-S-H are non-cross linked (Q^2) and (or) less-crosslinked (Q^3) (Myers et al., 2013; Wang et al., 1995). Whereas N-A-S-H is a highly cross-linked three-dimensional structure (Q^4) consisted of tetrahedral aluminum and silicon. The component peaks and simulated spectra were given according to the assignment in the reference papers. The peak at −71 ppm is assigned to Q^0 in monomer silicate (Q. Wan et al., 2018). The peaks at -77, -82, 87.8 and 96.4 ppm are due to Q^1, Q^2 (1Al), Q^2, and Q^3 presented in the binder C-(A)-S-H, respectively (Richardson, 1999; Singh et al., 2005). In N-A-S-H gel, the Q^4 (4Al), Q^4 (3Al), Q^4 (2Al), Q^4 (1Al), Q^4 (0Al) resonate at approximately −84, −89, −93, −99, and −108 ppm, respectively (Duxson et al., 2005). The peak at -104 ppm was observed in many previous studies (Günzler and Gremlich, 2002; Olejniczak et al., 2005), which represents Q^3 (R) when H in OH is substituted by an alkali metal ion (Na^+ or K^+) in Q^3. The peaks present at values far than -110 ppm were attributed to some different crystalline silicon (Olejniczak et al., 2005).

Figure 3.2.3 depicts the ^{29}Si NMR spectra and their deconvolution of the alkali-activated MSWI fly ash-based pastes with the varying proportions of metakaolin. It should be noted that during deconvolution on the assigned peaks, peak position and width at half height were held constant. Meanwhile, the peaks of any crystalline silicon are subtracted to calculate deconvolution because they are non-reactive, supporting to probe the distribution of Si and Al atoms in the pastes associated with the gel phase via deconvolution (Kim, 2012). With the metakaolin from 0 to 20%, the percentage of tetrahedral Si coordination in C-(A)-S-H (Q^1, Q^2 (1Al), Q^2 and Q^3) was observed at 41.54%, 41.63%, 41.32%, 42%, and 41.24%, respectively. The percentage of tetrahedral Si coordination in N-A-S-H gel (Q^4(m Al), $0 \leqslant m \leqslant 4$) was 47%, 47.92%, 50.74%, 53.74%, and 53.39%, respectively. And, the percentage of Q^3(R) were 11.46%, 10.43%, 7.92%, 4.26%, and 5.38% respectively. The percentage of C-(A)-S-H was constant in pastes. This result was contradicted with an earlier study in which major products converted from C-S-H gel to N-A-S-H

gel when substitution of metakaolin in slag varied from 0% to 50% (Wan et al., 2019a). It may be due to the decrease of calcium content in the source material when the substitution of metakaolin in slag is increased. In the current study, the amount of calcium content originated from MSWI fly ash was constant and the only variable was Si/Al ratio. Accordingly, the amount of C-(A)-S-H was maintained. It is well consistent with the study that the presence of calcium content serves in the formation of C-(A)-S-H (Yip and Deventer, 2003). Additionally, at the varying proportion from 0 to 20% of metakaolin, the percentage of N-A-S-H gel was slightly increased and a corresponding reduction of the Q^3(R) was observed. This indicates Q^3(R) was converted into Q^4 with the increase of aluminum dosage, which increased the crosslinking extent. It was reported that the incorporation of aluminum in the alkaline activation system leads to crosslinked (Ferna et al., 2006). Therefore Q^3(R) may be an intermediate species from non-cross linked (Q^2) and (or) less-cross linked (Q^3) to highly-cross linked phase (Q^4). As predicted, the spectra of NMR was shifted to a higher frequency with varying proportions of metakaolin from 0 to 20%. This may be attributed to the main species of Q^4 (0Al) and Q^4 (1Al) converted into Q^4 (2Al), Q^4 (3Al), and Q^4 (4Al).The percentage of Q^4 (4Al), Q^4 (3Al) and Q^4 (2Al) were 18.06%, 30.79%, 36.22%, 43.83% and 45.28%, respectively.

The effective Si/Al ratio was calculated for the N-A-S-H gel using Eq. (3.2.1) (Engelhardt et al., 1981). The results are shown in Table 3.2.1. The effective Si/Al in N-A-S-H gel is highly inconsistent with the original Si/Al calculated through the composition of raw materials. This may be due to the uneven distribution of silicon and aluminum resources in C-(A)-S-H and N-A-S-H gel. The C-(A)-S-H gel has a limited capacity to take up Al, which is restricted by the geometry of silicate chains and the thermodynamics of ionic substitution to a maximum Al/Si ratio slightly less than 0.2 (Pardal et al., 2009; Richardson et al., 1993). This caused much lower Si/Al in N-A-S-H than that in raw materials. It was reported that geopolymer gel with a Si/Al ratio of 2 exhibited the highest compressive strength (Wan et al., 2017a), which is consistent well with the current study that pastes with an effective Si/Al ratio of 1.9 (close to 2) possesses the highest compressive strength of 10.94 MPa. This indicates that the compressive strength of pastes containing the mixture of C-(A)-S-H and N-A-S-H gel is dependent on the ratio of Si/Al in N-A-S-H gel. Further, an increasing proportion of metakaolin produced more aluminum in the reactive system, which promotes the formation of Al-rich gel with low mechanical properties (Ferna et al., 2006).

Accordingly, the compressive strength constantly decreased in the synthesized pastes with 10% to 20% proportion of metakaolin, as can be seen in Figure 3.2.1.

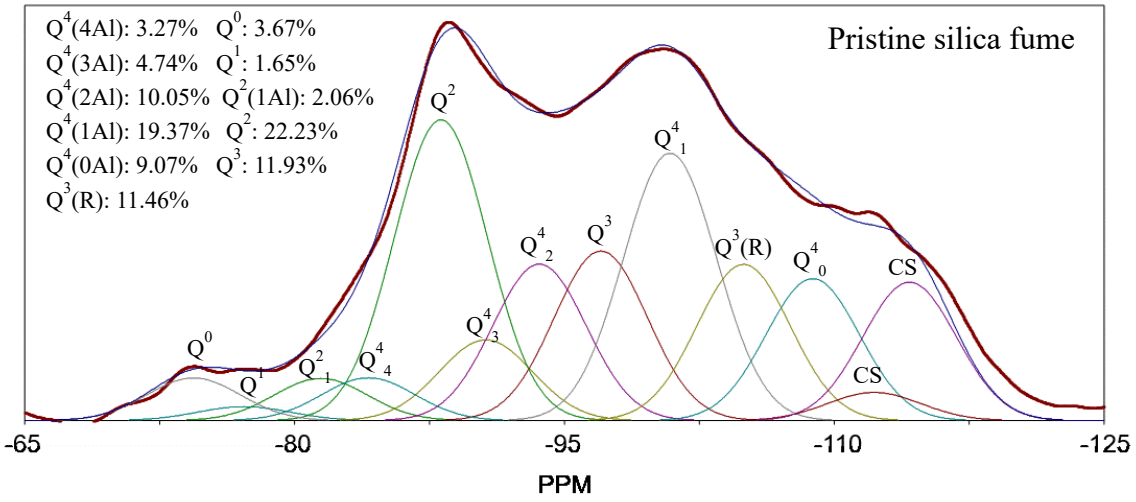

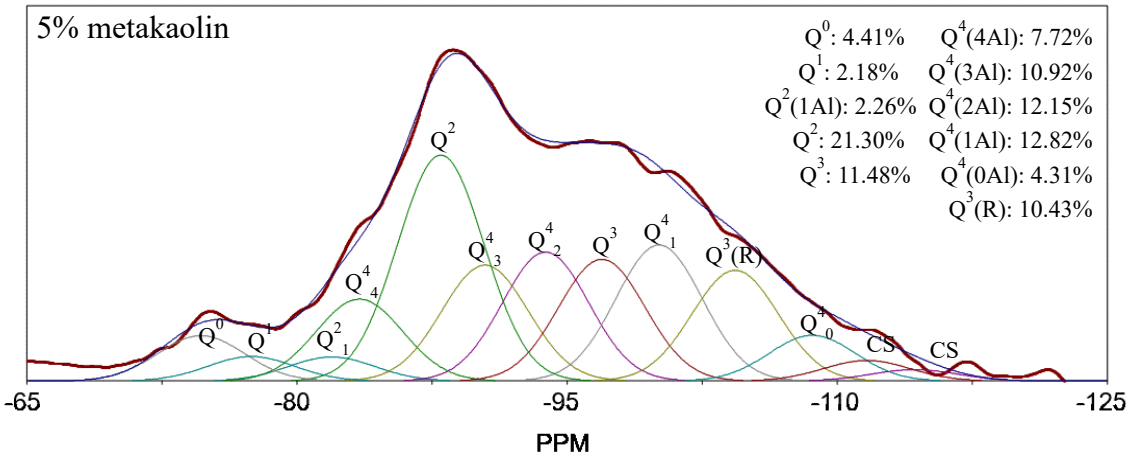

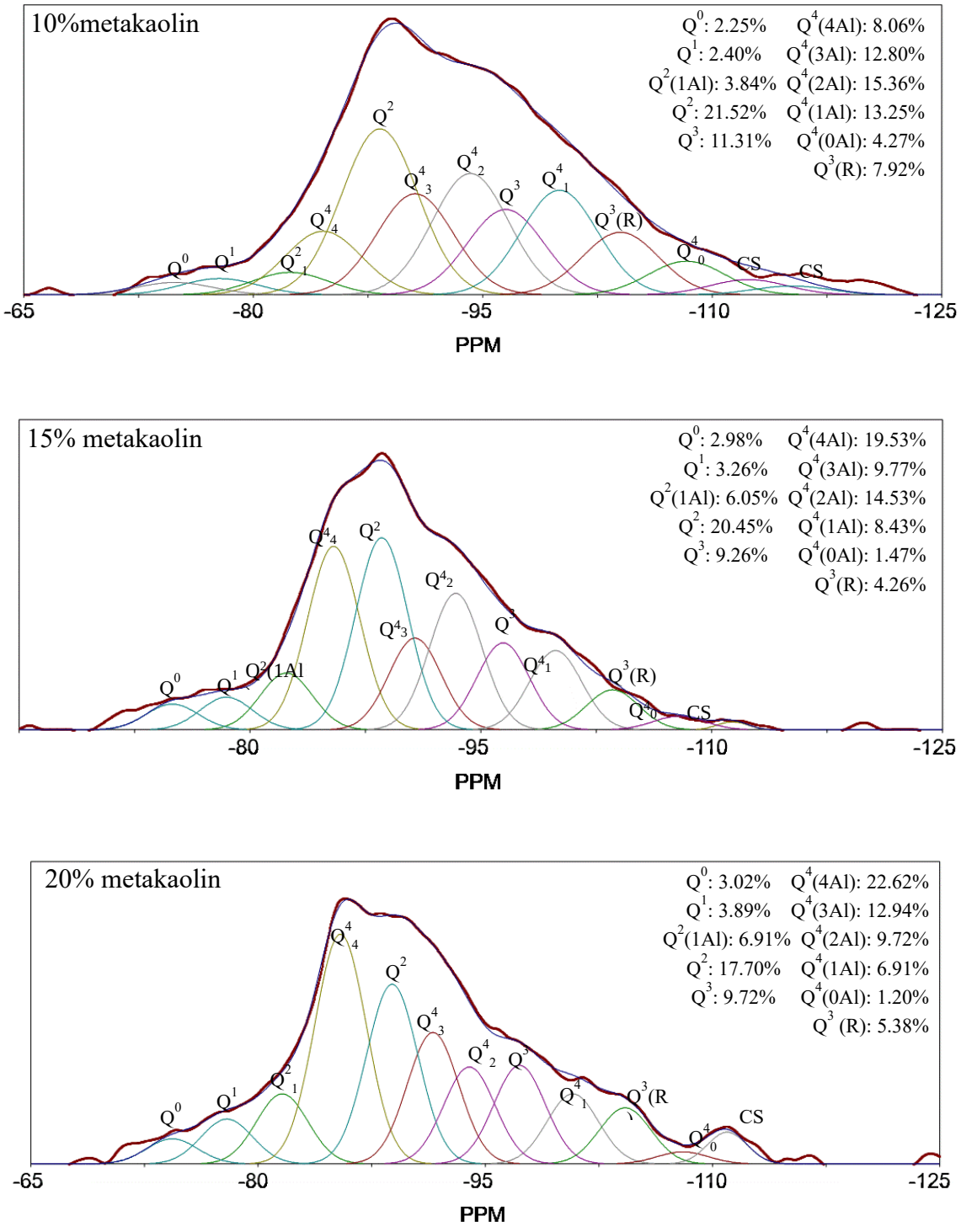

Figure 3.2.3. ^{29}Si NMR spectra and their deconvolution of alkali-activated MSWI fly ash-based pastes synthesized with varying proportions of metakaolin. (CS: crystalline silicon)

$$Si/Al = \frac{\sum_{m=0}^{4} I_{Si(mAl)}}{\sum_{m=0}^{4} \frac{m}{4} I_{Si(mAl)}} \quad [3.2.1]$$

Table 3.2.1. Effective Si/Al ratio in N-A-S-H gel

Pastes	Pristine silica fume	5% metakaolin	10% metakaolin	15% metakaolin	20% metakaolin
Si/Al	2.78	1.90	1.87	1.21	0.97

Figure 3.2.4 shows SEM images of alkali-activated MSWI fly ash-based pastes that are synthesized with varying proportions of metakaolin. As can be seen, with 0 and 5% metakaolin, the pastes show a high degree of homogeneity and compacted structure. It corresponds well with the study that silica fume promotes the formation of silicate oligomers and geopolymer gel, resulting in homogenous structures (Wan et al., 2017c). With 15% and 20% metakaolin, the pastes show a porous structure and heterogeneity. Notably, a large amount of unbridged particles were presented in the synthesized paste with a 20% proportion of metakaolin. It may be due to less formation of gel (as shown in XRD structure) and more Al-rich gel (as shown in NMR) formed in the synthesized paste with a 20% metakaolin in counterparts of pastes with 0 to 15%. Accordingly, paste synthesized with a 20% metakaolin exhibited structural discontinuity with the presence of a large number of unreactive particles.

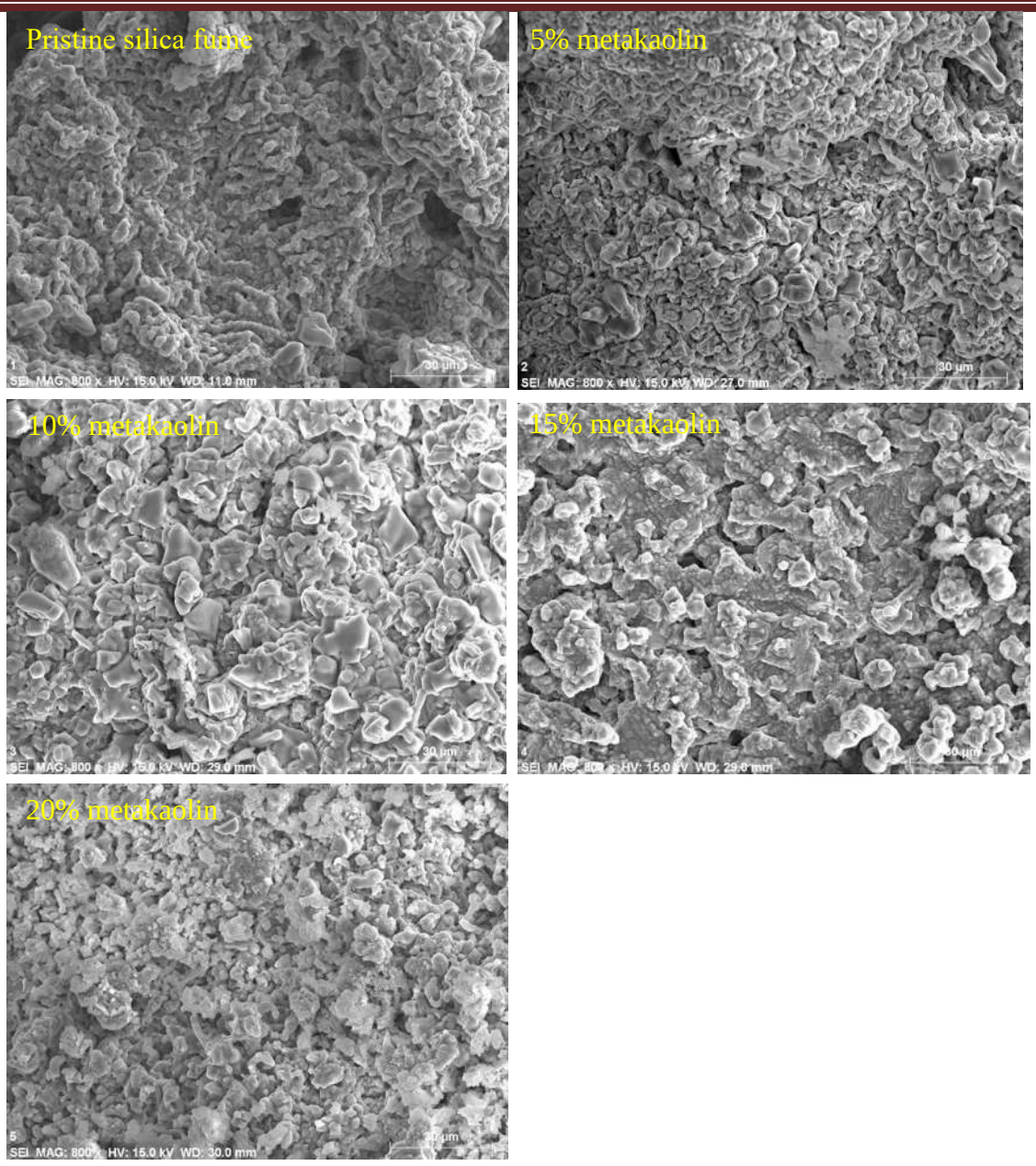

Figure 3.2.4. SEM images of alkali-activated MSWI fly ash-based pastes synthesized with varying proportions of metakaolin

3.2.3. Heavy metals immobilization

Table 3.2.2. TCLP leaching concentration (ppm) of heavy metal of alkali-activated MSWI fly ash-based pastes

Pastes	Pb	Cr(VI)	Cd	Cu	Zn
Pristine silica fume	3.2	3.1	ND	3.8	31.2
5% metakaolin	3.9	2.5	ND	3.1	30.2
10% metakaolin	4.3	1.8	0.3	4.3	32.6
15% metakaolin	6.8	3.3	0.6	5.2	35.5
20% metakaolin	11.6	6.1	0.8	8.2	40.6
TCLP limits	5	5	1	NL	NL

ND= not found; NL= no limit

Table 3.2.2 shows TCLP leaching concentrations of the existing heavy metals of alkali-activated MSWI fly ash-based pastes. As can be seen, with the addition of metakaolin from 0 to 20%, the leaching concentrations of Pb were increased gradually and exceeded the TCLP limits at 15% and 20%. Leaching concentrations of Cr exhibited a similar trend to Pb, and exceeded the TCLP limits at 20%. Initially, the leaching concentrations of Cd, Cu and Zn were increased and then decreased with the addition of metakaolin from 0 to 20%. The lowest leaching concentrations of Cr(VI), Cu and Zn were obtained in the synthesized pastes at 10%, 5% and 5% metakaolin, respectively.

From the TCLP leaching test, it is depicted that the immobilization of heavy metals was impacted by the substitution of metakaolin in silica fume in the synthesis process. As per the previous study, the possible mechanisms which affect the heavy metals immobilization due to varied dosages of aluminum can be summarized in three studies as follows. It was reported that formed Friedel's salt could stabilize the existing heavy metals by substitution of isomorphous (Chrysochoou and Dermatas, 2006; Shao et al., 2013). In addition, the substitution of the tetrahedral Al in the backbone of tetrahedral Si can produce more negative charges associated with tetrahedral Al(III), leading to additional metal cations bound into the structure for charge-balancing (Schilling et al., 1994). Also, the change in the compressive strength is related to the permeability of materials, i.e.,

an important parameter for immobilization of heavy metals. The stronger paste tends to possess less permeability and better encapsulation ability (Fernández-Pereira et al., 2018).

Further, the TCLP leaching test showed that the lowest leaching concentrations of Pb, Cd, Cu, and Zn were obtained as pastes synthesized with 0 and 5% metakaolin, and the highest leaching concentrations with a 20% metakaolin. Notably, the synthesized pastes with higher compressive strength tend to possess better immobilization ability. This indicates that the immobilization of heavy metals is dominated by encapsulation. It is interesting that the lowest leaching concentrations of Cr(VI) was obtained with a 10% metakaolin. Considering that the anion form of Cr(VI) is not capable of bonding with negative charged Al(III) due to the influence of electrostatic repulsion force. Thus, the immobilization of Cr(VI) may be attributed to the formation of Friedel's salt i.e. a trigonal crystal system of layered hexagonal structure in which sites like Ca^{2+}, $Al^{3+}$and Cl^{-} can be replaced by other ions (Taylor, 1997). It is reported that the stabilization of oxyanions like CrO_4^{2-} relies on the formation of Friedel's salt that immobilizing Cr(VI) by substitution of the isomorphous, resulted in solid-solutions of Cr-Friedel's salt (Qian et al., 2009; Shao et al., 2013). However, the immobilization mechanism seems effective only in the pastes with comparable strength. With a 10% to 20% of metakaolin, the compressive strength of paste was decreased. Subsequently, leaching concentrations of Cr(VI) were decreased abruptly. This indicates that isomorphous substitution and physical encapsulation act simultaneously on the immobilization of Cr(VI).

As can be seen in ^{29}Si NMR analysis, with the addition of metakaolin from 0 to 20%, more and more tetrahedral Al(III) in the backbone of the tetrahedral Si can produce negative charges and effectively immobilized more heavy metals. However, the opposite result was found in the TCLP test. For further clarification of the result, modeling and simulation tools were employed to calculate the binding energy related to charge-balanced ion in N-A-S-H gel, as shown in Figure 3.2.5. The binding energy of Na, Pb, Cd, Cu, and Zn exhibited the order of Na > Cd > Zn > Cu > Pb. This indicates that bonding of Na^{+} in N-A-S-H gel possesses the most stable molecular orientation. In the presence of a large amount of Na^{+} (calculated Na/Al in Table 2.3.2), it was preferentially bonded the N-A-S-H gel to balance the negative charge, causing hardly bonding of

heavy metals in the structure for charge-balancing. This result is well consistent with the TCLP results.

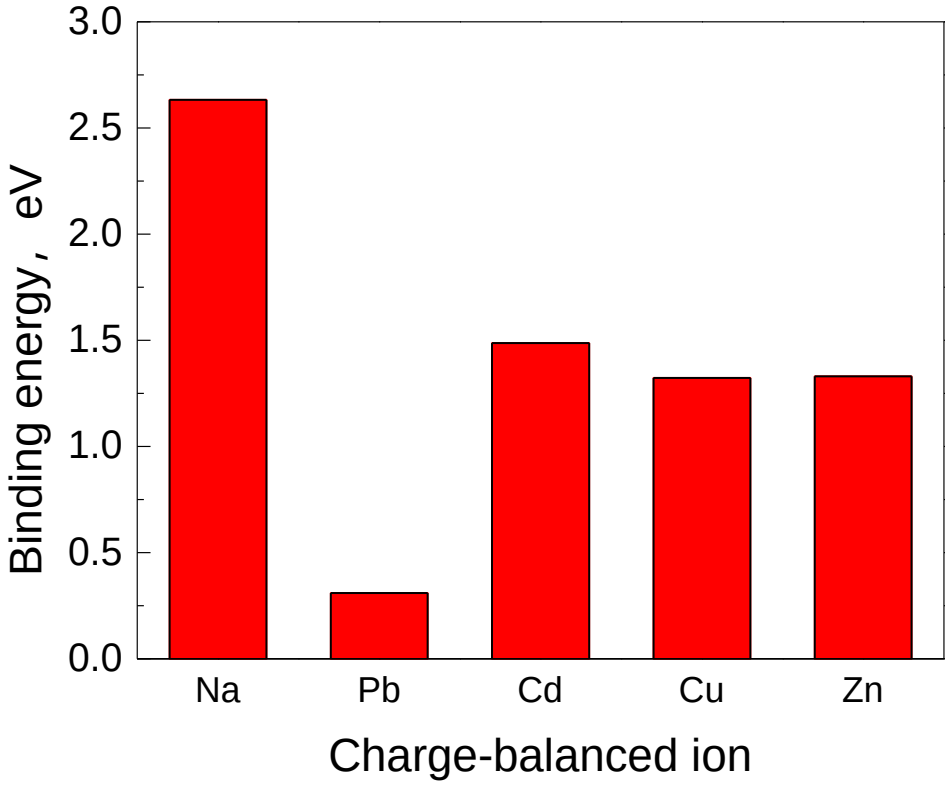

Figure 3.2.5. The binding energy related to charge-balanced ion in N-A-S-H gel

3.3. Influence of waste glass on immobilization effect of heavy metals

3.3.1. Compressive strength

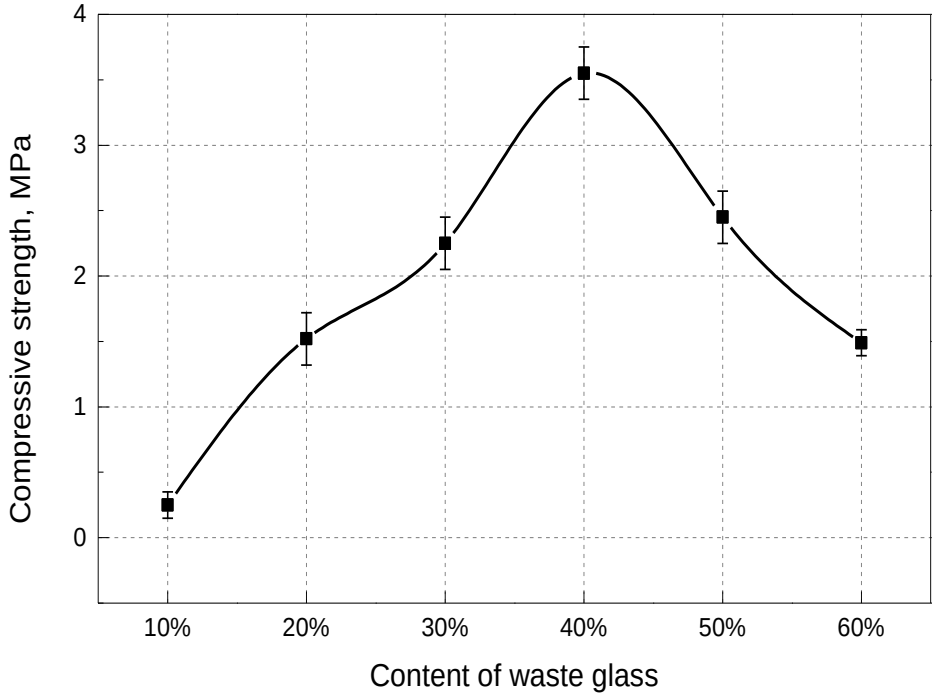

Figure 3.3.1. Compressive strength of alkali-activated MSWI fly ash-based pastes as a function of the proportions of waste glass

The consolidation process aims to transform powder waste into a monolithic solid with comparable strength through hydration reaction. The increase in structural strength and durability ensures long-term stability and structural integrity in landfill conditions (Phua et al., 2019). The acceptable strength for the Portland cement solidified matrix is more than 0.2 MPa (Lombardi et al., 1998; Mangialardi et al., 1999). However, in the UK, the Waste Regulation Authority (WRA) regulated the strength requirement for consolidation products is 0.7 MPa for 28 day age but the criteria may be as low as 0.35 MPa depending on the circumstances of testing (Hills and Pollard, 1997). Figure 3.3.1 shows the compressive strength of alkali-activated MSWI fly ash-based pastes as a function of the proportions of WA. With the increase of WA dosage from 10% to 40%, the compressive

strength of pastes increased and reached a maximum compressive strength of 3.55 MPa. This result demonstrates that WA addition effectively reinforced the consolidation of MSWI fly ash. In consideration of scarce silicon and aluminum in MSWI fly ash, the increase of compressive strength may be relative to the high content of silicon in WA, which supplies precursor for producing cementitious gel through alkaline activation reaction. Except for the paste synthesized with 10% WA, all the pastes meet the strength requirement. With the further increase in WA dosage, however, the compressive strength decreased. This result will be explained in detail in the later part.

3.3.2. Microstructure characterizations

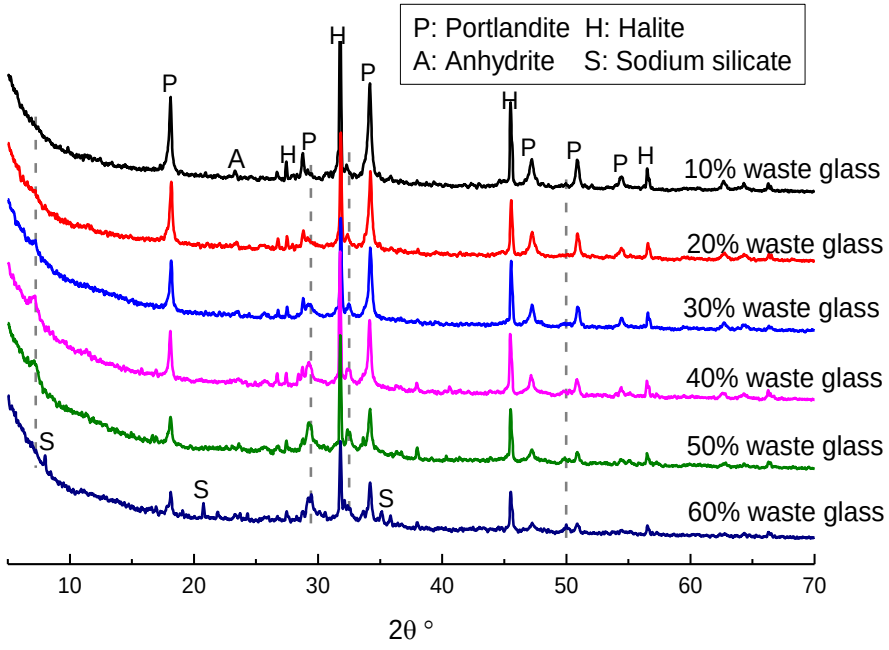

Figure 3.3.2. XRD patterns of alkali-activated MSWI fly ash-based pastes synthesized with varying proportions of waste glass

Figure 3.3.2 gives the XRD pattern of alkali-activated MSWI fly ash-based pastes synthesized with varying proportions of WA. Comparing with raw MSWI fly ash, calcium chloride hydroxide (CaClOH), calcite ($CaCO_3$) and sylvite (KCl) disappeared in pastes, and remained portlandite ($Ca(OH)_2$), halite (NaCl) and anhydrite ($CaSO_4$). Calcium chloride hydroxide is an unstable phase. It would be decomposed into $Ca(OH)_2$ and chloride when exposed in alkaline conditions (Zheng

et al., 2010). As a result, it existed in the form of $Ca(OH)_2$ and NaCl in pastes. Calcite usually is an inert phase in alkaline activation reaction in some studies (Jin et al., 2016; Wan and Rao, 2018; Ye et al., 2016b). However, it disappeared in the current study. This may be due to the generation of low crystalline $CaCO_3$ in the long period pre-stirring process, which was found when using a mixture of CaO and Na_2CO_3 as alkaline activator (J. Wang et al., 2018). The low crystalline $CaCO_3$ is highly reactive and reacted with added silicon source to form C-(A)-S-H gel. This was verified by the characteristic peaks of the C-(A)-S-H gel peaking at 7.07º , 29.3º and 49.83º of 2θ (Torres et al., 2009).

Further, with the increase of WA dosage, the intensity of the crystal phase originated from MSWI fly ash decreased. However, the intensity of a newly formed phase, locating at 2θ of 32.5º, increased as WA dosage increase from 10% to 50% and decreased when 60% WA addition. At the same time, the crystal sodium silicate is formed in pastes with 60% WA addition. We believe that the components of the newly formed phase could be associated with crystal sodium silicate. Previous studies found that the alkaline activation of WA produced C-S-H gel and sodium silicate gel (silica gel) when only calcium source is available, or C-S-H gel and sodium-alumino-silicate-hydrate (N-A-S-H) gel when both calcium and aluminum sources are available (Avila-López et al., 2015; Redden and Neithalath, 2014). In this reaction medium, aluminum is rarely presented (Tables 2.1.5 and 2.1.10), and thus the resultant formed cementitious gel are C-S-H gel and silica gel. Therefore, it is reasonable here to assign the phase locating at 2θ of 32.5º to silica gel. In a study of the alkaline activation of WA, silica gel exhibited an amorphous peak at 2θ from 25 º to 35 º (Zhu et al., 2019b). This may be attributed to the alkaline activator used, which could affect whether the crystal phase formation of gel. It has been reported that the alkaline activation of slag, regardless of the type of activator, the major product is always C-S-H gel. However, when sodium hydroxide was the alkaline activator, a poor-crystalline C-S-H gel was formed, while with water glass, crystallinity was invisible even after a full year of hydration (Huang et al., 2019). This is highly in support of our assignment for the newly formed crystal phase because we used sodium hydroxide as the alkaline activator, whereas the latter study used a mixture of sodium hydroxide and water glass as the alkaline activator.

Figure 3.3.3 shows SEM images of alkali-activated MSWI fly ash-based pastes synthesized with varying proportions of WA. With 10% and 20% WA addition, the pastes exhibited substantial indissoluble WA particles, as well as a scantly compacted structure. With the increase of WA to 30% and 40%, pastes tend to form more gel and a condensed structure. With continuously increase WA to 50% and 60%, pastes again presented WA particles and porous structure. The alkaline variation in the reaction medium and the dosage of WA could responsible for this result. In the stirring process to eliminate expansion, metallic aluminum and other impurities in MSWI fly ash would consume the dosage of NaOH (Tian et al., 2020c). Therefore, the more MSWI fly ash was added, the more NaOH was consumed. Keeping constant NaOH dosage, the reaction medium with high MSWI fly ash addition tends to be of a lower alkaline medium. At high MSWI fly ash (i.e.,10% and 20% WA addition), the low alkaline reaction medium is difficult to dissolve WA (Torres-Carrasco et al., 2014). This leads to less gel was formed in pastes and exhibited substantial indissoluble WA particles. With the decrease of MSWI fly ash (i.e., the increase of WA), the reaction medium tends to have a higher alkaline medium and dissolve more WA, pastes thus generated more gel and presented a homogeneous structure. With further increase of WA to 50% and 60%, the reaction medium failed to completely dissolve excess WA, resulting in WA particles remained in the pastes. Additionally, with the decrease of MSWI fly ash, the available calcium source decreased, inhibiting the formation of C-(A)S-H gel. Also, when 60% WA addition, partial silica gel turned into crystal sodium silicate (Figure 3.3.2). This leads to a porous structure and the decrease of the compressive strength of pastes.

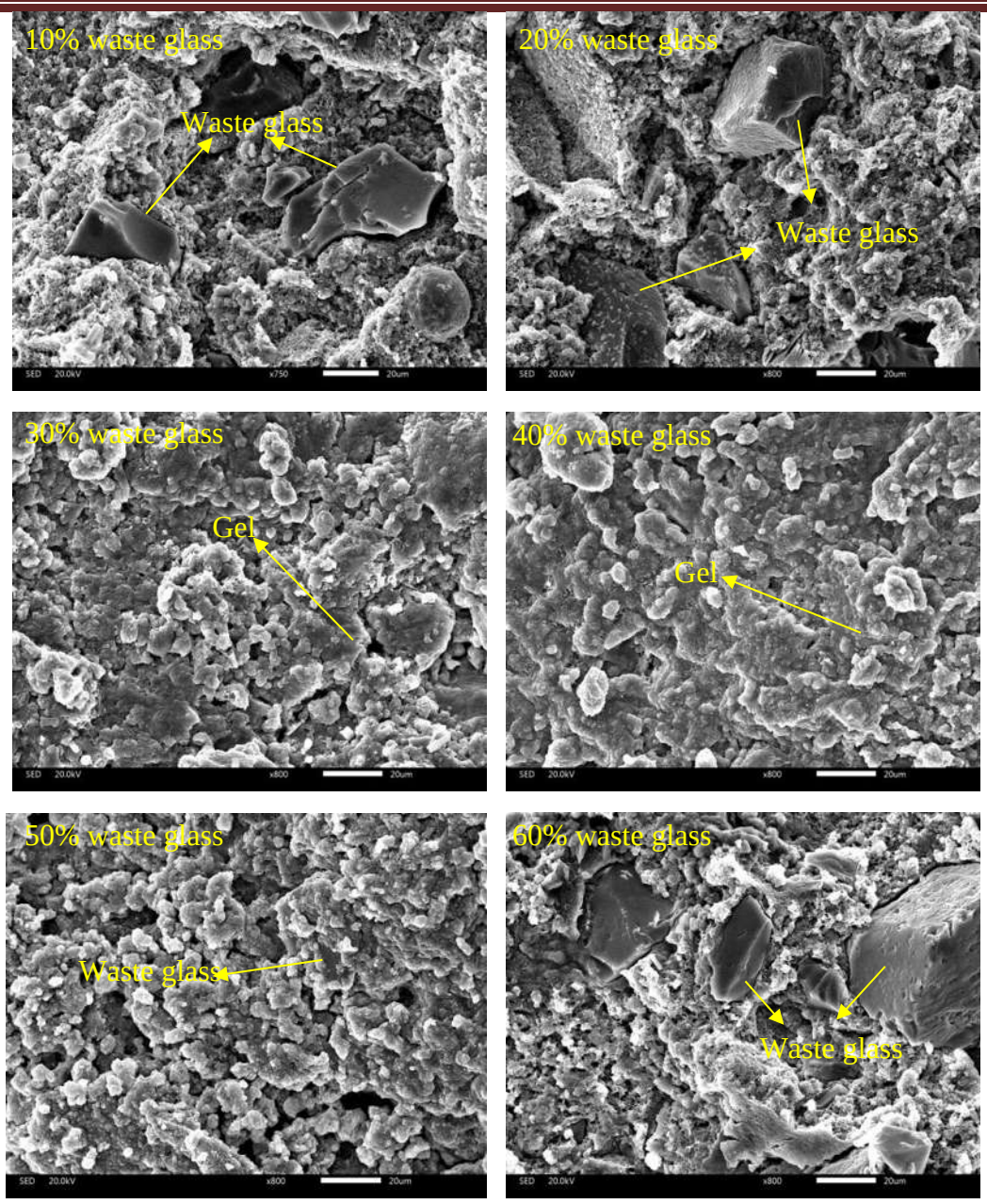

Figure 3.3.3. SEM images of alkali-activated MSWI fly ash-based pastes synthesized with varying proportions of waste glass

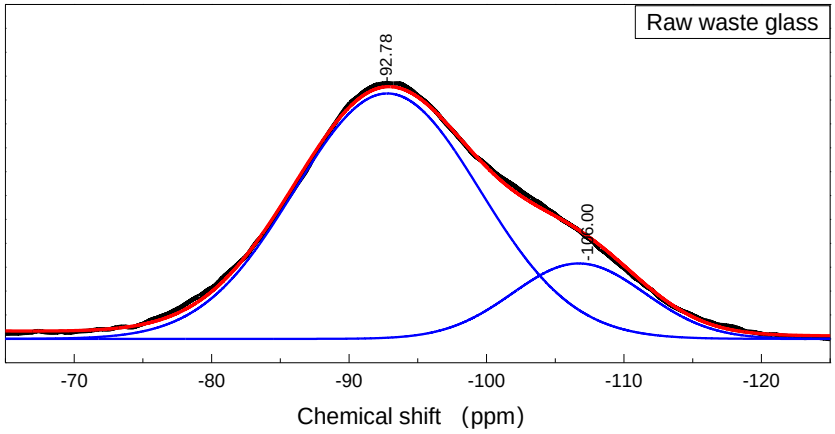
Raw waste glass
-92.78
-106.00
-70
-80
-90
-100
-110
-120
Chemical shift (ppm)

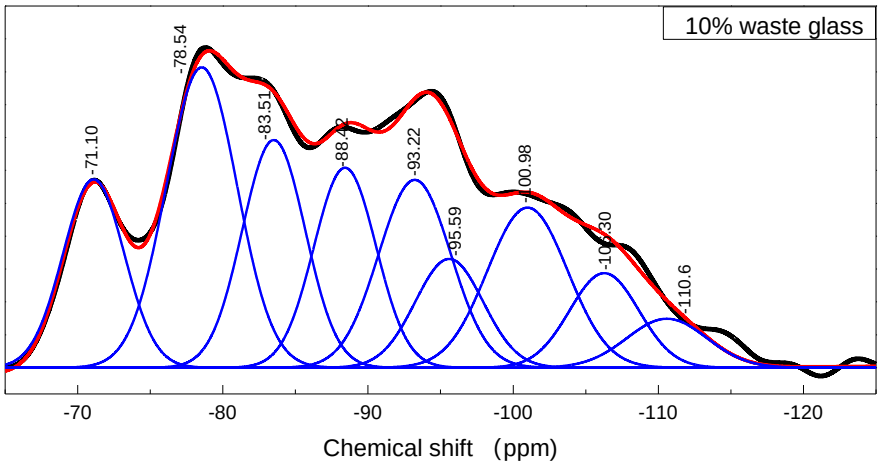
10% waste glass
-71.10
-78.54
-83.51
-88.42
-93.22
-95.59
-100.98
-106.30
-110.6
-70
-80
-90
-100
-110
-120
Chemical shift (ppm)

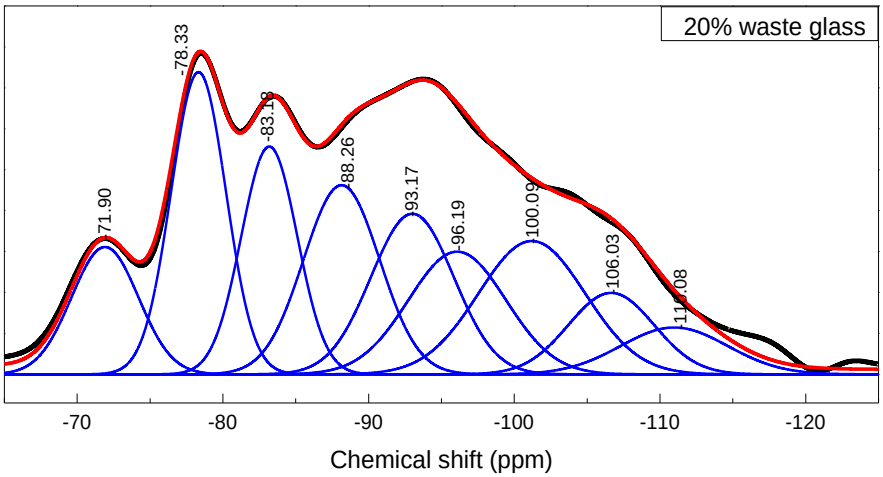
20% waste glass
-71.90
-78.33
-83.18
-88.26
-93.17
-96.19
-100.09
-106.03
-110.08
-70
-80
-90
-100
-110
-120
Chemical shift (ppm)

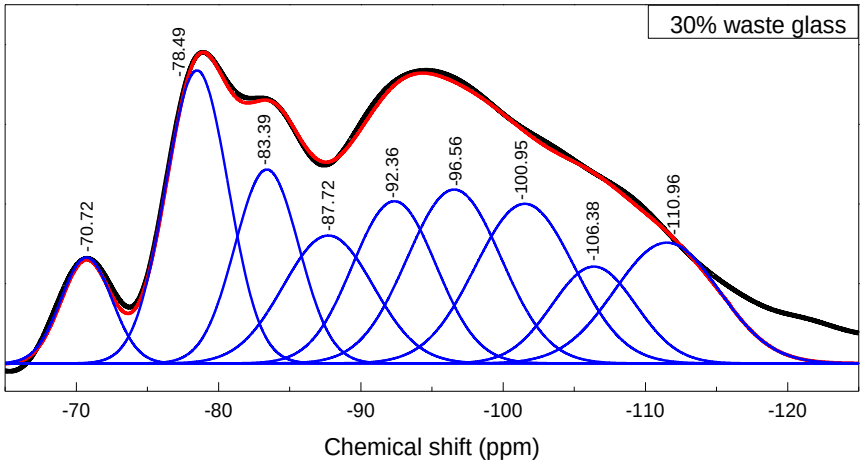
30% waste glass
-78.49
-83.39
-87.72
-92.36
-96.56
-100.95
-106.38
-110.96
-70.72
-70
-80
-90
-100
-110
-120
Chemical shift (ppm)

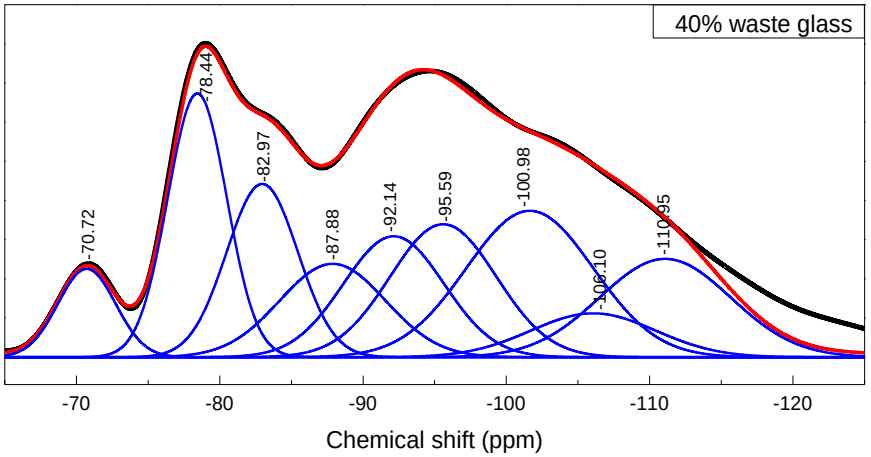
40% waste glass
-78.44
-82.97
-87.88
-92.14
-95.59
-100.98
-106.10
-110.95
-70.72
-70
-80
-90
-100
-110
-120
Chemical shift (ppm)

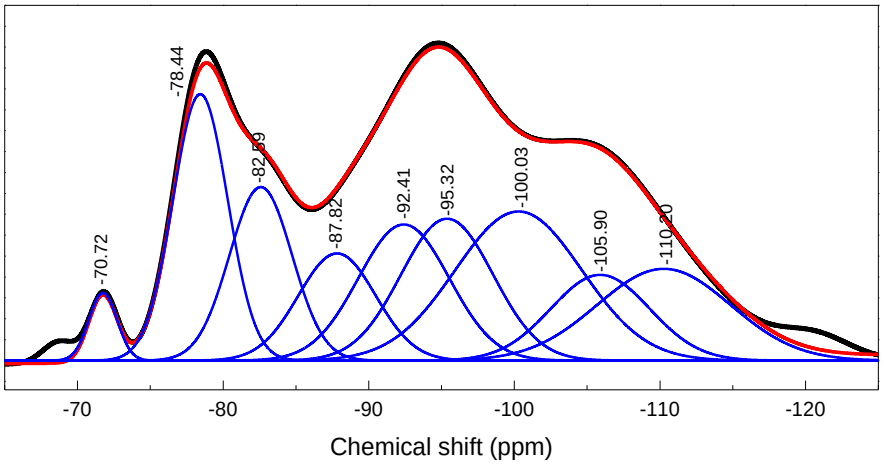
-78.44
-82.59
-87.82
-92.41
-95.32
-100.03
-105.90
-110.20
-70.72
-70
-80
-90
-100
-110
-120
Chemical shift (ppm)

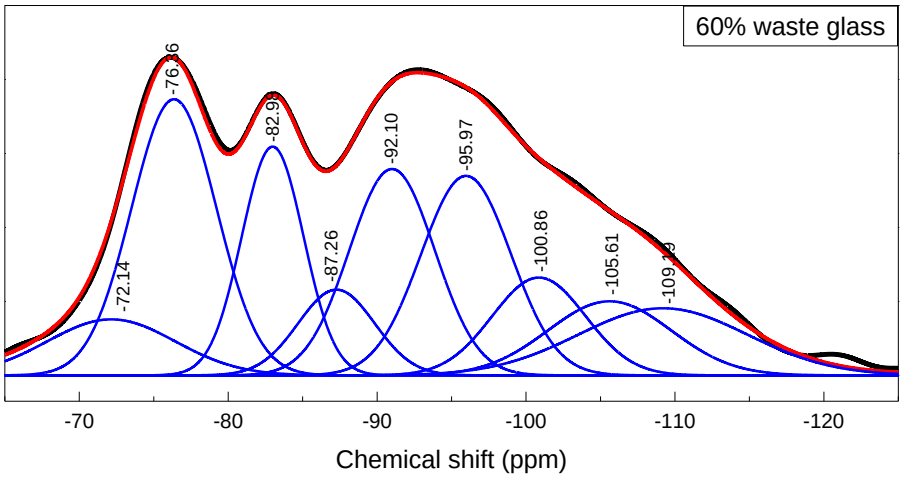

Figure 3.3.4. ^{29}Si NMR spectra of raw waste glass and alkali-activated MSWI fly ash-based pastes synthesized with varying proportions of waste glass

Table 3.3.1. ^{29}Si deconvolution data of alkali-activated MSWI fly ash-based pastes synthesized with varying proportions of waste glass

	Position center (error ±1)	Dosage of waste glass					
		10%	20%	30%	40%	50%	60%
Monomer	-71 ppm	11.10	8.19	4.72	4.78	1.93	6.14
C-S-H gel	-76 or -79 ppm	20.50	15.95	16.07	14.56	14.86	20.06
	-82 ppm	13.80	12.31	10.86	11.59	10.57	12.11
	-87.8 ppm	11.97	14.02	10.08	9.26	8.06	5.62
Silica gel	-95 ppm	7.11	11.52	14.31	13.25	13.14	15.38
	-100 ppm	12.37	13.72	13.87	17.50	18.70	7.81
	-110 ppm	3.76	4.82	11.05	12.11	12.48	9.72
Waste glass	-92 ppm	13.04	12.81	11.87	11.42	12.00	15.10
	-106 ppm	6.30	6.72	7.10	5.13	8.19	7.81

Figure 3.3.4 gives the ^{29}Si NMR spectra of raw WA and alkali-activated MSWI fly ash-based pastes synthesized with varying proportions of WA. WA predominantly peaked at -93 ppm and minor peaked at -106 ppm, which are indicative of the presence of the Q^4 Si site of characterizing WA (Torres-Carrasco et al., 2014). From the analysis of XRD and SEM, the silicon-bear substances contain C-(A)-S-H gel, silica gel and WA. In C-S-H gel, the peaks at -79 ppm, -82 ppm and -87.8 ppm are assigned to Q^1, Q^2 and Q^2(1Al) due to end-chains, middle-chains and Al is involved in middle-chains presented in C-S-H, respectively (Richardson, 1999; Wan and Rao, 2018). In silica gel, the peaks at -95ppm, -100 ppm and -110 ppm are assigned to Q^2, Q^3 and Q^4 Si site (Lutz et al., 2009; Zhu et al., 2019b). The peak at -71 ppm is assigned to monomer silicate (Q^0) (Q. Wan et al., 2018).

Table 3.3.1 gives the ^{29}Si deconvolution data of alkali-activated MSWI fly ash-based pastes synthesized with varying proportions of WA. With the increase of WA from 10% to 50%, the Si site in C-(A)-S-H gel decreased, which accounts for 46.27%, 42.28%, 37.01%, 35.41% and 33.49%, respectively. While the Si site in silica gel increase from 23.24%, 30.06%, 39.23%, 42.86% to 44.32%. This may be attributed to the variation in composition in the reaction medium. With the increase of WA, the silicon source increases and the calcium source originated from MSWI fly ash decreases accordingly, which facilitates the formation of silica gel and inhibits the formation of C-S-H gel from the perspective of thermodynamics. When 60% WA addition, the Si site in silica gel has an obvious decrease to 32.91%, and at the same time, the Si resonance at -78 ppm transferred to -76 ppm. This may be attributed to part of silica gel converting into crystal sodium silicate (Figure 3.3.2). Crystal sodium silicate is of similar constituents with silica gel (Redden and Neithalath, 2014). Differently, the Si site of silica gel peaks at -95ppm, -100 ppm and -110 ppm while that of sodium silicate peaks at -76.8 ppm (Mägi et al., 1984). The transformation of silica gel into crystal sodium silicate leads to a surging increase of Si site at -76 ppm. Furthermore, the Si site in WA exhibited a minimum percentage when 40% WA addition. This suggests the optimum reaction medium for WA dissolution, which further explained the paste synthesized with 40% WA exhibited the highest compressive strength and homogeneous structure.

3.3.3. Immobilization effect of heavy metals

Table 3.3.2. The heavy metals leaching concentration of raw MSWI fly ash

Heavy metals	Cu	Pb	Zn	Cr	Cd
Raw MSWI fly ash (mg/L)	5.43	10.92	52.88	0.24	5.73
Limit (mg/L)	100	5	100	5	1

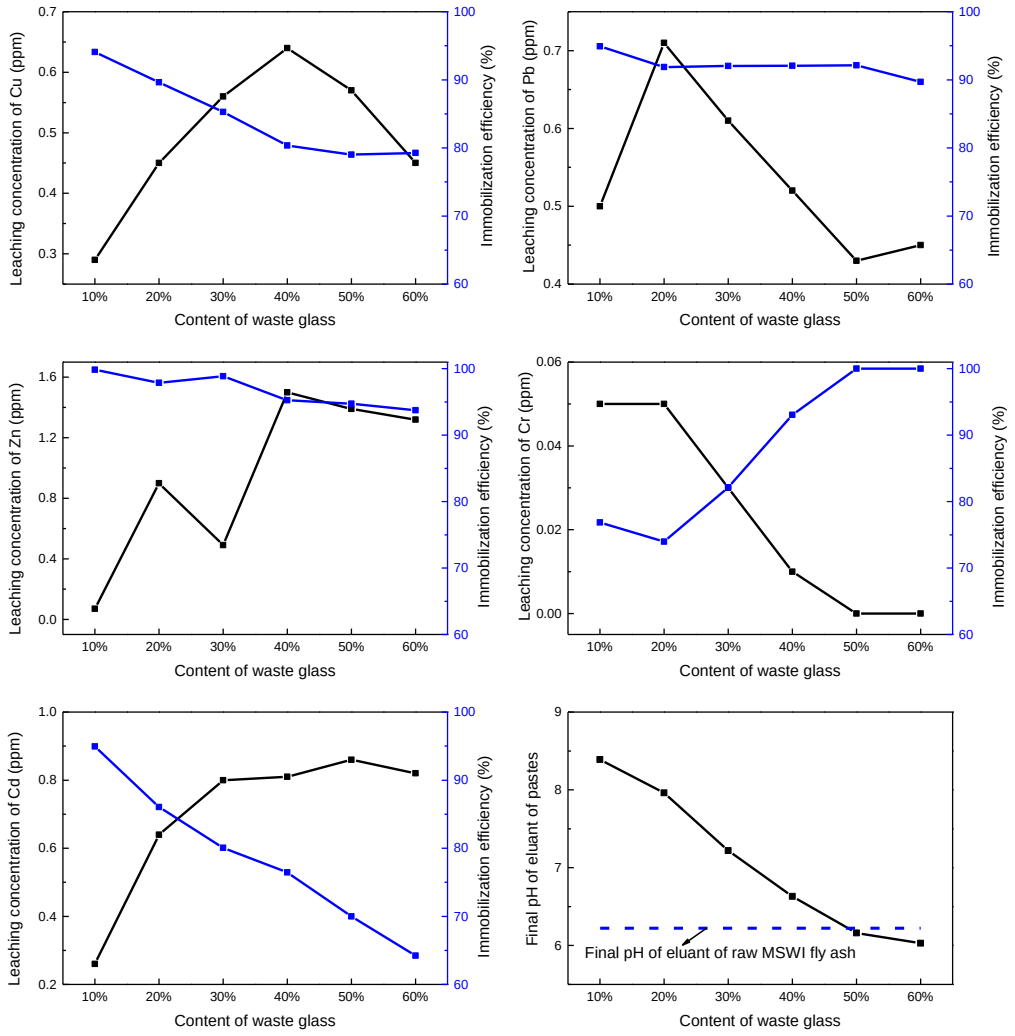

Figure 3.3.5. The leaching concentration and immobilization efficiency of heavy metals and eluant final pH of pastes synthesized with varying proportions of waste glass dosage

Table 3.3.2 gives the heavy metals leaching concentration of raw MSWI fly ash, in which the leaching concentration of Pb and Cd exceeds the acceptable limit of the environment. Figure 3.3.5 gives the leaching concentration and immobilization efficiency of heavy metals and eluant final pH of pastes synthesized with varying proportions of WA dosage. Compare to raw MSWI fly ash, the leaching concentration of the heavy metals decreased in the pastes synthesized with 10% to 60% WA, and all meet the acceptable limit of the environment. The immobilization efficiency of Cr increased with the increase of WA. However, the immobilization efficiency of Cu, Pb, Zn and Cd decreased with the increase of WA. This result may be related to the eluant final pH of pastes. With the addition of WA, the eluant final pH decreased, promoting the leaching of heavy metals that in the form of hydroxides, oxide and carbonate. Two factors could be responsible for the variation in the eluant final pH value. Firstly, as a lower dosage addition of WA, less alkaline activation reaction occurred in pastes, consuming less alkaline activator (Ye et al., 2016b). Secondly, MSWI fly ash itself is of high alkalinity due to it contains substantial portlandite ($Ca(OH)_2$), calcium chloride hydroxide (CaClOH) and calcite ($CaCO_3$) (Figure 2.2.3). The pH of its aqueous solution is higher than 12 and exhibited a strong buffering capacity against acidification (Luo et al., 2019). Therefore, keeping constant alkaline activator, pastes synthesized with a low dosage of WA (i.e., high dosage of MSWI fly ash) exhibited a strong alkaline environment. On the other hand, as 50% WA addition, the eluant final pH of paste is comparable with that of raw MSWI fly ash. However, the immobilization efficiency reached to 77.8%, 92.3%, 94.56%, 100% and 69.98% for Cu, Pb, Zn, Cr and Cd, respectively. This indicates that the immobilization of heavy metals is not only controlled by alkalinity, but also enhanced by alkaline activation reation. Moreover, the immobilization efficiency of Cu and Cd are more susceptible to eluant final pH than that of Pb and Zn, suggesting different immobilization form of heavy metals. To explore the immobilization form of heavy metals, we chose two kinds of heavy metals (Cd and Pb) with different leaching behavior as candidates for further study.

3.3.4. Immobilization forms of heavy metals

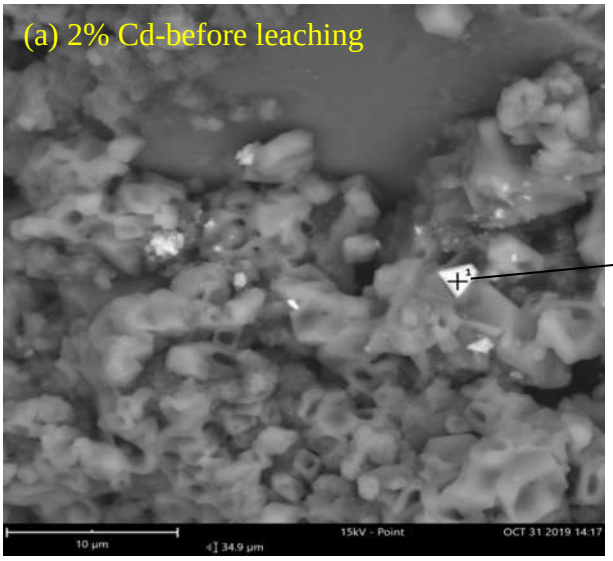

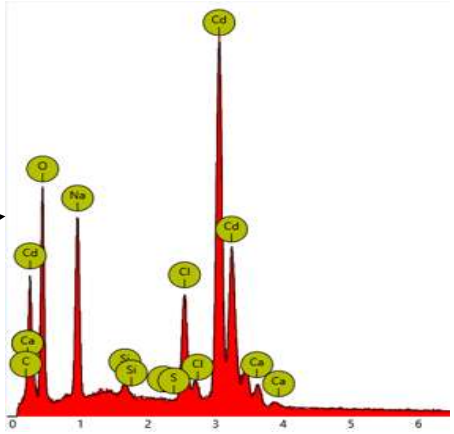

Element	O	Na	Cd	Cl	C	Ca	Si	S	Total
Mass percent (%)	34.37	14.16	45.39	4.55	0.38	0.78	0.35	0.02	100
Atomic percent (%)	63.93	18.33	12.02	3.83	0.93	0.58	0.37	0.02	100

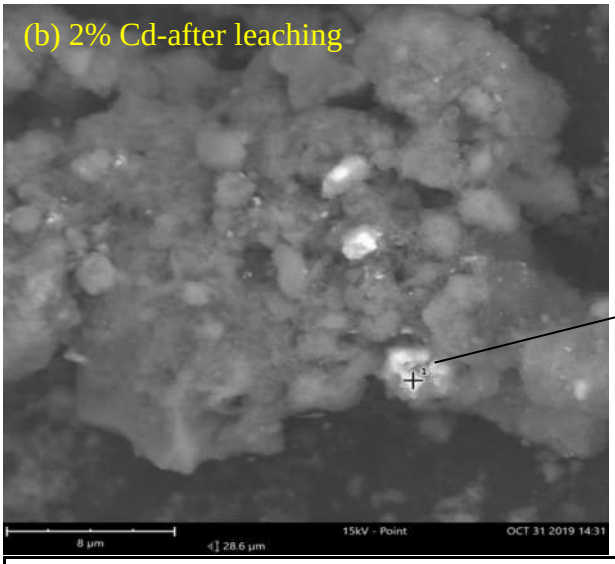

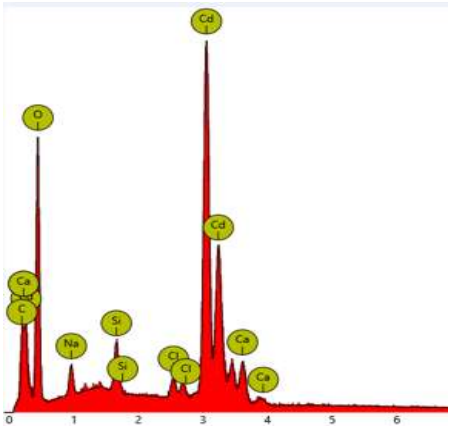

Element	O	Na	Cd	Cl	C	Ca	Si	Total
Mass percent (%)	44.79	2.63	47.26	0.88	0.77	2.24	1.42	100
Atomic percent (%)	79.31	3.25	11.91	0.71	1.82	1.58	1.43	100

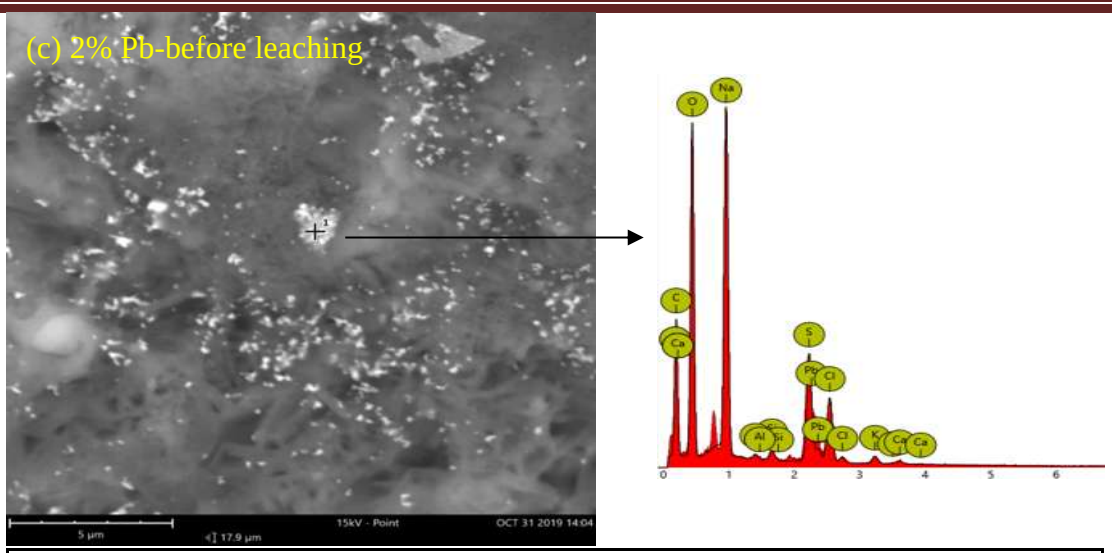

Element	O	Na	Pb	Cl	C	Ca	S	Si	K	Al	Total
Mass percent (%)	44.18	34.03	3.63	5.52	4.86	0.31	6.05	0.49	0.68	0.26	100
Atomic percent (%)	54.57	29.25	0.35	3.07	8.00	0.15	3.73	0.34	0.34	0.19	100

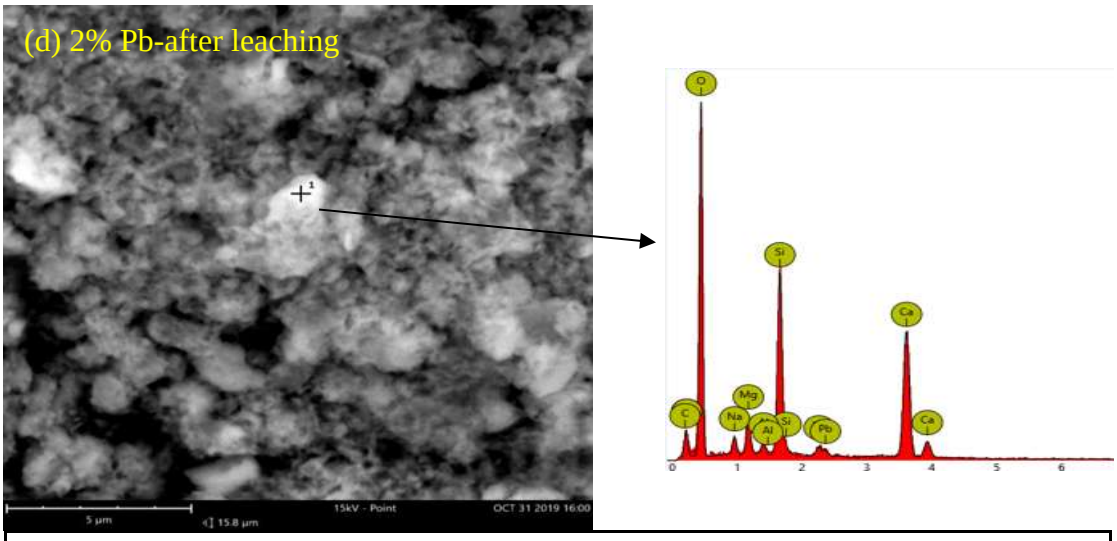

Element	O	Na	Pb	C	Ca	Si	Mg	Al	Total
Mass percent (%)	64.30	2.38	3.14	0.72	15.62	9.73	3.53	0.58	100
Atomic percent (%)	78.80	2.03	0.30	1.18	7.64	6.79	2.85	0.42	100

Figure 3.3.6. Backscattered electron (BSE/EDS) microscopy of alkali-activated MSWI fly ash-based paste synthesized with 2% $Cd(NO_3)_2$ and 2% $Pb(NO_3)_2$ addition before and after leaching

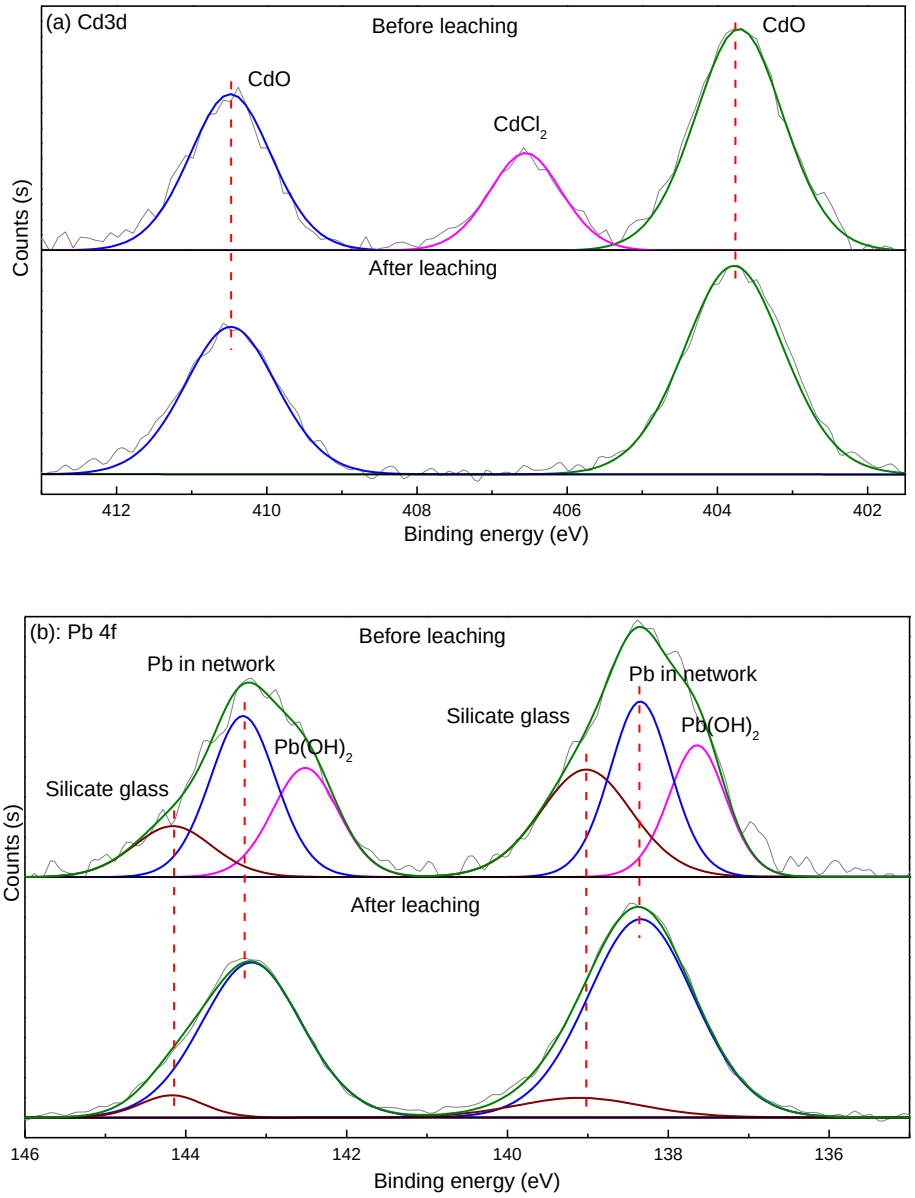

Figure 3.3.7. XPS spectra of alkali-activated MSWI fly ash-based pastes synthesized with 2% $Cd(NO_3)_2$ and $Pb(NO_3)_2$ addition

The backscattered electron (BSE/EDS) microscopy was given to examine heavy metals distribution in pastes. The brightness of the areas is proportional to the atomic number in BSE microscopy. Point analysis by EDS indicates that the bright areas contained Cd and Pb in pastes synthesized with $Cd(NO_3)_2$ and $Pb(NO_3)_2$ addition, respectively. Figure 3.3.6 (a) and (b) show the BSE/EDS microscopy of paste synthesized with 2% $Cd(NO_3)_2$ addition before and after leaching, respectively.

As can be seen from the EDS results, the possible elements to chemically combine with Cd in the paste before leaching include O, Cl, C, Si and S, corresponding to compounds CdO or $Cd(OH)_2$, $CdCl_2$, $CdCO_3$, $CdSiO_3$ and $CdSO_4$, respectively. After leaching, the S disappeared in the bright area. Therefore, the possible compounds to immobilize Cd include CdO, $Cd(OH)_2$, $CdCl_2$, $CdCO_3$ and $CdSiO_3$. However, $CdCl_2$, $CdCO_3$ and $CdSiO_3$ have little possibility to immobilize Cd from the perspective of the atomic ratio. The atomic percent of Cd (11.91%) is much higher than that of Cl (0.71%), C (0.93%) and Si (0.37%). Previous study concluded that Cd could be effectively immobilized in high calcium matrix because Cd substitute for Ca^{2+} to form Cd/Ca silicate hydrate gels (Diez et al., 1997; Pomiès et al., 2001). Here, we found that the formation of Cd/Ca silicate hydrate gels seem not the dominant immobilization form. Therefore, the possible forms to immobilize Cd only include CdO and $Cd(OH)_2$.

To further confirm the immobilization form, XPS was performed. Figure 3.3.7 (a) gives the Cd 3d spectra of pastes synthesized with 2% $Cd(NO_3)_2$ addition before and after leaching. In the Cd 3d spectra of the paste before leaching, the binding energy of Cd $3d^{5/2}$ peaks at 406.10 eV for $CdCl_2$ (Seals et al., 1973). After leaching, the peak of $CdCl_2$ disappeared. In the Cd 3d spectra of paste before and after leaching, the binding energy of Cd $3d^{5/2}$ and $Cd3d^{3/2}$ peaking at 404.00 eV and 410.38 eV are assigned to CdO (Seyama and Soma, 1984). While the binding energy of $Cd3d^{5/2}$ for $Cd(OH)_2$ peaked at 404.8 eV (Hammond et al., 1975). Therefore, the remaining Cd-bear compounds in paste is CdO. The CdO is rarely soluble when pH higher than 7. However at pH of 6, it is highly soluble (El-eswed, 2020). As 50% WA addition, the eluant final pH of paste is 6.16, while immobilization efficiency of Cd reached 69.98% (Figure 3.3.5). This immobilization effect may be attributed to physical encapsulation and the alkaline environment formation. After alkaline activation reaction, the enhanced properties of paste exhibited lower hydraulic conductivity and lower porosity and thus limited the leachability of the heavy metals by reducing contact with the outer environment (Mangialardi et al., 1999). On the other hand, the alkaline environment formation in the pore solution buttered the contacted acid extraction liquid, keeping the alkaline condition of the internal environment and thus immobilizing the CdO.

Figure 3.3.6 (c) and (d) show the BSE/EDS microscopy of paste synthesized with 2% $Pb(NO_3)_2$ addition before and after leaching, respectively. Before leaching, the possible elements to

chemically combine with Pb include O, Cl, C, S and Si, corresponding to compounds PbO or $Pb(OH)_2$, $PbCl_2$, $PbCO_3$, $PbSO_4$ and the combination forms of Pb and Si. In previous studies, the combination forms of Pb and Si include the formation of lead silicate glass ($PbO{\cdot}nSiO_2$) (Wang and Zhang, 1996) and lead in network that refers to Pb covalently bonds to O to form PbO_n pyramidal units with silicate (Boddenberg, 1988). After leaching, the possible elements to chemically combine with Pb include O, C and Si, corresponding to compounds of PbO or $Pb(OH)_2$, $PbCO_3$ and lead silicate glass or lead in network.

Figure 3.3.7 (b) gives the Pb4f spectra of paste synthesized with 2% $Pb(NO_3)_2$ addition before and after leaching. In the Pb4f spectra of paste before leaching, 6 peaks could be fitted, which is 137.95 eV,138.20 eV, 139.00 eV 142. 90 eV,143.10 eV and 144.10 eV. After leaching, 4 peaks remained, which is located at 138.20 eV, 139.00 eV, 143.10 eV and 144.10 eV. Combing with the possible compounds in paste before and after leaching, the binding energies peaking at 137.95eV 142.90 eV may be attributed to $Pb(OH)_2$ (Pederson, 1982), the binding energies peaking at 138.2 eV and 143.2 eV are assigned to lead in the network (C. Zhang et al., 2016), and binding energies peaking at 139.0 eV and 144.1 eV are assigned to lead silicate glass (Wang and Zhang, 1996). As can be seen from Figure 3.3.7 (b), Pb is immobilized mainly by lead in a network with a minor amount of lead silicate glass formation.

3.4. Co-disposal of MSWI fly ash and spent caustic

3.4.1. Consolidation of MSWI fly ash

3.4.1.1. X-ray diffraction (XRD) examination

To determine the existing phase and phase transformation of alkali-activated MSWI fly ash-based pastes, XRD examination was carried out. Figure 3.4.1 shows the XRD of spent caustic-pastes and NaOH-pastes synthesized with the varying dosage of BFS. Comparing to the XRD spectra of raw MSWI fly ash (Figure 2.2.2), the phase of calcium chlorine hydroxide (CaClOH) disappeared and hydrocalumite ($Ca_4Al_2O_6Cl_2{\cdot}10H_2O$) formed in both species' pastes. CaClOH was an unstable phase when exposed to alkaline surroundings, and it would be decomposed into $Ca(OH)_2$ and chloride ions (Zheng et al., 2010). In the presence of a large amount of calcium source and chloride ions, aluminum source into the system with the introduction of BFS facilitates hydrocalumite

generation. The chemical equations can be expressed as Eq. (3.4.1). Differently, ettringite ($Ca_6Al_2(SO_4)_3(OH)_{12}$ $26H_2O$) formed in spent caustic-pastes, whereas none formed in NaOH-pastes. This may due to SO_4^{2-} contained in spent caustic, supplying the precursor for forming ettringite. This can be verified by the fade away of peaks of anhydrite in spent caustic-pastes with the BFS addition, and meanwhile, the ettringite peaks intensity increased. This chemical equation can be deduced to Eq. (3.4.2). On the other hand, the peak of 2θ=29.3º, which assigning to calcite, is slightly higher in spent caustic-pastes. This may due to Na_2CO_3 presented in spent caustic facilitates the calcite formation when mixing spent caustic in the system full of calcium ion. The other crystalline phases produced in both species' pastes are similar. This may be due to major element Na and similar alkalinity exist in both alkaline activators.

$$2AlO_2^- + 4Ca^{2+} + 2Cl^- + 4OH^- + 8H_2O = Ca_4Al_2O_6Cl_2 \cdot 10H_2O \quad (3.4.1)$$

$$3SO_4^{2-} + 2AlO_2^- + 6Ca^{2+} + 4OH^- + 28H_2O = Ca_6Al_2(SO_4)_3(OH)_{12} \cdot 26H_2O \quad (3.4.2)$$

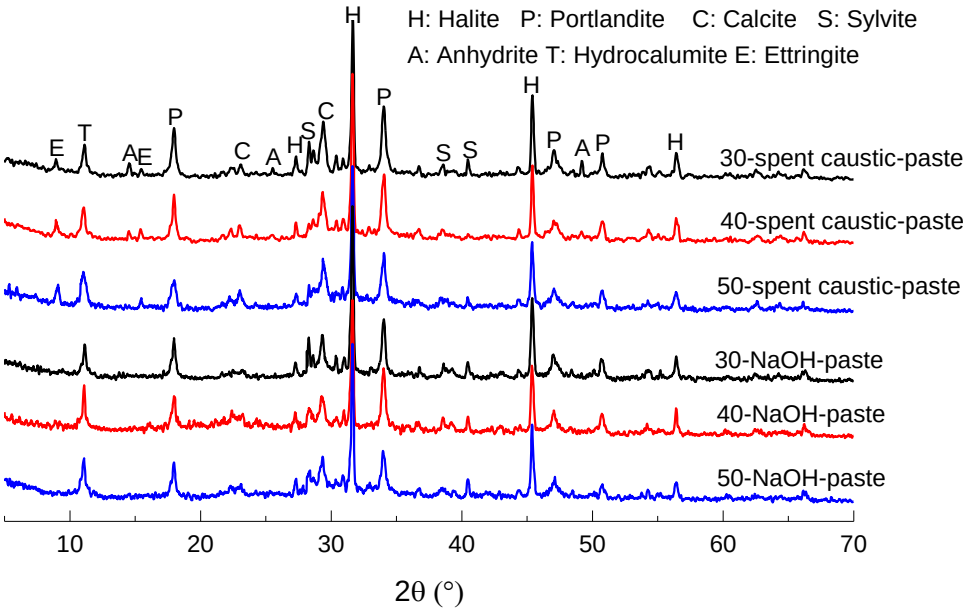

Figure 3.4.1. XRD spectra of spent caustic-activated MSWI fly ash-based pastes (spent caustic-pastes) and NaOH-activated MSWI fly ash-based pastes (NaOH-pastes) synthesized with the varying dosage of BFS (30%, 40%, and 50%)

3.4.1.2. Fourier transform infrared (FTIR) spectroscopy

FTIR spectroscopy was usually used to investigate the chemical covalent bond's vibration environment, by which some chemical covalent of organics could be detected in spent caustic-pastes. Figure 3.4.2 gives the FTIR spectra of spent caustic-pastes and NaOH-pastes synthesized with the varying dosage of BFS. The absorption bands that occurred in the 3400–3700 cm^{-1} region are characteristic of the stretching vibration of O-H (Yi et al., 2020, 2019). The sharp absorption band at 3644 cm^{-1} is assigned to the O-H in portlandite (Stoch et al., 1999). The broadband located at 3440 cm^{-1} is assigned to stretching vibration of water lattice in C-(A)-S-H, and the band at 1640 cm^{-1} is assigned to its bending vibrations (Baharom and Mamat, 2015). The bands at 1420, 875 and 713 cm^{-1} are assigned to the vibration of CO_3^{2-} in calcite (Lodeiro et al., 2009; Zhu et al., 2018). The band around at 998 cm^{-1} is asymmetric stretching vibration of Si-O-T (T is tetrahedral Si or Al) in N-A-S-H gel (Wan et al., 2017c). The band at 954 cm^{-1} is attributed to C-(A)-S-H gel (Baharom and Mamat, 2015). Obviously, the band's intensity at 954 cm^{-1} is much stronger than that at 998 cm^{-1}, indicating that the dominant C-A-S-H gel was formed in both species' pastes. The band at 620 cm^{-1} is assigned to Si-O-Al bending vibrations in N-A-S-H gel (Nogami et al., 1989).

Different bands occurred in spent caustic-pastes (marked by the grey rectangle). The bands at 2957, 2925, 2845 and 1460 cm^{-1} are due to asymmetric stretching of CH_3, asymmetric stretching of CH_2, symmetric stretching of CH_2 and bending vibration of C–H, respectively (Coelho et al., 2006; Mansur et al., 2008; Palaniappan and Pramod, 2010; Peng et al., 2020). This may be because spent caustic contains large amounts of organics, as shown in Figure 2.1.9. The band at 1120 cm^{-1} in spent caustic-pastes is attributed to the presence of SO_4^{2-} in spent caustic, corresponding to the formed anhydrite and ettringite in spent caustic-pastes (Böke and Akkurt, 2003). This result is well consistent with the XRD analysis (Figure 3.4.1).

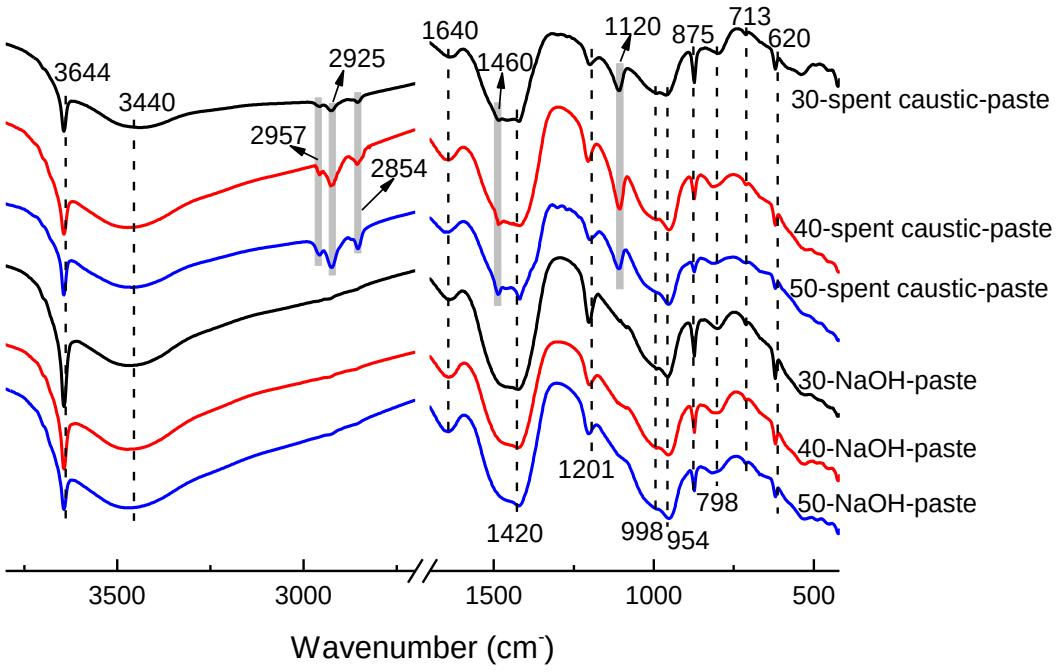

Figure 3.4.2. FTIR spectra of spent caustic-activated MSWI fly ash-based pastes (spent caustic-pastes) and NaOH-activated MSWI fly ash-based pastes (NaOH-pastes) synthesized with the varying dosage of BFS (30%, 40%, and 50%)

3.4.1.3. Nuclear magnetic resolution (NMR) spectra

In alkaline activation reaction, the formed cementitious binders are N-A-S-H and C-(A)-S-H gel (Criado et al., 2007; Tian et al., 2020d), which can't be detected by XRD owing to most of them are non-crystalline (Wang et al., 2005). The short-range ordering and molecular structure of AAMs have been investigated with great success using NMR spectroscopy (Duxson et al., 2005). It is thus an effective tool in exploring amorphous gel in AAMs. The lack of spectral resolution for silicon in AAMs has been overcome by adopting Gaussian peak deconvolution to separate and quantify Qn(mAl) species ($0 \leqslant m \leqslant n \leqslant 4$, n = integer) (S.K. Lee, 1999). The resonances at -71 and -73 ppm were due to the presence of two different types of isolated silicate (Q^0). According to assignment in reference papers (Cong and Kirkpatrick, 1996; Singh et al., 2005; Wieker et al., 1982), the Q^0 usually resonates from -66 to -74 ppm. This is because isolated silicate can be bonded to Ca^{2+}, $Na^{+,}$ and H^+ as charge-balancing sites (Le Saoût et al., 2011). Therefore, the distinct

bonding environments cause a different chemical shift of the Q^0 site. The same is true that the resonances at -77 and -79 ppm were assigned to the end-chain groups (Q^1) in C-(A)–S–H gels due to it can either be bonded to Si or Al (Bernal et al., 2013). The resonance at -87.8 ppm was assigned to the middle-chain (Q^2) in C-S-H gel, and the resonance at -82 ppm was assigned to Q^2 (1Al) when Al substitute for Si in Q^2 (Singh et al., 2005). The resonance at -84, -89.and -93 ppm were assigned to Q^4 (4Al), Q^4 (3Al), and Q^4 (2Al) in N-A-S-H gel, respectively (Wan et al., 2020).

Figure 3.4.3 gives the ^{29}Si NMR spectra of BFS, spent caustic-pastes and NaOH-pastes. The Si site in BFS is predominantly composed of Q^0, which are well consistent with other studies (Schneider et al., 2001; Wang and Scrivener, 2003) The spectra of BFS exhibited a certain tendency to a higher frequency. This may be attributed to some extent of crosslinking between silicate monomers. Table 3.4.1 gives the ^{29}Si deconvolution of spent caustic-pastes and NaOH-pastes synthesized with the varying dosage of BFS. After the alkaline activation reaction, the percentage of Q^0 decreased sensibly in two species' pastes, indicating alkaline activation reaction occurred in both species' pastes. The gel formed in both species is mainly C-(A)-S-H gel. This is consistent with the study that the major C-(A)-S-H gel formed in alkali-activated BFS pastes (Fernández - Jiménez et al., 2003; Huanhai et al., 1993). Comparing to spent caustic-pastes, NaOH-pastes contains more Al-rich N-A-S-H gel with a predominance of Q^4 (4Al) environment, whereas less C-(A)-S-H gel. This can be attributed to the high pH environment caused by the NaOH alkaline activator, which inhibits the dissolution of calcium ion and thus the formation of C-(A)-S-H (S Alonso and Palomo, 2001).

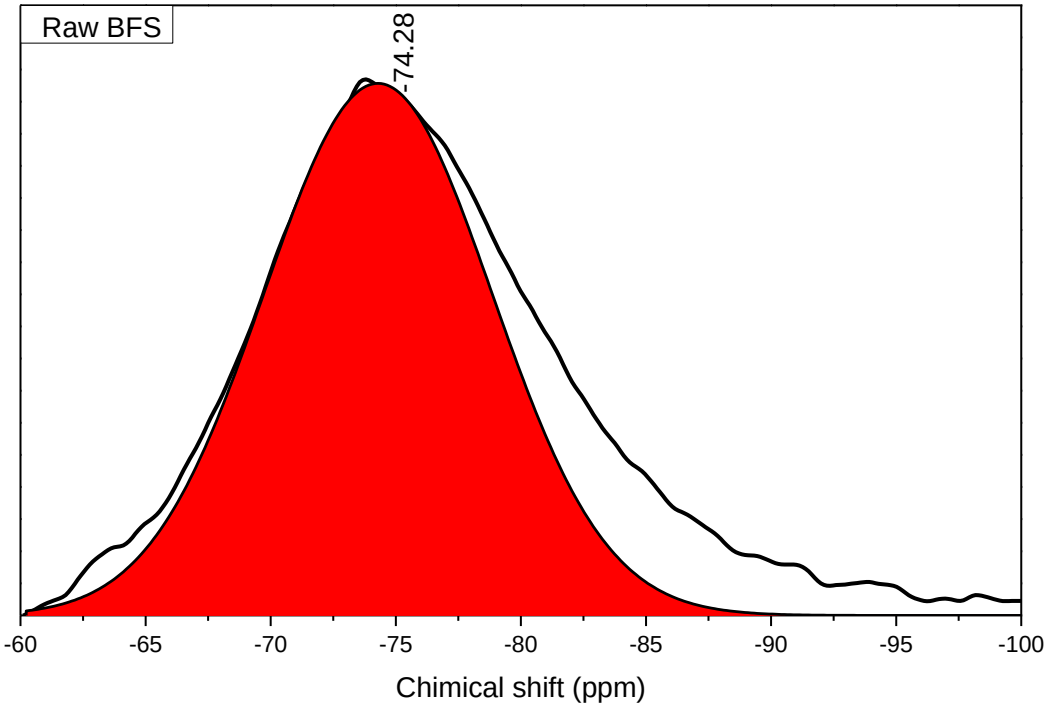

Table 3.4.1. ^{29}Si deconvolution of spent caustic-pastes and NaOH-pastes synthesized with the varying dosage of BFS (%)

Components	Q^n (mAl)	30-spent caustic-paste	40-spent caustic-paste	50-spent caustic-paste	30-NaOH-paste	40-NaOH-paste	50-NaOH-paste
Isolated silicate	Q^0	10.5	12.46	7.71	10.80	12.03	9.11
C-(A)-S-H gel	Q^1	41.44	38.89	39.99	38.46	36.87	38.08
	Q^2(1Al)	22.72	25.74	30.51	22.02	22.87	23.89
	Q^2	8.06	6.76	7.73	6.53	6.05	5.56
N-A-S-H gel	Q^4(4Al)	11.95	12.65	9.52	17.92	17.12	17.62
	Q^4(3Al)	2.97	2.27	3.26	2.27	2.80	3.95
	Q^4(2Al)	2.36	1.23	1.25	1.93	2.29	1.80

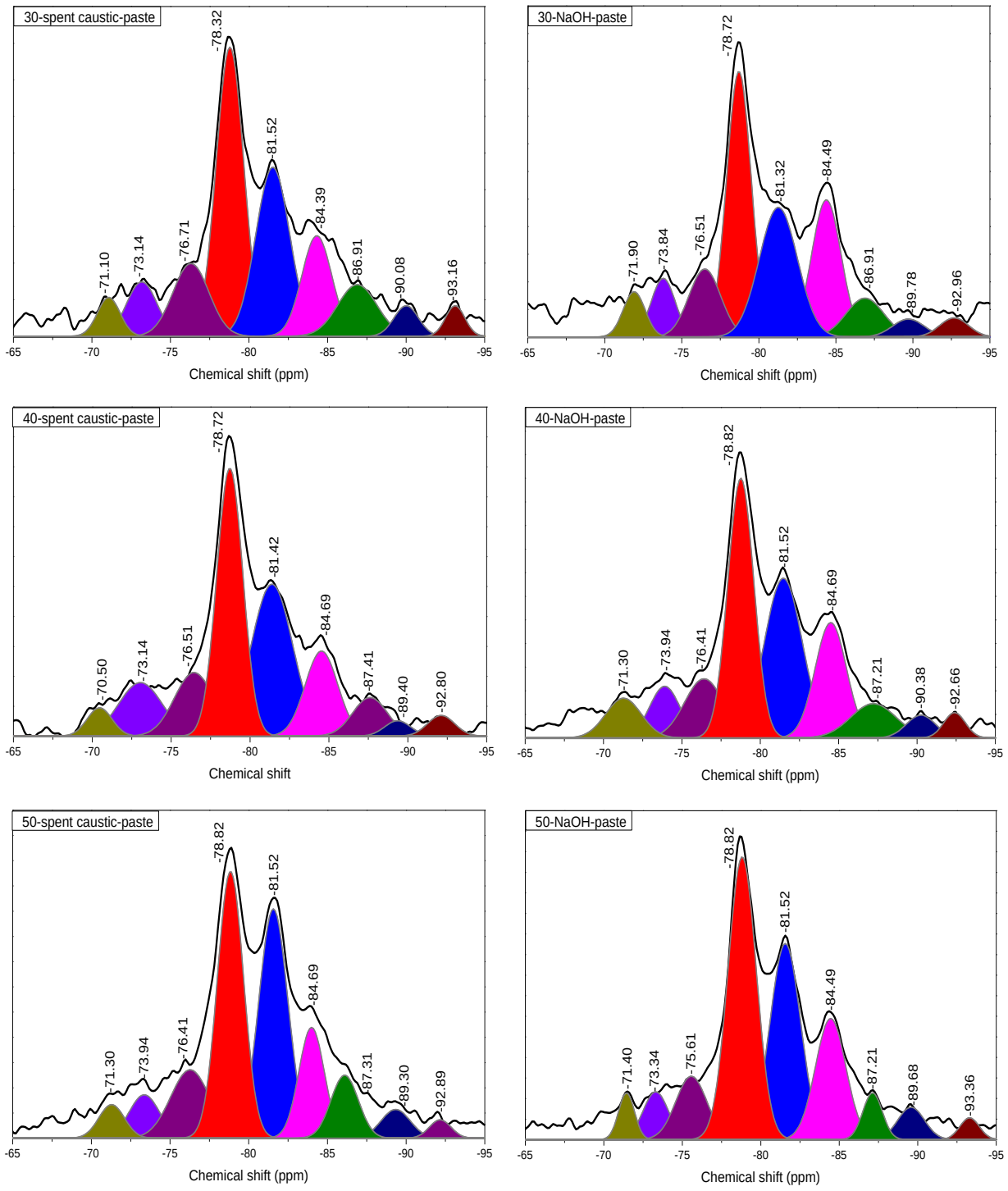

Figure 3.4.3 ^{29}Si NMR spectra of raw BFS, and spent caustic-activated MSWI fly ash-based pastes (spent caustic-pastes) and NaOH-activated MSWI fly ash-based pastes (NaOH-pastes) synthesized with the varying dosage of BFS (30%, 40%, and 50%)

3.4.1.4. Compressive strength

Figure 3.4.4 shows the compressive strength of spent caustic-pastes and NaOH-pastes synthesized with the varying dosage of BFS. The compressive strength of spent caustic-pastes is much higher than their counterpart NaOH-pastes. Some possible factors may contribute to this result. Firstly, ettringite formation can enhance the compressive strength of alkaline activation materials (Sebök et al., 2001). Secondly, the presence of organics in spent caustic facilitates the improvement of compressive strength. Many researchers studied that organics (e.g., polypropylene and polyvinyl alcohol) as additives can improve the mechanical compressive strength of alkaline activation materials because organics can control the generation of cracks through by bonding effect between cracks and increasing the fracture toughness of the brittle alkaline activation materials. (Dias and Thaumaturgo, 2005; Ferone et al., 2013; Li and Xu, 2009). Thirdly, NaOH-pastes produced more Al-rich N-A-S-H gel (Q^4 (4Al)) than that in spent caustic-pastes, which usually exhibited low compressive strength (Ferna et al., 2006; Tian et al., 2020a). Therefore NaOH-pastes exhibited lower compressive strength than spent caustic-pastes. Lastly, Na_2CO_3 contained in spent caustic can enhance the compressive strength of alkaline activated materials. Jiao et al. studied the combined effect of Na_2CO_3 and NaOH as an alkaline activator in the synthesis of alkali-activated slag pastes. They concluded that the increase of Na_2CO_3 in the combined activator prolong the setting time, whereas increased the compressive strength (Jiao et al., 2019, 2018). In spent caustic, the major alkaline activated composition is Na_2CO_3, resulting in a higher compressive strength of spent caustic-pastes.

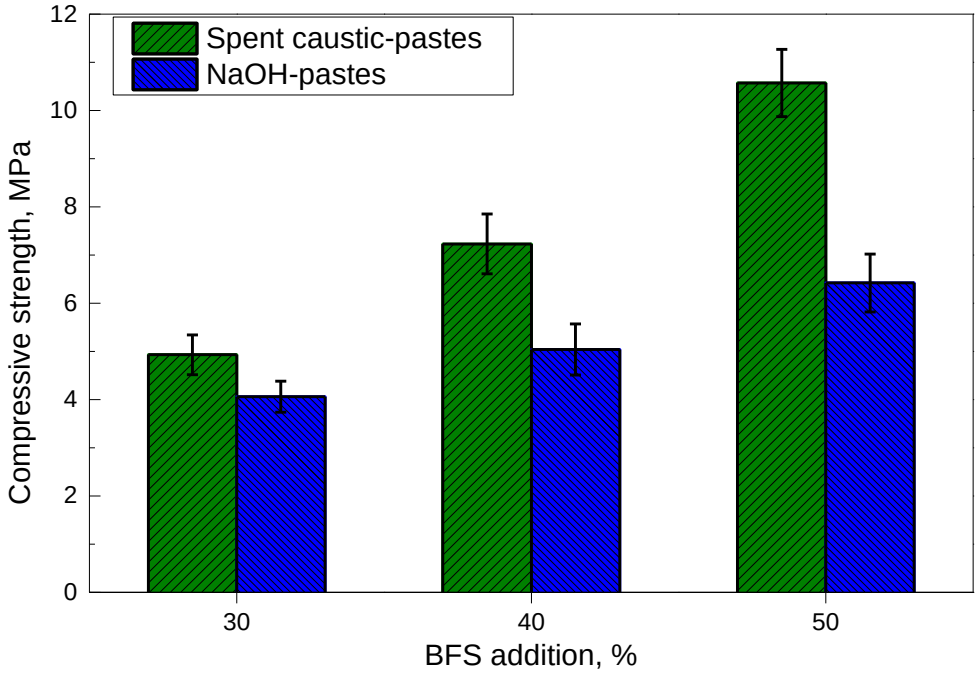

Figure 3.4.4. Compressive strength of spent caustic-pastes and NaOH-pastes synthesized with the varying dosage of BFS

3.4.1.5. Scanning electron microscope (SEM) morphological analysis

Figure 3.4.5 gives the fracture surface SEM image of spent caustic-pastes and NaOH-pastes. As can be seen, both species' pastes exhibit quite different morphology. In spent caustic-pastes, large amounts of needle structure were produced, which can be attributed to ettringite formation (X. Liu et al., 2018). In NaOH-pastes, some unreacted particles were exposed to the fracture surface, whereas none of them presented in spent caustic-pastes. This indicates the unreacted particles are a weakness in NaOH-pastes. Under high pressure, the pastes break in the surface containing the unreacted particles. However, the fracture surface of spent caustic-pastes seldom presented unreacted particles. This may be due to the reaction in spent caustic-pastes increased the adhesion between unreacted particles and gel, thus strengthening the weakness. This result is well consistent with compressive strength.

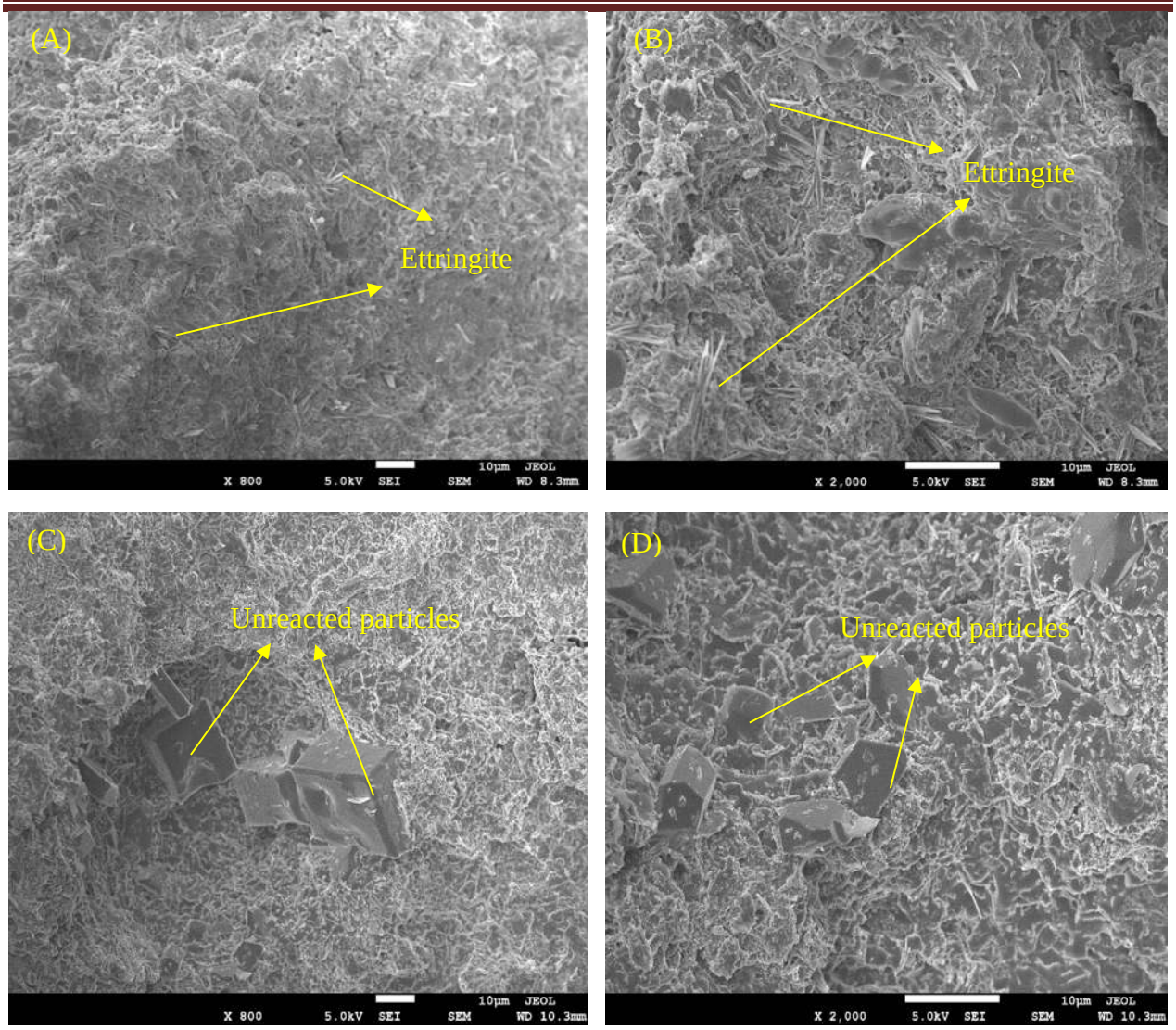

Figure 3.4.5. Fracture surface SEM image of spent caustic-pastes and NaOH-pastes. (A) (B): spent caustic-pastes, and (C) (D): NaOH-pastes

3.4.2. Immobilization of heavy metals and organics

3.4.2.1. Static pH leaching test for MSWI fly ash

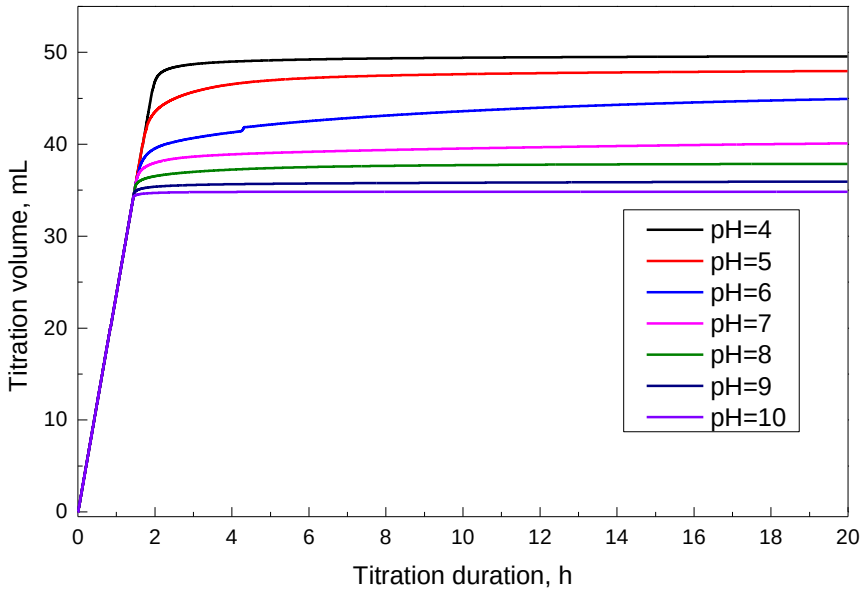

Figure 3.4.6. Static pH titration curves of MSWI fly ash

MSWI fly ash contains a large number of alkaline substances, i.e., hydroxide and carbonate. When it was exposed to landfill, these substances exhibited the buffering capacity against acidification called acid neutralization capacity (ANC), through which the long-term heavy metals leaching behavior could be analyzed because it is related to the precipitation/dissolution of heavy metals (Quina et al., 2009). In the previous study, pH = 7 (ANC_{pH7}) and pH = 4 (ANC_{pH4}) were considered as reference pH to evaluate ANC (Quina et al., 2008b). Figure 3.4.6 shows the static pH titration curves of MSWI fly ash. Calculated by the titration data, the ANC_{pH7} and ANC_{pH4} are 10.01 meq g^{-1} and 12.39 meq g^{-1}, respectively. This value is much higher than that was reported by (Quina et al., 2008b), in which the estimated ANC_{pH7} ranged 4.2 from 6.3 meq g^{-1}, and ANC_{pH4} ranged from7.6 to 9.3 meq g^{-1}. This may be attributed to different sample collection locations in the current study that the used MSWI fly ash only collected from the acidic gas purification process. According to Phua et al. (2019), most incineration plants collect the horizontal flue fly ash (generated prior to the acidic gas purification process) and air pollution control (APC) residues (generated during the acidic gas purification process) together. Therefore, researchers refer to these two residues as

MSWI fly ash and study them together. However, compared to horizontal flue fly ash, APC residues are of higher alkalinity due to the hydrated lime was added in the capturing of acid gases in the purification process. The mixture of horizontal flue fly ash significantly dilutes the alkalinity of APC residues. This causes MSWI fly ash to be studied in the current study to present a much higher ANC than in the previous studies.

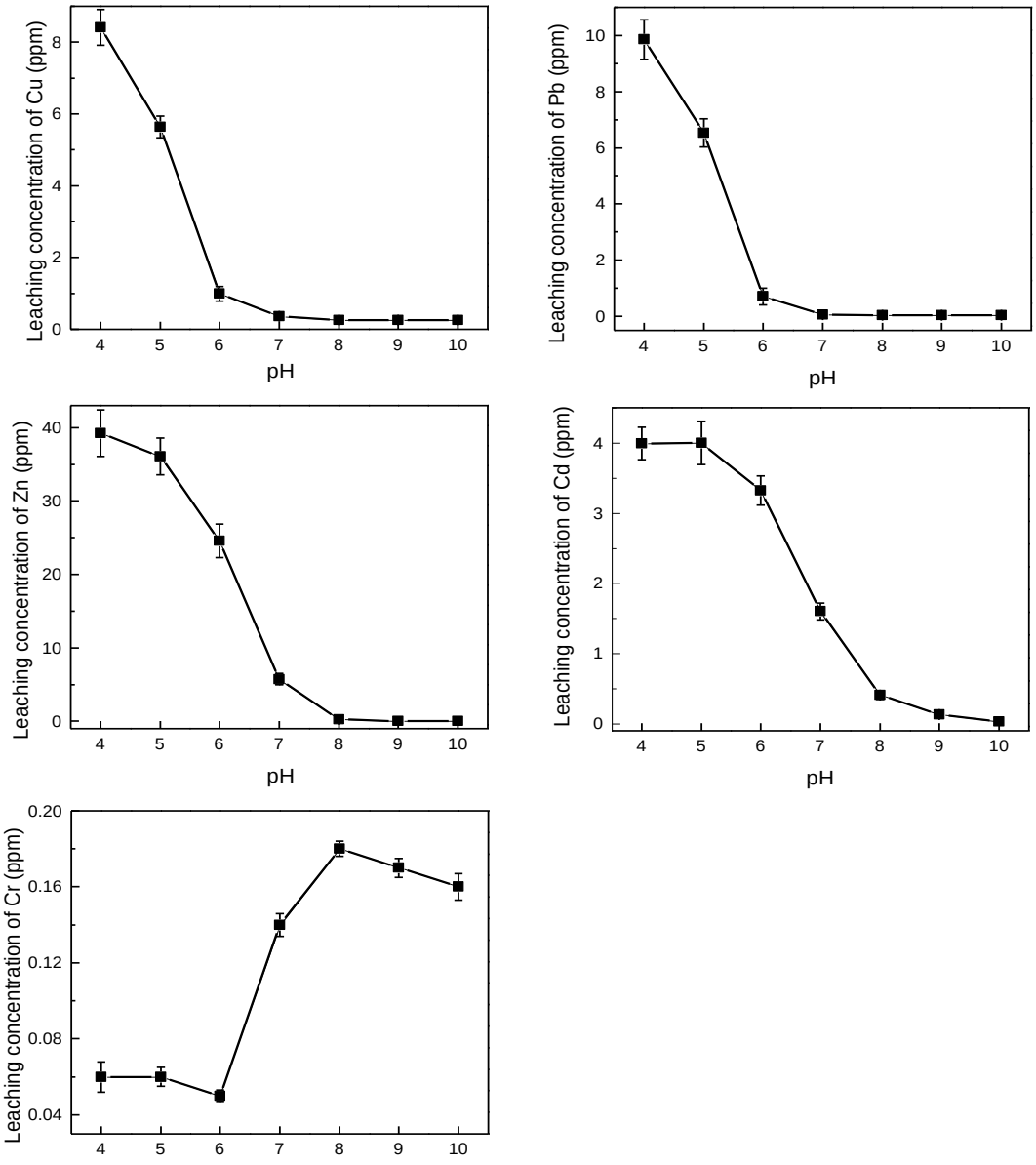

Figure 3.4.7. Leaching concentration of heavy metals in MSWI fly ash under varying pH

3.4.2.2. Heavy metals immobilization

Table 3.4.2. Leaching concentration and leaching ratio of heavy metals in MSWI fly ash

Heavy metals	Cu	Pb	Zn	Cd	Cr(VI)
Leaching concentration	13.06	16.97	54.90	6.03	0.18
Leaching ratio (%)	69.7	32.37	39.02	61.85	2.32
Limit (mg/L)	100	5	100	1	5

Table 3.4.3. Leaching concentration and immobilization efficiency of heavy metals in spent caustic-activated MSWI fly ash-based pastes (spent caustic-pastes) and NaOH-activated MSWI fly ash-based pastes (NaOH-pastes) synthesized with the varying dosage of BFS (30%, 40%, and 50%)

Samples	Leaching concentration (ppm)					Immobilization efficiency (%)			
	Cu	Pb	Zn	Cd	Cr(VI)	Cu	Pb	Zn	Cd
30-spent	4.59	4.37	36.63	3.00	0.21	49.98	63.21	4.68	28.93
40-spent	2.34	2.86	30.08	1.99	0.24	70.14	71.91	8.68	45.00
50-spent	1.09	0.94	24.81	0.95	0.22	83.31	88.92	9.63	68.49
30-NaOH-	3.08	3.62	33.83	2.43	0.28	66.31	69.52	11.96	42.43
40-NaOH-	1.85	2.59	27.92	1.56	0.27	76.39	74.56	15.24	56.88
50-NaOH-	0.64	0.65	22.89	0.63	0.26	90.20	92.34	16.61	79.10

Figure 3.4.7 shows the leaching concentration of heavy metals in MSWI fly ash under varying pH. As can be seen, the leaching concentration of heavy metals is strongly dependent on the pH value.

Cu, Pb, Zn and Cd are rarely leached out as pH higher than 6, 6, 7 and 8, respectively. Many published papers reported that minimal solubility of Pb and Zn occurred in the range pH of 8.5-10 and 9-10, respectively. They also found that when pH higher than 10, the leaching of Pb and Zn would increase, thereby presenting a "V-shaped" amphoteric nature (Benassi et al., 2016; Quina et al., 2009). Zhou et al. reported that the leaching concentration of Pb is higher as MSWI fly ash was extracted with water than that with an aggressive condition (pH=4) (Zhou et al., 2017). Therefore, it is noteworthy that the high solubility of Pb and Zn at the natural condition (pH＞12). The leaching concentration of Cu and Cd steadily increased with decreasing pH value. This is well consistent with the previous study that the Cu and Cd did not show amphoteric nature under a wide pH range from 2 to 14, and reach the maximum leaching concentration under most aggressive acid conditions (Y. Zhang et al., 2016). The maximum leaching concentration of Cr occurred at the pH of 8, which differs from the previous study that the leaching concentration under the acid and basic conditions are higher than that in the neutral condition (Zhou et al., 2017). Cr exhibits two valence states in the environment, thus more complex leaching behavior. Sperling et al. (1992) found that the predominant species in solution to control leaching is CrO_4^{2-} as pH higher than 7; and the Cr (III) compounds are rarely soluble as pH above 5. This result suggests that the CrO_4^{2-} dominates the leaching behavior of Cr in the MSWI fly ash.

Table 3.4.2 gives the heavy metals leaching concentration of MSWI fly ash extracted by HJ/T 300–2007. The leaching concentration of Cu, Pb, Zn, Cd and Cr is 13.06, 16.97, 54.90, 6.03 and 0.18 mg/L, respectively, corresponding to leaching ratio of 69.7%, 32.37%, 39.02%, 61.85% and 2.32%, respectively. The leaching ratio difference is attributed to different chemical speciation of each heavy metal in MSWI fly ash, which will be further discussed in the later part. Analyzed by UV-vis spectrophotometer, the soluble Cr in eluate predominantly exists as Cr (VI). This result is well consistent with the study that Cr (VI) is the most available Cr species in MSWI fly ash (Zhou et al., 2017). It is noteworthy that the leaching concentration of Pb and Cd exceeds the acceptable limit of the environment.

Table 3.4.3 shows the leaching concentration and immobilization efficiency of heavy metals in spent caustic-pastes and NaOH-pastes synthesized with the varying dosage of BFS. Compared to raw MSWI fly ash, the leaching concentration of Cu, Pb, Zn and Cd in both species' pastes

decreased sensibly, indicating an outstanding heavy metals immobilization effect by alkaline activation reaction. However, the leaching concentration of Cr in both species' pastes is slightly higher than that in raw MSWI fly ash. This may be due to comparable Cr content contained in BFS with that in raw MSWI fly ash, contributing to the amount of leaching of Cr (VI). Alkali-activated BFS binders exhibited effective immobilization for Cr (VI) due to it could reduce Cr (VI) to rarely soluble Cr (III) by the redox environment caused by the addition of BFS (Zhang et al., 2017). The increase of leaching concentration of Cr (VI) in pastes may be attributed to Cr (VI) content introduced by BFS surpasses that it could reduce. With the BFS addition from 30% to 50%, the immobilization efficiency of Cu, Pb, Cd and Zn in both species' pastes increased. This suggests that the leaching concentration decrease with the increase of BFS dosage is not only a dilution effect by incorporating BFS, but also an immobilization effect caused by alkaline activation reaction. Regardless of the alkaline activator used, the immobilization efficiency of Cu and Pb is much higher than that of Zn and Cd, which indicates the both species' pastes are of better immobilization effect for Cu and Pb than Zn and Cd. This is well consistent with studies that Cu and Pb were more effectively immobilized than Cd in alkali-activated pastes (El-Eswed et al., 2017; Zhang et al., 2008). However, the immobilization efficiency of Zn in the current study (around 10%) is much lower than other studies that the immobilization efficiency of Zn reached 99.99% in alkali-activated pastes (Kirkpatrick et al., 2002; Kiventerä et al., 2018). This may be attributed to different extraction methods that the TANK method and European standard EN 12457 were used in their studies, in which the extraction liquid is only water. This could lead to Zn in the form of hydroxide retained in pastes due to the alkaline environment caused by alkaline added in alkaline activation reaction. In the current study, much aggressive extraction was used, which significantly increased the leachability of heavy metals. Another study found that the immobilization of Zn mainly depends on the physical and adsorption by generated gel (Wan et al., 2019a). These ways are less effective because they depend on the porosity of the matrix and the changes in water ionic composition that is likely to affect sorption-desorption processes. The aggressive acid conditions in the current study dissolved the hydroxide and significantly promoted the desorption of Zn, resulting in the low immobilization efficiency. With 50% BFS addition, both species' pastes meet the environmental requirement that the leaching concentration of all the heavy metals lower than the acceptable limit of the environment.

Compared to the counterpart NaOH-pastes, spent caustic-pastes exhibited slightly higher leaching concentration for Cu, Pb, Zn and Cd, and slightly lower leaching concentration for Cr (VI). This is because the presence of organics could promote heavy metals leaching by forming heavy metal-organic complexes with high mobility in water (Arickx et al., 2010; Luo et al., 2019). Substantial organics in spent caustic-pastes may enhance the leaching for Cu, Pb, Zn and Cd. The lower leaching concentration for Cr (VI) in spent caustic-pastes may be attributed to two factors. Firstly, the ettringite formed in spent caustic-pastes (Figure S4) could uptake oxyanion $CrO4^{2-}$ by isomorphous substitution to form solid solution phase (Chrysochoou and Dermatas, 2006), which is a crucial mechanism for Cr (VI) leaching control. Secondly, the presence of organics in spent caustic-pastes could be reducing agents for Cr (VI) being reduced to Cr (III) (Abbas et al., 2001; Sabbas et al., 2003). The Cr (III) compounds are sparingly soluble and thus control the leaching of Cr. This result indicates spent caustic-pastes, compared to NaOH-pastes, are of weaker immobilization effect for Cu, Pb, Zn and Cd, and better immobilization effect for Cr (VI).

3.4.2.3. BCR chemical speciation analysis

In BCR speciation analysis, five fractions of heavy metals exhibit different risk releases in the environment. The water-soluble fraction presents in the form of soluble salt and would directly dissolve in water solution. The exchangeable fraction contains the content that is adsorbed on the surface of MSWI fly ash by complexation and diffusion and that co-precipitate with the carbonate in the MSWI fly ash. This fraction would be susceptible to variation in pH and can be extracted by ion exchange under weak acid conditions (Tessier et al., 1979). The reducible fraction represents the content bound to iron and manganese oxides that could be released as subjected to more reducing conditions (Usero et al., 1998). The oxidizable fraction refers to the content bound to the organic matter and sulfur species, which would be released oxidizing environment (Li et al., 2014). The residual fraction is usually assigned to heavy metals being hold in the mineral lattice, which could exist stably under the conditions normally encountered in nature (Tessier et al., 1979). The change of chemical fractions can be used to assess the immobilization effect of alkali-activated pastes (Ji and Pei, 2020).

Figure 3.4.8 shows the chemical speciation of heavy metals in raw MSWI fly ash, spent caustic-pastes and NaOH-pastes synthesized with the varying dosage of BFS. In raw MSWI fly ash, heavy

metals rarely exhibited in water-soluble fraction, suggesting they rarely exist in the form of soluble salt. This explained the results in previous studies that water washing is less effective for removing heavy metals in MSWI fly ash (Chiang and Hu, 2010; Colangelo et al., 2012; Wang et al., 2001). In the bioavailable fractions, Cu, Zn and Cd mainly present in the reducible fraction, whereas Pb is mainly distributed in exchange fraction. Similar data were found in (Li et al., 2014). This indicates that heavy metals have certain orientations to form certain compounds in MSWI fly ash. Cr (VI) exist in most residual fractions, making it the least bioavailable metal. The residual fraction of Cu, Pb, Zn, Cd and Cr accounted for 19.76%, 59.57%, 48.84%, 35.87% and 96.12%, respectively. In consideration of residual fraction unavailable for leaching, this data indicate that heavy metal bioavailability in the environment followed the order of Cu > Cd >Zn> Pb > Cr (VI). This result is well corresponding to the leaching ratio of heavy metals in MSWI fly ash extracted by HJ/T 300–2007 test (Table 3.4.3), in which the leaching ratio of Cu, Cd, Zn, Pb and Cr are 69.7%, 61.85%, 39.02%, 32.37% and 2.32%, respectively.

Compared to heavy metals chemical speciation in raw MSWI fly ash, Cu, Pb, Zn and Cd transferred into more stable speciation in both species' pastes. However, the magnitude of each speciation in each heavy metal was changed differently. For spent caustic-paste with the 30% BFS addition, most of the reducible fractions of Cu was transferred into residual fraction, leading to the residual fractions sensibly increase from 19.76% to 60.39%. For Pb, the main speciation change occurred from exchangeable fractions into residual fractions, which causes an increase of residual fractions from 59.57% to 85.09%. Zn and Cd exhibit similar tendencies, in which the speciation change mainly occurred from a slight amount of reducible fractions transferred into residual fractions, causing the slight increase of residual fractions from 48.84% to 56.99% for Zn, and from 35.87% to 52.39% for Cd. The increase of residual fraction indicates more heavy metals being hold in the mineral lattice. It has been reported that Cu-O, Pb-O and Si-O bonds have similar ionic character of about 45%, while Zn-O, Cd-O and Al-O have similar ionic character of about 55% (El-eswed, 2020). According to Goldschmidt rules, when ions have similar electronegativity, they are possible to substitute each other and form bonds with similar ionic character (Hautier et al., 2011). This allows Cu and Pb, which are of similar electronegativity to Si, to substitute Si in the N-A-S-H gel network, whereas Cd and Zn could not undergo such substitution because the ionic character Cd-O and Zn-O is about 55% (El-eswed, 2020). This substitution makes more Cu and Pb transferred

into residual fractions than Zn and Cd. This further explained the HJ/T 300–2007 extraction test results that Cu and Pb exhibited higher immobilization efficiency than Zn and Cd. Differently, the residual fractions of Cr (VI) have a slight decrease from 96.12% to 95.08%, which also explained Cr VI) leaching concentration slightly increased in pastes.

With BFS addition from 30% to 50%, the residual fractions of Cu, Pb, Zn and Cd increased persistently, which from 60.39% to 85.15%, 85.09% to 91.97%, 56.99% to 63.51 and 52.39% to 71.00%, respectively. This confirmed that BFS addition enhanced the immobilization effect for heavy metals. Compared to spent caustic-pastes, the counterpart NaOH-pastes exhibited slightly higher residual fractions for Cu, Pb, Zn and Cd, whereas slightly lower residual fractions for Cr (VI). This data once again verified the results that spent caustic-pastes are of weaker immobilization effect for Cu, Pb, Zn and Cd, and better immobilization effect for Cr (VI) compared to NaOH-paste.

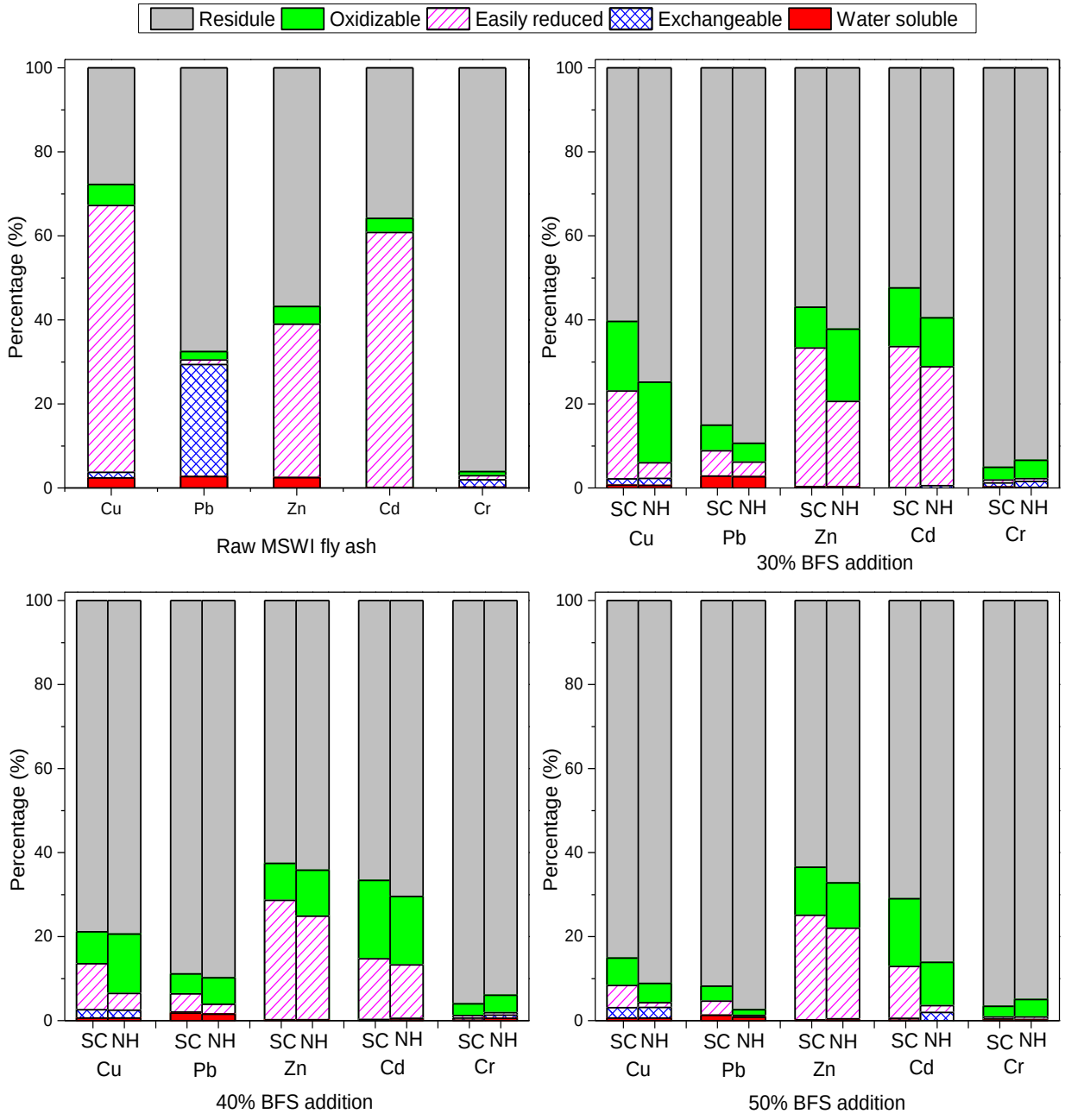

Figure 3.4.8. Chemical speciation of heavy metals in raw MSWI fly ash, spent caustic-activated MSWI fly ash-based pastes (spent caustic-pastes) and NaOH-activated MSWI fly ash-based pastes (NaOH-pastes) synthesized with the varying dosage of BFS (SC: spent caustic-pastes, NH: NaOH-pastes)

3.4.2.3. Organics immobilization

Table 3.4.4. TOC of spent caustic, of raw MSWI fly ash eluate contributed by MSWI fly ash and of spent caustic-pastes eluate contributed by pastes

Materials	Spent caustic	MSWI fly ash	30-spent caustic -paste	40-spent caustic -paste	50-spent caustic -paste
TOC (mg/L)	3561	52	43	38	27

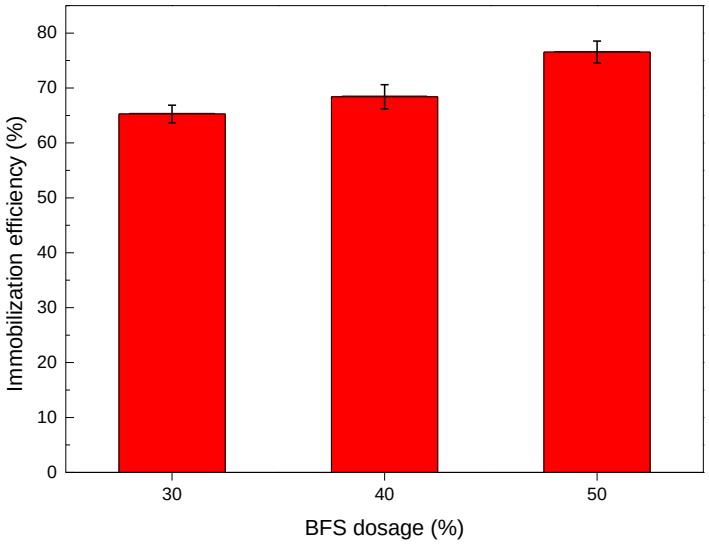

Figure 3.4.9. The organics immobilization efficiency of spent caustic-activated MSWI fly ash-based pastes synthesized with the varying dosage of BFS

Leached organics from pastes could be quantified by means of measuring total organic carbon (TOC) (Luo et al., 2019). Table 3.4.4 gives the TOC of spent caustic, of raw MSWI fly ash eluate contributed by MSWI fly ash and of spent caustic-pastes eluate contributed by pastes. The TOC of spent caustic is 3561mg/L, indicating large quantities of organics in it. The TOC of MSWI fly ash eluate contributed by MSWI fly ash is 52 mg/L, equivalents to 1.04 mg/g organics leached out from MSWI fly ash. The TOC of spent caustic-pastes eluate contributed by pastes is 43, 38 and 27 mg/L as the addition of BFS of 30%, 40% and 50%, respectively. Figure 3.4.9 gives the organics

immobilization efficiency of spent caustic-pastes calculated by Eq. (2.4.10). The immobilization efficiency of organics is 65.72%, 68.40% and 76.53% as the addition of BFS of 30%, 40% and 50%, respectively. The previous study reported that the immobilization of organics mainly relies on the adsorption by zeolite-like structure produced in alkaline activation reaction (C.Gokhale, n.d.). Also, alkaline activation material is an effective encapsulation matrix for the retention of organics due to its low porosity (Al-Mashaqbeh et al., 2018). Al-Mashaqbeh et al. (2018) studied the utilization of a metakaolin-based geopolymer to immobilize organics, i.e., methylene blue, acid blue, Congo red and crystal violet. It was found that all the organics were effectively immobilized and the immobilization efficiency higher than 94%. However, in the current study, organics immobilization efficiency is much less than 94%. This may be due to alkali-activated MSWI fly ash-based pastes containing substantial salts and heavy metals (Figure 3.4.2). Many published papers confirmed that the presence of chloride (e.g., KCl and NaCl) retards the formation of N-A-S-H gel in alkaline activation system (Lee and Van Deventer, 2002a, 2002b; Zheng et al., 2011), and the migration of K^+, Na^+ and Cl^- in the leaching process causes the visual cracks of matrix (Zheng et al., 2011). The organics usually penetrated the alkali-activated matrix (Ferone et al., 2013); the dissolution of salts in pastes may facilitate the leaching of organics bonded in pastes. Additionally, the formation of heavy metal-organic complexes facilitated the leaching because of their high mobility in water. The presence of salts and heavy metals in spent caustic-pastes weakens the immobilization capacity of alkaline activation matrix for organics.

Table 3.4.5. Organics identified in spent caustic and 50-spent caustic-paste eluate

Retention time, min	Compounds	C.A.S. No.	Probability, %
2.380	Cyclopropyl carbinol	002516-33-8	90
4.324	2,4-Dimethylamphetamine	075659-61-9	59
4.569	Methylene chloride	000075-09-2	95
7.192	Trichloromethane	000067-66-3	64

8.190	Benzene	000071-43-2	91
13.603	Cyclotrisiloxane-hexamethyl-	000541-05-9	83
20.056	Stannane-tributylmethyl-	001528-01-4	90
22.730	1-Pentene-4,4-dimethyl-	000762-62-9	49
24.309	2-Amino-4-methylphenol	1000373-28-1	90
27.701	Benzothiazole	000095-16-9	93
30.608	Cyclotrisiloxane-hexamethyl-	000541-05-9	45
3.988	Sodium acetate	000127-09-3	59
17.910	2-methoxy-5-methyl-4-phenyl	107939-25-3	55

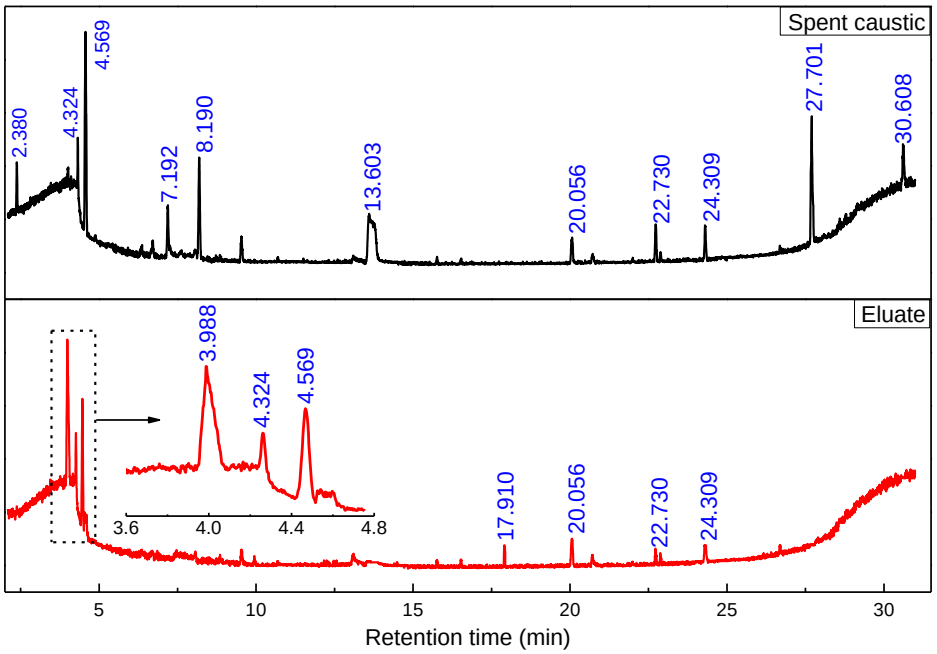

Figure 3.4.10. GC-MS chromatogram of spent caustic and eluate of 50-spent caustic-paste.

Figure 3.4.10 gives the GC-MS chromatogram of spent caustic of the 50-spent caustic-paste eluate. Spent caustic contains 11 kinds of detectable organics. However, the kind of detectable organics in the eluate decreases to 7. Table 3.4.5 gives the organics identified in the spent caustic and 50-spent caustic-paste eluate. In eluate, the sodium acetate may be attributed to acetic extraction liquid reacts with sodium salt that rich in pastes (Figure 3.4.1). The 2-methoxy-5-methyl-4-phenyl may be from MSWI fly ash owning to some toxic organics contained in it (Harmsen, 1983; Zhang et al., 2004). Previous studies found that the immobilization of organics depends on solubility (Al-Degs et al., 2008). This leads to some organics that can be effectively immobilized, and others cannot. For instance, benzene, which is insoluble in water, could be effectively immobilized; Whereas the hydrophilic 2,4-dimethylamphetamine was not immobilized. However, cyclopropyl methanol, which is easily soluble in water, also did not appear in the eluent. This indicates that the immobilization of organics does not only depend on the solubility of organics. Some other factors, such as group electronegativity and alkyl chain length, should be taken into consideration. The mechanism of the immobilization of organics should be further studied in the future.

CHAPTER 4.

Conclusions

1) The MSWI fly ash is a CaO-SiO_2-Al_2O_3-SO_3-Cl based system which is rich in the elements of calcium, chlorine and sulfur, and relatively have scarcity in silicon and aluminum. Meanwhile, it contains a large amount of heavy metals that threaten the environment and eco-systems.

2) In the solidification of MSWI fly ash through alkaline activation, metallic aluminum reacts with the alkalis and releases H_2, leading to expansion, cracks and low compressive strength of the alkali-activated MSWI fly ash-based pastes. This effect can be mitigated by optimizing the synthesis process, in which sodium hydroxide is added separately and reacted with the raw materials, and the amount used of sodium hydroxide is related to the dosage of MSWI fly ash. A small amount of aluminosilicate is required to consolidate MSWI fly ash well.

3) The crystal phases in alkali-activated MSWI fly ash-based pastes contain portlandite ($Ca(OH)_2$), halite (NaCl), anhydrite (CaSO4), sylvite (KCl) and F: Friedel's salt. The amorphous phases contain silica gel, C-(A)-S-H and N-(A)-S-H gel, which are responsible for the consolidation of MSWI fly ash.

4) The variation in aluminum dosage could lead to a modification in the compressive strength of the synthesized pastes. Additionally, the aluminum dosage can transfer the soluble chloride salt into Friedel's salt which supports the immobilization of Cr(VI). The addition of aluminum dosage affects heavy metal immobilization dominantly by changing the encapsulation ability of the pastes. A 5% metakaolin substitution in the synthesis process can improve the immobilization effect of the Cr (VI), Cu and Zn significantly. Moreover, the addition of metakaolin in synthesis process did not change the ratio of C-(A)-S-H and N-A-S-H gel in pastes, though it kicked out Q^4 (0Al) and Q^4 (1Al) conversion into Q^4 (2Al), Q^4 (3Al), and Q^4 (4Al) in N-A-S-H gel.

5) MSWI fly ash could be solidified by the addition of waste glass to form C-S-H and silica gel. The addition of waste glass effectively immobilized heavy metals in MSWI fly ash. The heavy metal immobilization mechanisms include physical encapsulation and the alkaline environment formation, as well as the generation of silicate compounds.

6) Spent caustic was of alkalinity concentration comparable to 4.416 M NaOH solution. It could be an alkaline activator in the consolidation of MSWI fly ash and immobilization of heavy metals. MSWI fly ash was successfully consolidated using spent caustic through the alkaline activation reaction. Comparing to NaOH-activated pastes, spent caustic-activated pastes formed ettringite and

more C-(A)-S-H. The spent caustic-activated pastes exhibited higher compressive strength than NaOH-activated pastes, which reached 4.93, 7.23, and 10.94 MPa as addition BFS of 30%, 40%, and 50%, respectively. Additionally, spent caustic-activated pastes exhibited weaker immobilization effect for Cu, Pb, Zn and Cd, and better immobilization effect for Cr (VI). The immobilization efficiency of Cu and Pb is higher than that of Zn and Cd in both species' pastes. With the BFS dosage increased, the heavy metals immobilization efficiency improved. The presence of salts and heavy metals in MSWI fly ash harms organics immobilization for spent caustic-activated pastes.

Recommendations for future work

In the thesis work, we focused on the consolidation of MSWI fly ash and the immobilization of heavy metals through alkaline activation reaction. The immobilization mechanism of cation was intensively investigated. However, for anion immobilization and the MSWI fly ash as a raw material in preparing road materials through alkaline activation reaction, should be conducted in future work.

References

Abbas, Z., Steenari, B.-M., Lindqvist, O., 2001. A study of Cr (VI) in ashes from fluidized bed combustion of municipal solid waste: leaching, secondary reactions and the applicability of some speciation methods. Waste Manag. 21, 725–739.

Ahmed, S.A., Metwally, M.E.A., Zakey, S.E., 2018. Utilizing industrial waste-water as alkali activator in sand-cement kiln dust bricks. Constr. Build. Mater. 182, 284–289. https://doi.org/10.1016/j.conbuildmat.2018.06.129

Al-Degs, Y.S., El-Barghouthi, M.I., El-Sheikh, A.H., Walker, G.M., 2008. Effect of solution pH, ionic strength, and temperature on adsorption behavior of reactive dyes on activated carbon. Dye. Pigment. 77, 16–23.

Al-Mashaqbeh, A., El-Eswed, B., Banat, R., Khalili, F.I., 2018. Immobilization of organic dyes in geopolymeric cementing material. Environ. nanotechnology, Monit. Manag. 10, 351–359.

Albitar, M., Ali, M.S.M., Visintin, P., Drechsler, M., 2017. Durability evaluation of geopolymer and conventional concretes. Constr. Build. Mater. 136, 374–385.

Alhadj-Mallah, M.-M., Huang, Q., Cai, X., Chi, Y., Yan, J., 2015. Vitrification of municipal solid waste incineration fly ash using biomass ash as additives. Environ. Technol. 36, 654–660.

Alipour, Z., Azari, A., 2020. COD removal from industrial spent caustic wastewater: A review. J. Environ. Chem. Eng. 8, 103678. https://doi.org/10.1016/j.jece.2020.103678

Alonso, Santiago, Palomo, A., 2001. Calorimetric study of alkaline activation of calcium hydroxide ± metakaolin solid mixtures 31.

Alonso, S, Palomo, A., 2001. Alkaline activation of metakaolin and calcium hydroxide mixtures: influence of temperature, activator concentration and solids ratio. Mater. Lett. 47, 55–62.

Arickx, S., Borger, V. De, Gerven, T. Van, Vandecasteele, C., 2010. Effect of carbonation on the leaching of organic carbon and of copper from MSWI bottom ash. Waste Manag. 30, 1296–1302. https://doi.org/10.1016/j.wasman.2009.10.016

Assi, A., Bilo, F., Zanoletti, A., Ponti, J., Valsesia, A., La Spina, R., Zacco, A., Bontempi, E., 2020. Zero-waste approach in municipal solid waste incineration: Reuse of bottom ash to stabilize fly ash. J. Clean. Prod. 245, 118779. https://doi.org/10.1016/j.jclepro.2019.118779

Aubert, J.-E., Husson, B., Sarramone, N., 2006. Utilization of municipal solid waste incineration (MSWI) fly ash in blended cement: Part 1: Processing and characterization of MSWI fly ash. J. Hazard. Mater. 136, 624–631. https://doi.org/https://10.1016/j.jhazmat.2005.12.041

Audry, S., Schäfer, J., Blanc, G., Jouanneau, J.-M., 2004. Fifty-year sedimentary record of heavy metal pollution (Cd, Zn, Cu, Pb) in the Lot River reservoirs (France). Environ. Pollut. 132, 413–426.

Avila-López, U., Almanza-Robles, J.M., Escalante-García, J.I., 2015. Investigation of novel waste glass and limestone binders using statistical methods. Constr. Build. Mater. 82, 296–303. https://doi.org/10.1016/j.conbuildmat.2015.02.085

Baharom, M.I.N.H., Mamat, C.R. Bin, 2015. Hydration and Properties of Blended Cement System Incorporatiing Aerogel.

Bakharev, T., 2005. Resistance of geopolymer materials to acid attack. Cem. Concr. Res. 35, 658–670. https://doi.org/https://10.1016/j.cemconres.2004.06.005

Bakri, A.M., Kamarudin, H., Binhussain, M., Nizar, I.K., Rafiza, A.R., Zarina, Y., 2013. Comparison of geopolymer fly ash and ordinary portland cement to the strength of concrete. Adv. Sci. Lett. 19, 3592–3595. https://doi.org/https://10.1166/asl.2013.5187

Baun, D.L., Christensen, T.H., 2004. Speciation of heavy metals in landfill leachate: a review. Waste Manag. Res. 22, 3–23.

Bayuseno, A.P., Schmahl, W.W., Muellejans, T., 2009. Hydrothermal processing of MSWI Fly Ash-towards new stable minerals and fixation of heavy metals. J. Hazard. Mater. 167, 250–259.

Benassi, L., Pasquali, M., Zanoletti, A., Dalipi, R., Borgese, L., Depero, L.E., Vassura, I., Quina, M.J., Bontempi, E., 2016. Chemical stabilization of municipal solid waste incineration fly ash without any commercial chemicals: first pilot-plant scaling up. ACS Sustain. Chem. Eng. 4, 5561–5569.

Bernal, S.A., Provis, J.L., Walkley, B., San Nicolas, R., Gehman, J.D., Brice, D.G., Kilcullen, A.R., Duxson, P., van Deventer, J.S.J., 2013. Gel nanostructure in alkali-activated binders based on slag and fly ash, and effects of accelerated carbonation. Cem. Concr. Res. 53, 127–144.

Bie, R., Chen, P., Song, X., Ji, X., 2015. Characteristics of municipal solid waste incineration fly ash with cement solidification treatment. J. Energy Inst. S1743967114204028.

Boccaccini, A.R., Schawohl, J., Kern, H., Schunck, B., Rincon, J.M., Romero, M., 2000. Sintered glass ceramics from municipal incinerator fly ash. Glas. Technol. 41, 99–105.

Boddenberg, B., 1988. High-resolution solid-state NMR of silicates and zeolites. Appl. Catal. 42, 187–188.

Böke, H., Akkurt, S., 2003. Ettringite formation in historic bath brick-lime plasters. Cem. Concr. Res. 33, 1457–1464. https://doi.org/10.1016/S0008-8846(03)00094-2

Bolan, N., Kunhikrishnan, A., Thangarajan, R., Kumpiene, J., Park, J., Makino, T., Kirkham, M.B., Scheckel, K., 2014. Remediation of heavy metal (loid) s contaminated soils–to mobilize or to immobilize? J. Hazard. Mater. 266, 141–166. https://doi.org/https://10.1016/j.jhazmat.2013.12.018

Bosshard, P.P., Bachofen, R., Brandl, H., 1996. Metal leaching of fly ash from municipal waste incineration by Aspergillus niger. Environ. Sci. Technol. 30, 3066–3070.

C.Gokhale, L.L. and . T.S.J.V.D., n.d. THE IMMOBILISATION OF ORGANIC WASTE BY GEOPOLYMERISATION.

Čarnogurská, M., Lázár, M., Puškár, M., Lengyelová, M., Václav, J., Širillová, Ľ., 2015. Measurement and evaluation of properties of MSW fly ash treated by plasma. Measurement 62, 155–161.

Cetin, B., Aydilek, A.H., Li, L., 2012. Experimental and numerical analysis of metal leaching from fly ash-amended highway bases. Waste Manag. 32, 965–978.

Chandler, A.J., Eighmy, T.T., Hjelmar, O., Kosson, D.S., Sawell, S.E., Vehlow, J., Van der Sloot, H.A., Hartlén, J., 1997. Municipal solid waste incinerator residues. Elsevier.

Chen, W., Kirkelund, G.M., Jensen, P.E., Ottosen, L.M., 2018. Electrodialytic extraction of Cr from water-washed MSWI fly ash by changing pH and redox conditions. Waste Manag. 71, 215–223.

Chen, W., Kirkelund, G.M., Jensen, P.E., Ottosen, L.M., 2017. Comparison of different MSWI fly ash treatment processes on the thermal behavior of As, Cr, Pb and Zn in the ash. Waste Manag. 68, 240–251.

Chen, X., Bi, Y., Zhang, H., Wang, J., 2016. Chlorides removal and control through water-washing process on MSWI fly ash. Procedia Environ. Sci. 31, 560–566.

Chiang, K.-Y., Hu, Y.-H., 2010. Water washing effects on metals emission reduction during municipal solid waste incinerator (MSWI) fly ash melting process. Waste Manag. 30, 831–838.

Chimenos, J.M., Fernández, A.I., Cervantes, A., Miralles, L., Fernández, M.A., Espiell, F., 2005. Optimizing the APC residue washing process to minimize the release of chloride and heavy metals. Waste Manag. 25, 686–693.

Chou, S.-Y., Lo, S.-L., Hsieh, C.-H., Chen, C.-L., 2009. Sintering of MSWI fly ash by microwave energy. J. Hazard. Mater. 163, 357–362.

Chrysochoou, M., Dermatas, D., 2006. Evaluation of ettringite and hydrocalumite formation for heavy metal immobilization: literature review and experimental study. J. Hazard. Mater. 136, 20–33.

Coelho, R.R., Hovell, I., De Mello Monte, M.B., Middea, A., De Souza, A.L., 2006. Characterisation of aliphatic chains in vacuum residues (VRs) of asphaltenes and resins using molecular modelling and FTIR techniques. Fuel Process. Technol. 87, 325–333. https://doi.org/10.1016/j.fuproc.2005.10.010

Colangelo, F., Cioffi, R., Montagnaro, F., Santoro, L., 2012. Soluble salt removal from MSWI fly ash and its stabilization for safer disposal and recovery as road basement material. Waste Manag. 32, 1179–1185.

Conesa, H.M., Pérez-Chacón, J.A., Arnaldos, R., Moreno-Caselles, J., Faz-Cano, Á., 2010. In situ heavy metal accumulation in lettuce growing near a former mining waste disposal area: implications for agricultural management. Water. Air. Soil Pollut. 208, 377–383.

Cong, X., Kirkpatrick, R.J., 1996. 29Si and 17O NMR investigation of the structure of some crystalline calcium silica hydrates. Adv. Cem. Based Mater. 3, 133–143. https://doi.org/10.1016/s1065-7355(96)90045-0

Conner, J.R., Hoeffner, S.L., 1998. A Critical Review of Stabilization/Solidification Technology. C R C Crit. Rev. Environ. Control 28, 397–462.

Criado, M., Fernández-Jiménez, A., De La Torre, A.G., Aranda, M.A.G., Palomo, A., 2007. An XRD study of the effect of the SiO2/Na2O ratio on the alkali activation of fly ash. Cem. Concr. Res. 37, 671–679.

Cyr, M., Idir, R., Escadeillas, G., 2012. Use of metakaolin to stabilize sewage sludge ash and municipal solid waste incineration fly ash in cement-based materials. J. Hazard. Mater. 243, 193–203.

Dabo, D., Badreddine, R., De Windt, L., Drouadaine, I., 2009. Ten-year chemical evolution of leachate and municipal solid waste incineration bottom ash used in a test road site. J. Hazard. Mater. 172, 904–913.

De Boom, A., Degrez, M., 2015. Combining sieving and washing, a way to treat MSWI boiler fly ash. Waste Manag. 39, 179–188.

De Boom, A., Degrez, M., 2012. Belgian MSWI fly ashes and APC residues: a characterisation study. Waste Manag. 32, 1163–1170.

Derie, R., 1996. A new way to stabilize fly ash from municipal incinerators. Waste Manag. 16, 711–716.

Di Gianfilippo, M., Costa, G., Pantini, S., Allegrini, E., Lombardi, F., Astrup, T.F., 2016a. LCA of management strategies for RDF incineration and gasification bottom ash based on experimental leaching data. Waste Manag. 47, 285–298.

Di Gianfilippo, M., Costa, G., Verginelli, I., Gavasci, R., Lombardi, F., 2016b. Analysis and interpretation of the leaching behaviour of waste thermal treatment bottom ash by batch and column tests. Waste Manag. 56, 216–228. https://doi.org/10.1016/j.wasman.2016.07.034

Dias, D.P., Thaumaturgo, C., 2005. Fracture toughness of geopolymeric concretes reinforced with basalt fibers. Cem. Concr. Compos. 27, 49–54.

Diaz-Loya, E.I., Allouche, E.N., Eklund, S., Joshi, A.R., Kupwade-Patil, K., 2012. Toxicity mitigation and solidification of municipal solid waste incinerator fly ash using alkaline

activated coal ash. Waste Manag. 32, 1521–1527. https://doi.org/https://10.1016/j.wasman.2012.03.030

Diez, J.M., Madrid, J., Macias, A., 1997. Characterization of cement-stabilized Cd wastes. Cem. Concr. Res. 27, 337–343.

Dou, X., Ren, F., Nguyen, M.Q., Ahamed, A., Yin, K., Chan, W.P., Chang, V.W.-C., 2017. Review of MSWI bottom ash utilization from perspectives of collective characterization, treatment and existing application. Renew. Sustain. Energy Rev. 79, 24–38.

Du, B., Li, J., Fang, W., Liu, J., 2019. Comparison of long-term stability under natural ageing between cement solidified and chelator-stabilised MSWI fly ash. Environ. Pollut. 250, 68–78. https://doi.org/10.1016/j.envpol.2019.03.124

Du, W., Zhang, C.Y., Kong, X.M., Zhuo, Y.Q., Zhu, Z.W., 2018. Mercury release from fly ashes and hydrated fly ash cement pastes. Atmos. Environ. 178, 11–18.

Duxson, P., Provis, J.L., Lukey, G.C., Separovic, F., van Deventer, J.S.J., 2005. 29Si NMR study of structural ordering in aluminosilicate geopolymer gels. Langmuir 21, 3028–3036.

Ecke, H., 2003. Sequestration of metals in carbonated municipal solid waste incineration (MSWI) fly ash. Waste Manag. 23, 631–640.

Ecke, H., Sakanakura, H., Matsuto, T., Tanaka, N., Lagerkvist, A., 2000. State-of-the-art treatment processes for municipal solid waste incineration residues in Japan. Waste Manag. Res. 18, 41–51.

Eighmy, T.T., Crannell, B.S., Butler, L.G., Cartledge, F.K., Emery, E.F., Oblas, D., Krzanowski, J.E., Eusden, J.D., Shaw, E.L., Francis, C.A., 1997. Heavy metal stabilization in municipal solid waste combustion dry scrubber residue using soluble phosphate. Environ. Sci. Technol. 31, 3330–3338. https://doi.org/10.1021/es970407c

El-eswed, B.I., 2020. Chemical evaluation of immobilization of wastes containing Pb, Cd, Cu and Zn in alkali-activated materials: A critical review. J. Environ. Chem. Eng. 8, 104194. https://doi.org/10.1016/j.jece.2020.104194

El-Eswed, B.I., Aldagag, O.M., Khalili, F.I., 2017. Efficiency and mechanism of stabilization/solidification of Pb(II), Cd(II), Cu(II), Th(IV) and U(VI) in metakaolin based geopolymers. Appl. Clay Sci. 140, 148–156. https://doi.org/10.1016/j.clay.2017.02.003

Ellis, C.E., 1998. Wet air oxidation of refinery spent caustic. Environ. Prog. 17, 28–30. https://doi.org/10.1002/ep.670170116

Engelhardt, G., Lippmaa, E., Mägi, M., 1981. Ordering of silicon and aluminium ions in the framework of NaX zeolites. A solid-state high-resolution ^{29}Si N.M.R. study. J. Chem. Soc. Chem. Commun. 67, 712–713. https://doi.org/10.1039/C39810000712

Fedje, K.K., Ekberg, C., Skarnemark, G., Steenari, B.-M., 2010. Removal of hazardous metals from MSW fly ash—an evaluation of ash leaching methods. J. Hazard. Mater. 173, 310–317.

Ferna, A., Palomo, A., Sobrados, I., Sanz, J., 2006. The role played by the reactive alumina content in the alkaline activation of fly ashes 91, 111–119. https://doi.org/10.1016/j.micromeso.2005.11.015

Fernández-Pereira, C., Luna-Galiano, Y., Pérez-Clemente, M., Leiva, C., Arroyo, F., Villegas, R., Vilches, L., 2018. Immobilization of heavy metals (Cd, Ni or Pb) using aluminate geopolymers. Mater. Lett. 227, S0167577X18307699.

Fernández-Jiménez, A., Puertas, F., Sobrados, I., Sanz, J., 2003. Structure of calcium silicate hydrates formed in alkaline-activated slag: influence of the type of alkaline activator. J. Am. Ceram. Soc. 86, 1389–1394.

Ferone, C., Roviello, G., Colangelo, F., Cioffi, R., Tarallo, O., 2013. Novel hybrid organic-geopolymer materials. Appl. Clay Sci. 73, 42–50. https://doi.org/10.1016/j.clay.2012.11.001

Ferreira, C., Ribeiro, A., Ottosen, L., 2003. Possible applications for municipal solid waste fly ash. J. Hazard. Mater. 96, 201–216.

Florea, M.V.A., Quaas, L.C., Brouwers, H.J.H., Schmidt, W., Msinjili, N., 2016. MSWI by-products and immobilisates as concrete constituents, in: Advances in Cement and Concrete Technology in Africa: 2nd International Conference, Dar Es Salaam, Tanzania.

Funari, V., Mäkinen, J., Salminen, J., Braga, R., Dinelli, E., Revitzer, H., 2017. Metal removal from Municipal Solid Waste Incineration fly ash: A comparison between chemical leaching and bioleaching. waste Manag. 60, 397–406.

Galiano, Y.L., Pereira, C.F., Vale, J., 2011. Stabilization/solidification of a municipal solid waste incineration residue using fly ash-based geopolymers. J. Hazard. Mater. 185, 373–381.

Gao, X., Yuan, B., Yu, Q.L., Brouwers, H.J.H., 2017. Characterization and application of municipal solid waste incineration (MSWI) bottom ash and waste granite powder in alkali activated slag 164, 410–419. https://doi.org/10.1016/j.jclepro.2017.06.218

Gerven, T. Van, Baelen, D. Van, Dutré, V., Vandecasteele, C., 2004. Influence of carbonation and carbonation methods on leaching of metals from mortars. Cem. Concr. Res. 34, 149–156.

Ghouleh, Z., Shao, Y., 2018. Turning municipal solid waste incineration into a cleaner cement production. J. Clean. Prod. 195, 268–279.

Günzler, H., Gremlich, H.-U., 2002. IR spectroscopy. An introduction.

Guo, X., Zhang, T., 2020. Utilization of municipal solid waste incineration fly ash to produce autoclaved and modified wall blocks. J. Clean. Prod. 252, 119759. https://doi.org/10.1016/j.jclepro.2019.119759

Haider, G.M., Sanjayan, J.G., Ranjith, P.G., 2014. Complete triaxial stress–strain curves for geopolymer. Constr. Build. Mater. 69, 196–202.

Haiying, Z., Youcai, Z., Jingyu, Q., 2010. Thermal characterization of fly ash from one municipal solid waste incinerator (MSWI) in Shanghai. Process Saf. Environ. Prot. 88, 269–275.

Hammond, J.S., Gaarenstroom, S.W., Winograd, N., 1975. X-ray photoelectron spectroscopic studies of cadmium-and silver-oxygen surfaces. Anal. Chem. 47, 2193–2199.

Harmsen, J., 1983. Identification of organic compounds in leachate from a waste tip. Water Res. 17, 699–705.

Hautier, G., Fischer, C., Ehrlacher, V., Jain, A., Ceder, G., 2011. Data mined ionic substitutions for the discovery of new compounds. Inorg. Chem. 50, 656–663.

Hills, C.D., Pollard, S.J.T., 1997. The influence of interference effects on the mechanical, microstructural and fixation characteristics of cement-solidified hazardous waste forms. J. Hazard. Mater. 52, 171–191. https://doi.org/10.1016/S0304-3894(96)01806-7

Hu, H.-Y., Liu, H., Zhang, Q., Zhang, P.-A., Li, A.-J., Yao, H., Naruse, I., 2016. Sintering characteristics of CaO-rich municipal solid waste incineration fly ash through the addition of Si/Al-rich ash residues. J. Mater. Cycles Waste Manag. 18, 340–347.

Hu, S.H., 2005. Stabilization of heavy metals in municipal solid waste incineration ash using mixed ferrous/ferric sulfate solution. J. Hazard. Mater. 123, 158–164.

Hu, Y., PengfeiZhang, DezhenChen, BinZhou, Li, J., Li, X.W., 2012. Hydrothermal treatment of municipal solid waste incineration fly ash for dioxin decomposition. J. Hazard. Mater. 207–208, 79–85.

Hu, Y., Zhang, P., Li, J., Chen, D., 2015. Stabilization and separation of heavy metals in incineration fly ash during the hydrothermal treatment process. J. Hazard. Mater. 299, 149–157.

Huang, G., Yuan, L., Ji, Y., Liu, B., Xu, Z., 2019. Cooperative action and compatibility between Portland cement and MSWI bottom ash alkali-activated double gel system materials. Constr. Build. Mater. 209, 445–453. https://doi.org/10.1016/j.conbuildmat.2019.03.141

Huanhai, Z., Xuequan, W., Zhongzi, X., Mingshu, T., 1993. Kinetic study on hydration of alkali-activated slag. Cem. Concr. Res. 23, 1253–1258.

Huber, F., Blasenbauer, D., Mallow, O., Lederer, J., Winter, F., Fellner, J., 2016. Thermal co-treatment of combustible hazardous waste and waste incineration fly ash in a rotary kiln. Waste Manag. 58, 181–190.

Ishigaki, T., Nakanishi, A., Tateda, M., Ike, M., Fujita, M., 2005. Bioleaching of metal from municipal waste incineration fly ash using a mixed culture of sulfur-oxidizing and iron-oxidizing bacteria. Chemosphere 60, 1087–1094.

Jensen, P.E., Kirkelund, G.M., Pedersen, K.B., Dias-Ferreira, C., Ottosen, L.M., 2015. Electrodialytic upgrading of three different municipal solid waste incineration residue types with focus on Cr, Pb, Zn, Mn, Mo, Sb, Se, V, Cl and SO4. Electrochim. Acta 181, 167–178.

Ji, Z., Pei, Y., 2020. Immobilization efficiency and mechanism of metal cations (Cd2+, Pb2+ and Zn2+) and anions (AsO43- and Cr2O72-) in wastes-based geopolymer. J. Hazard. Mater. 384, 121290. https://doi.org/10.1016/j.jhazmat.2019.121290

Jiao, Z., Wang, Y., Zheng, W., Huang, W., 2019. Effect of the activator on the performance of alkali-activated slag mortars with pottery sand as fine aggregate. Constr. Build. Mater. 197, 83–90. https://doi.org/10.1016/j.conbuildmat.2018.11.178

Jiao, Z., Wang, Y., Zheng, W., Huang, W., 2018. Effect of dosage of sodium carbonate on the strength and drying shrinkage of sodium hydroxide based alkali-activated slag paste. Constr. Build. Mater. 179, 11–24. https://doi.org/10.1016/j.conbuildmat.2018.05.194

Jin, M., Zheng, Z., Sun, Y., Chen, L., Jin, Z., 2016. Resistance of metakaolin-MSWI fl y ash based geopolymer to acid and alkaline environments. J. Non. Cryst. Solids 450, 116–122. https://doi.org/10.1016/j.jnoncrysol.2016.07.036

Joseph, A.M., Van den Heede, P., Snellings, R., Van, A., 2017. Comparison of different beneficiation techniques to improve utilization potential of municipal solid waste incineration fly ash concrete. Constr. Mater. Syst. 49.

Kanhar, A.H., Chen, S., Wang, F., 2020. Incineration Fly Ash and Its Treatment to Possible Utilization: A Review. Energies 13, 6681. https://doi.org/10.3390/en13246681

Karamalidis, A.K., Voudrias, E.A., 2007. Leaching of VOCs from cement-based stabilized/solidified refinery oily sludge using solid phase microextraction. Environ. Technol. 28, 1173–1185.

Karlfeldt, K., Steenari, B.-M., 2007. Assessment of metal mobility in MSW incineration ashes using water as the reagent. Fuel 86, 1983–1993.

Kim, E., 2012. Understanding effects of silicon/aluminum ratio and calcium hydroxide on chemical composition, nanostructure and compressive strength for metakaolin geopolymers.

Kirkpatrick, T.J., Weyers, R.E., Anderson-Cook, C.M., Sprinkel, M.M., 2002. Immobilization of Cr6+, Cd2+, Zn2+ and Pb2+ in alkali-activated slag binders. Cem. Concr. Res. 32, 1971–1979. https://doi.org/10.1016/S0008-8846(02)00904-3

Kiventerä, J., Lancellotti, I., Catauro, M., Poggetto, F.D., Leonelli, C., Illikainen, M., 2018. Alkali activation as new option for gold mine tailings inertization. J. Clean. Prod. 187, 76–84. https://doi.org/10.1016/j.jclepro.2018.03.182

Komárek, M., Vaněk, A., Ettler, V., 2013. Chemical stabilization of metals and arsenic in contaminated soils using oxides–a review. Environ. Pollut. 172, 9–22.

Komonweeraket, K., Cetin, B., Aydilek, A.H., Benson, C.H., Edil, T.B., 2015. Effects of pH on the leaching mechanisms of elements from fly ash mixed soils. Fuel 140, 788–802.

Kouamo, H.T., Elimbi, A., Mbey, J.A., Sabouang, C.J.N., Njopwouo, D., 2012. The effect of adding alumina-oxide to metakaolin and volcanic ash on geopolymer products: A comparative study. Constr. Build. Mater. 35, 960–969.

Kupwade-patil, K., Soto, F., Kunjumon, A., Allouche, E.N., Mainardi, D.S., 2013. Multi-scale modeling and experimental investigations of geopolymeric gels at elevated temperatures. Comput. Struct. 122, 164–177. https://doi.org/10.1016/j.compstruc.2013.01.005

Kwan, W.H., Cheah, C.B., Ramli, M., Chang, K.Y., 2018. Alkali-resistant glass fiber reinforced high strength concrete in simulated aggressive environment. Mater. Construcción 68, 147.

Lam, C.H.K., Ip, A.W.M., Barford, J.P., McKay, G., 2010. Use of incineration MSW ash: a review. Sustainability 2, 1943–1968.

Lancellotti, I., Kamseu, E., Michelazzi, M., Barbieri, L., Corradi, A., Leonelli, C., 2010. Chemical stability of geopolymers containing municipal solid waste incinerator fly ash. Waste Manag. 30, 673–679.

Le Saoût, G., Ben Haha, M., Winnefeld, F., Lothenbach, B., 2011. Hydration degree of alkali-activated slags: A 29 Si NMR study. J. Am. Ceram. Soc. 94, 4541–4547. https://doi.org/10.1111/j.1551-2916.2011.04828.x

Lee, W.K.W., Van Deventer, J.S.J., 2002a. The effects of inorganic salt contamination on the strength and durability of geopolymers. Colloids Surfaces A Physicochem. Eng. Asp. 211, 115–126. https://doi.org/10.1016/S0927-7757(02)00239-X

Lee, W.K.W., Van Deventer, J.S.J., 2002b. Effects of anions on the formation of aluminosilicate gel in geopolymers. Ind. Eng. Chem. Res. 41, 4550–4558. https://doi.org/10.1021/ie0109410

Li, C., Sun, H., Li, L., 2010. A review: The comparison between alkali-activated slag (Si+ Ca) and metakaolin (Si+ Al) cements. Cem. Concr. Res. 40, 1341–1349.

Li, H., Liu, G., Cao, Y., 2015. Levels and environmental impact of PAHs and trace element in fly ash from a miscellaneous solid waste by rotary kiln incinerator, China. Nat. Hazards 76, 811–822.

Li, R., Li, Y., Yang, T., Wang, L., Wang, W., 2015. A new integrated evaluation method of heavy metals pollution control during melting and sintering of MSWI fly ash. J. Hazard. Mater. 289, 197–203.

Li, X., Bertos, M.F., Hills, C.D., Carey, P.J., Simon, S., 2007. Accelerated carbonation of municipal solid waste incineration fly ashes. Waste Manag. 27, 1200–1206.

Li, X., Chen, Q., Zhou, Y., Tyrer, M., Yu, Y., 2014. Stabilization of heavy metals in MSWI fly ash using silica fume. Waste Manag. 34, 2494–2504. https://doi.org/10.1016/j.wasman.2014.08.027

Li, Y., Xu, L., 2009. Multicolor illumination device using moving plate with wavelength conversion materials.

Lin, X., Chen, Z., Lu, S., Zhang, S., Zhang, M., Li, X., Yan, J., 2018. Emission characteristics of polychlorinated dibenzo-p-dioxins and dibenzofurans from the co-combustion of municipal solid waste in a lab-scale drop-tube furnace. Energy & fuels 32, 5396–5404.

Liu, J., Hu, L., Tang, L., Ren, J., 2021. Utilisation of municipal solid waste incinerator (MSWI) fly ash with metakaolin for preparation of alkali-activated cementitious material. J. Hazard. Mater. 402. https://doi.org/10.1016/j.jhazmat.2020.123451

Liu, Shutang, Li, Zhuozhi, Yingyong, Cao, Weidong, 2018. Strength properties of Bayer red mud stabilized by lime-fly ash using orthogonal experiments. Constr. Build. Mater.

Liu, X., Zhao, X., Yin, H., Chen, J., Zhang, N., 2018. Intermediate-calcium based cementitious materials prepared by MSWI fly ash and other solid wastes: hydration characteristics and heavy metals solidification behavior. J. Hazard. Mater. 349, 262–271. https://doi.org/10.1016/j.jhazmat.2017.12.072

Lo, H.-M., Liao, Y.-L., 2007. The metal-leaching and acid-neutralizing capacity of MSW incinerator ash co-disposed with MSW in landfill sites. J. Hazard. Mater. 142, 512–519.

Lodeiro, I.G., Macphee, D.E., Palomo, A., Fernández-Jiménez, A., 2009. Effect of alkalis on fresh C–S–H gels. FTIR analysis. Cem. Concr. Res. 39, 147–153.

Lombardi, F., Mangialardi, T., Piga, L., Sirini, P., 1998. Mechanical and leaching properties of cement solidified hospital solid waste incinerator fly ash. Waste Manag. 18, 99–106. https://doi.org/10.1016/S0956-053X(98)00006-3

Lu, J.-W., Zhang, S., Hai, J., Lei, M., 2017. Status and perspectives of municipal solid waste incineration in China: A comparison with developed regions. Waste Manag. 69, 170–186.

Luo, H., Cheng, Y., He, D., Yang, E.-H., 2019. Review of leaching behavior of municipal solid waste incineration (MSWI) ash. Sci. Total Environ. 668, 90–103.

Lura, P., Jensen, O.M., 2007. Measuring techniques for autogenous strain of cement paste. Mater. Struct. 40, 431–440. https://doi.org/https://10.1617/s11527-006-9180-2

Lutz, W., Täschner, D., Kurzhals, R., Heidemann, D., Hübert, C., 2009. Characterization of silica gels by29Si MAS NMR and IR spectroscopic □ measurements. Zeitschrift fur Anorg. und Allg. Chemie 635, 2191–2196. https://doi.org/10.1002/zaac.200900237

Ma, W., Fang, Y., Chen, D., Chen, G., Xu, Y., Sheng, H., Zhou, Z., 2017. Volatilization and leaching behavior of heavy metals in MSW incineration fly ash in a DC arc plasma furnace. Fuel 210, 145–153.

Mägi, M., Lippmaa, E., Samoson, A., Engelhardt, G., Grimmer, A.R., 1984. Solid-state high-resolution silicon-29 chemical shifts in silicates. J. Phys. Chem. 88, 1518–1522. https://doi.org/10.1021/j150652a015

Mangialardi, T., 2001. Sintering of MSW fly ash for reuse as a concrete aggregate. J. Hazard. Mater. 87, 225–239.

Mangialardi, T., Paolini, A.E., Polettini, A., Sirini, P., 1999. Optimization of the solidification/stabilization process of MSW fly ash in cementitious matrices. J. Hazard. Mater. 70, 53–70. https://doi.org/10.1016/S0304-3894(99)00132-6

Mansur, H.S., Sadahira, C.M., Souza, A.N., Mansur, A.A.P., 2008. FTIR spectroscopy characterization of poly (vinyl alcohol) hydrogel with different hydrolysis degree and chemically crosslinked with glutaraldehyde. Mater. Sci. Eng. C 28, 539–548. https://doi.org/10.1016/j.msec.2007.10.088

Margallo, M., Taddei, M.B.M., Hernández-Pellón, A., Aldaco, R., Irabien, A., 2015. Environmental sustainability assessment of the management of municipal solid waste incineration residues: a review of the current situation. Clean Technol. Environ. Policy 17, 1333–1353.

Mccarthy, M.J., Zheng, L., Dhir, R.K., Tella, G., 2017. Dry-processing of long-term wet-stored fly ash for use as an addition in concrete. Cem. Concr. Compos. S0958946516306849.

Meza, S.L., Kalbe, U., Berger, W., Simon, F.-G., 2010. Effect of contact time on the release of contaminants from granular waste materials during column leaching experiments. Waste Manag. 30, 565–571.

Miller, F.A., Wilkins, C.H., 1952. Infrared spectra and characteristic frequencies of inorganic ions. Anal. Chem. 24, 1253–1294. https://doi.org/https://10.1021/ac60068a007

Mizutani, S., Yoshida, T., Sakai, S., Takatsuki, H., 1996. Release of metals from MSW I fly ash and availability in alkali condition. Waste Manag. 16, 537–544.

Moraes, J.C.B., Font, A., Soriano, L., Akasaki, J.L., Tashima, M.M., Monzó, J., Borrachero, M. V., Payá, J., 2018. New use of sugar cane straw ash in alkali-activated materials: A silica source for the preparation of the alkaline activator. Constr. Build. Mater. 171, 611–621. https://doi.org/10.1016/j.conbuildmat.2018.03.230

Mroueh, U.-M., Eskola, P., Laine-Ylijoki, J., 2001. Life-cycle impacts of the use of industrial by-products in road and earth construction. Waste Manag. 21, 271–277.

Myers, R.J., Bernal, S.A., San Nicolas, R., Provis, J.L., 2013. Generalized structural description of calcium–sodium aluminosilicate hydrate gels: the cross-linked substituted tobermorite model. Langmuir 29, 5294–5306.

Nagib, S., Inoue, K., 2000. Recovery of lead and zinc from fly ash generated from municipal incineration plants by means of acid and/or alkaline leaching. Hydrometallurgy 56, 269–292.

Nogami, M., Ogawa, S., Nagasaka, K., 1989. Preparation of cordierite glass by the sol-gel process. J. Mater. Sci. 24, 4339–4342.

Nowak, B., Frías, S., Aschenbrenner, P., Rechberger, H., Winter, F., 2012. Heavy metal removal from MSW fly ash by means of chlorination and thermal treatment : Influence of the chloride type. Chem. Eng. J. 179, 178–185. https://doi.org/10.1016/j.cej.2011.10.077

Ntagia, E., Fiset, E., Truong Cong Hong, L., Vaiopoulou, E., Rabaey, K., 2019. Electrochemical treatment of industrial sulfidic spent caustic streams for sulfide removal and caustic recovery. J. Hazard. Mater. 121770. https://doi.org/10.1016/j.jhazmat.2019.121770

Nzihou, A., Sharrock, P., 2002. Calcium phosphate stabilization of fly ash with chloride extraction. Waste Manag. 22, p.235-239.

Okada, T., Tojo, Y., Tanaka, N., Matsuto, T., 2007. Recovery of zinc and lead from fly ash from ash-melting and gasification-melting processes of MSW–Comparison and applicability of chemical leaching methods. Waste Manag. 27, 69–80.

Okada, T., Tomikawa, H., 2012. Leaching characteristics of lead from melting furnace fly ash generated by melting of incineration fly ash. J. Environ. Manage. 110, 207–214.

Olejniczak, Z., Łęczka, M., Cholewa-Kowalska, K., Wojtach, K., Rokita, M., Mozgawa, W., 2005. 29Si MAS NMR and FTIR study of inorganic–organic hybrid gels. J. Mol. Struct. 744, 465–471.

Ottosen, L.M., Jensen, P.E., Kirkelund, G.M., 2016. Phosphorous recovery from sewage sludge ash suspended in water in a two-compartment electrodialytic cell. Waste Manag. 51, 142–148.

Ouellet-Plamondon, C., Habert, G., 2015. Life cycle assessment (LCA) of alkali-activated cements and concretes, in: Handbook of Alkali-Activated Cements, Mortars and Concretes. Elsevier, pp. 663–686.

Palaniappan, P.L.R.M., Pramod, K.S., 2010. FTIR study of the effect of nTiO2 on the biochemical constituents of gill tissues of Zebrafish (Danio rerio). Food Chem. Toxicol. 48, 2337–2343. https://doi.org/10.1016/j.fct.2010.05.068

Pardal, X., Pochard, I., Nonat, A., 2009. Cement and Concrete Research Experimental study of Si – Al substitution in calcium-silicate-hydrate (C-S-H) prepared under equilibrium conditions. Cem. Concr. Res. 39, 637–643. https://doi.org/10.1016/j.cemconres.2009.05.001

Park, Y.J., 2009. Stabilization of a chlorine-rich fly ash by colloidal silica solution. J. Hazard. Mater. 162, 819–822.

Pederson, L.R., 1982. Two-dimensional chemical-state plot for lead using XPS. J. Electron Spectros. Relat. Phenomena 28, 203–209.

Peng, W., Wang, W., Han, G., Huang, Y., Zhang, Y., 2020. Fabrication of 3D flower-like MoS2/graphene composite as high-performance electrode for capacitive deionization. Desalination 473, 114191.

Phair, J.W., Deventer, J.S.J.V.A.N., 2001. EFFECT OF SILICATE ACTIVATOR pH ON THE LEACHING AND MATERIAL CHARACTERISTICS OF WASTE-BASED INORGANIC POLYMERS 14, 289–304.

Phoungthong, K., Xia, Y., Zhang, H., Shao, L., He, P., 2016. Leaching toxicity characteristics of municipal solid waste incineration bottom ash. Front. Environ. Sci. Eng. 10, 399–411.

Phua, Z., Giannis, A., Dong, Z.L., Lisak, G., Ng, W.J., 2019. Characteristics of incineration ash for sustainable treatment and reutilization. Environ. Sci. Pollut. Res. 26, 16974–16997. https://doi.org/10.1007/s11356-019-05217-8

Pomiès, M.-P., Lequeux, N., Boch, P., 2001. Speciation of cadmium in cement: Part I. Cd2+ uptake by CSH. Cem. Concr. Res. 31, 563–569.

Qian, G., Yang, X., Dong, S., Zhou, J., Sun, Y., Xu, Y., Liu, Q., 2009. Stabilization of chromium-bearing electroplating sludge with MSWI fly ash-based Friedel matrices. J. Hazard. Mater. 165, 955–960. https://doi.org/https://doi.org/10.1016/j.jhazmat.2008.10.078

Quina, M.J., Bordado, J.C., Quinta-Ferreira, R.M., 2008a. Treatment and use of air pollution control residues from MSW incineration: an overview. Waste Manag. 28, 2097–2121.

Quina, M.J., Bordado, J.C.M., Quinta-Ferreira, R.M., 2010. Chemical stabilization of air pollution control residues from municipal solid waste incineration. J. Hazard. Mater. 179, 382–392.

Quina, M.J., Bordado, J.C.M., Quinta-Ferreira, R.M., 2009. The influence of pH on the leaching behaviour of inorganic components from municipal solid waste APC residues. Waste Manag. 29, 2483–2493.

Quina, M.J., Santos, R.C., Bordado, J.C., Quinta-Ferreira, R.M., 2008b. Characterization of air pollution control residues produced in a municipal solid waste incinerator in Portugal. J. Hazard. Mater. 152, 853–869.

Redden, R., Neithalath, N., 2014. Microstructure, strength, and moisture stability of alkali activated glass powder-based binders. Cem. Concr. Compos. 45, 46–56. https://doi.org/10.1016/j.cemconcomp.2013.09.011

Richardson, I.G., 1999. The nature of CSH in hardened cements. Cem. Concr. Res. 29, 1131–1147.

Richardson, I.G., Brough, A.R., Brydson, R., Groves, G.W., Dobsont, C.M., 1993. Location of Aluminum in Substituted Calcium Silicate Hydrate (C-S-H) Gels as Determined by 29Si and 27AI NMR and EELS.

S.K. Lee, J.F.S., 1999. The degree of aluminum avoidance in aluminosilicate glasses. Mineral 84, 937–945. https://doi.org/10.1007/978-3-540-47108-0-4

Sabbas, T., Polettini, A., Pomi, R., Astrup, T., Hjelmar, O., Mostbauer, P., Cappai, G., Magel, G., Salhofer, S., Speiser, C., 2003. Management of municipal solid waste incineration residues. Waste Manag. 23, 61–88.

Sagoe-Crentsil, K., Brown, T., Taylor, A., 2013. Drying shrinkage and creep performance of geopolymer concrete. J. Sustain. Cem. Mater. 2, 35–42. https://doi.org/https://10.1080/21650373.2013.764963

Saikia, N., Mertens, G., Van Balen, K., Elsen, J., Van Gerven, T., Vandecasteele, C., 2015. Pre-treatment of municipal solid waste incineration (MSWI) bottom ash for utilisation in cement mortar. Constr. Build. Mater. 96, 76–85. https://doi.org/https://10.1016/j.conbuildmat.2015.07.185

Sakai, S., Hiraoka, M., 2000. Municipal solid waste incinerator residue recycling by thermal processes. Waste Manag. 20, 249–258.

Sarker, P.K., Kelly, S., Yao, Z., 2014. Effect of fire exposure on cracking, spalling and residual strength of fly ash geopolymer concrete. Mater. Des. 63, 584–592.

Sarker, P.K., Mcbeath, S., 2015. Fire endurance of steel reinforced fly ash geopolymer concrete elements. Constr. Build. Mater. 90, 91–98.

Sarmiento, L.M., Clavier, K.A., Paris, J.M., Ferraro, C.C., Townsend, T.G., 2019. Critical examination of recycled municipal solid waste incineration ash as a mineral source for portland cement manufacture–A case study. Resour. Conserv. Recycl. 148, 1–10.

Schilling, P.J., Butler, L.G., Roy, A., Eaton, H.C., 1994. 29Si and 27Al MAS-NMR of NaOH-activated blast-furnace slag. J. Am. Ceram. Soc. 77, 2363–2368.

Schneider, J., Cincotto, M.A., Panepucci, H., 2001. 29Si and 27Al high-resolution NMR characterization of calcium silicate hydrate phases in activated blast-furnace slag pastes. Cem. Concr. Res. 31, 993–1001.

Seals, R.D., Alexander, R., Taylor, L.T., Dillard, J.G., 1973. Core electron binding energy study of group IIb-VIIa compounds. Inorg. Chem. 12, 2485–2487.

Sebök, T., Šimoník, J., Kulísek, K., 2001. The compressive strength of samples containing fly ash with high content of calcium sulfate and calcium oxide. Cem. Concr. Res. 31, 1101–1107.

Seyama, H., Soma, M., 1984. X-ray photoelectron spectroscopic study of montmorillonite containing exchangeable divalent cations. J. Chem. Soc. Faraday Trans. 1 Phys. Chem. Condens. Phases 80, 237–248.

Shao, Y., Zhou, M., Wang, W., Hou, H., 2013. Identification of chromate binding mechanisms in Friedel's salt. Constr. Build. Mater. 48, 942–947.

Shi, H.-S., Kan, L.-L., 2009. Leaching behavior of heavy metals from municipal solid wastes incineration (MSWI) fly ash used in concrete. J. Hazard. Mater. 164, 750–754.

Singh, P.S., Bastow, T., Trigg, M., 2005. Structural studies of geopolymers by 29 Si and 27 Al MAS-NMR. J. Mater. Sci. 40, 3951–3961.

Sperling, M., Xu, S., Welz, B., 1992. Determination of chromium (III) and chromium (VI) in water using flow injection on-line preconcentration with selective adsorption on activated alumina and flame atomic absorption spectrometric detection. Anal. Chem. 64, 3101–3108.

Stoch, A., Zdaniewicz, M., Paluszkiewicz, C., 1999. The effect of polymethylsiloxanes on hydration of clinker phases. J. Mol. Struct. 511, 319–325.

Tabata, Y., Saitsu, T., Okihara, Y., Itoh, N., Ueda, R., Tanimura, Y., Ohta, K., 2013. Apparatus for concentrating and diluting specific gas and method for concentrating and diluting specific gas.

Tang, P., Florea, M.V.A., Spiesz, P., Brouwers, H.J.H., 2016. Application of thermally activated municipal solid waste incineration (MSWI) bottom ash fines as binder substitute. Cem. Concr. Compos. 70, 194–205. https://doi.org/https://10.1016/j.cemconcomp.2016.03.015

Taylor, H.F.W., 1997. Cement chemistry. Thomas Telford London.

Tessier, A., Campbell, P.G.C., Bisson, M., 1979. Sequential Extraction Procedure for the Speciation of Particulate Trace Metals. Anal. Chem. 51, 844–851. https://doi.org/10.1021/ac50043a017

Tian, S., Li, J., Liu, F., Guan, J., Dong, L., Wang, Q., 2012. Behavior of heavy metals in the vitrification of MSWI fly ash with a pilot-scale diesel oil furnace. Procedia Environ. Sci. 16, 214–221.

Tian, X., Rao, F., Estrella, R.M., Song, S., 2020a. Effects of aluminum dosage on gel formation and heavy metals immobilization in alkali-activated MSWI fly ash. Energy & Fuels. https://doi.org/https://doi.org/10.1021/acs.energyfuels.9b04493

Tian, X., Rao, F., Morales-Estrella, R., Song, S., 2020b. Effects of Aluminum Dosage on Gel Formation and Heavy Metal Immobilization in Alkali-Activated Municipal Solid Waste Incineration Fly Ash. Energy and Fuels 34, 4727–4733. https://doi.org/10.1021/acs.energyfuels.9b04493

Tian, X., Song, S., Rao, F., 2020c. Effects of aluminum on the expansion and microstructure of alkali-activated MSWI fl y ash-based pastes. Chemosphere 240, 2–6. https://doi.org/10.1016/j.chemosphere.2019.124986

Tian, X., Xu, W., Song, S., Rao, F., Xia, L., 2020d. Effects of curing temperature on the compressive strength and microstructure of copper tailing-based geopolymers. Chemosphere 253, 126754. https://doi.org/10.1016/j.chemosphere.2020.126754

Tian, X., Zhang, H., Zhang, T., Fernández, C.A., 2020e. Alkali-activated copper tailings-based pastes: compressive strength and microstructural characterization. J. Mater. Res. Technol.

Torres-Carrasco, M., Palomo, J.G., Puertas, F., 2014. Sodium silicate solutions from dissolution of glasswastes. Statistical analysis. Mater. Constr. 64. https://doi.org/10.3989/mc.2014.05213

Torres, J.J., Palacios, M., Hellouin, M., Puertas, F., 2009. Alkaline Chemical Activation of Urban Glass Wastes to Produce Cementitious Materials. 1st Spanish Natl. Conf. Adv. Mater. Recycl. Eco – Energy Madrid, 12-13 Novemb. 2009 12–13.

Usero, J., Gamero, M., Morillo, J., Gracia, I., 1998. Comparative study of three sequential extraction procedures for metals in marine sediments. Environ. Int. 24, 487–496.

Valls, S., Vazquez, E., 2002. Leaching properties of stabilised/solidified cement-admixtures-sewage sludges systems. Waste Manag. 22, 37–45.

Viader, R.P., Jensen, P.E., Ottosen, L.M., 2017. Electrodialytic remediation of municipal solid waste incineration residues using different membranes. Chemosphere 169, 62–68.

Wan, Q., Rao, F., 2018. Consolidation of mine tailings through geopolymerization at ambient temperature 1–11. https://doi.org/10.1111/jace.16183

Wan, Q., Rao, F., Song, S., Cholico-González, D.F., Ortiz, N.L., 2017a. Combination formation in the reinforcement of metakaolin geopolymers with quartz sand. Cem. Concr. Compos. 80, 115–122. https://doi.org/10.1016/j.cemconcomp.2017.03.005

Wan, Q., Rao, F., Song, S., García, R.E., Estrella, R.M., Patino, C.L., Zhang, Y., 2017b. Geopolymerization reaction, microstructure and simulation of metakaolin-based geopolymers at extended Si/Al ratios. Cem. Concr. Compos. 79, 45–52. https://doi.org/https://10.1016/j.cemconcomp.2017.01.014

Wan, Q., Rao, F., Song, S., García, R.E., Estrella, R.M., Patiño, C.L., Zhang, Y., 2017c. Geopolymerization reaction, microstructure and simulation of metakaolin-based geopolymers at extended Si/Al ratios. Cem. Concr. Compos. 79, 45–52. https://doi.org/10.1016/j.cemconcomp.2017.01.014

Wan, Q., Rao, F., Song, S., Leon-Patino, C.A., Ma, Y., Yin, W., 2019a. Consolidation of mine tailings through geopolymerization at ambient temperature. J. Am. Ceram. Soc. 102, 2451–2461.

Wan, Q., Rao, F., Song, S., Morales-estrella, R., Xie, X., Tong, X., 2018. Chemical forms of lead immobilization in alkali-activated binders based on mine tailings. Cem. Concr. Compos. 92, 198–204. https://doi.org/10.1016/j.cemconcomp.2018.06.011

Wan, Q., Rao, F., Song, S., Zhang, Y., 2019b. Immobilization forms of ZnO in the solidification / stabilization (S / S) of a zinc mine tailing through geopolymerization. Integr. Med. Res. 6–13. https://doi.org/10.1016/j.jmrt.2019.09.040

Wan, Q., Zhang, Y., Zhang, R., 2020. Using mechanical activation of quartz to enhance the compressive strength of metakaolin based geopolymers. Cem. Concr. Compos. 111, 103635. https://doi.org/10.1016/j.cemconcomp.2020.103635

Wan, S., Zhou, X., Zhou, M., Han, Y., Chen, Y., Geng, J., Wang, T., Xu, S., Qiu, Z., Hou, H., 2018. Hydration characteristics and modeling of ternary system of municipal solid wastes incineration fly ash-blast furnace slag-cement. Constr. Build. Mater. 180, 154–166.

Wang, F.H., Zhang, F., Chen, Y.J., Gao, J., Zhao, B., 2015. A comparative study on the heavy metal solidification/stabilization performance of four chemical solidifying agents in municipal solid waste incineration fly ash. J. Hazard. Mater. 300, 451–458.

Wang, H., Fan, X., Wang, Y.N., Li, W., Wu, G., 2017. Comparative leaching of six toxic metals from raw and chemically stabilized MSWI fly ash using citric acid. J. Environ. Manage. 208, 15.

Wang, H., Li, H., Yan, F., 2005. Synthesis and mechanical properties of metakaolinite-based geopolymer. Colloids Surfaces A Physicochem. Eng. Asp. 268, 1–6.

Wang, J., Lyu, X.J., Wang, L., Cao, X., Liu, Q., Zang, H., 2018. Influence of the combination of calcium oxide and sodium carbonate on the hydration reactivity of alkali-activated slag binders. J. Clean. Prod. 171, 622–629. https://doi.org/10.1016/j.jclepro.2017.10.077

Wang, K.-S., Chiang, K.-Y., Lin, K.-L., Sun, C.-J., 2001. Effects of a water-extraction process on heavy metal behavior in municipal solid waste incinerator fly ash. Hydrometallurgy 62, 73–81.

Wang, K.-S., Chiang, K.-Y., Perng, J.-K., Sun, C.-J., 1998. The characteristics study on sintering of municipal solid waste incinerator ashes. J. Hazard. Mater. 59, 201–210.

Wang, L., Jin, Y., Nie, Y., 2010a. Investigation of accelerated and natural carbonation of MSWI fly ash with a high content of Ca. J. Hazard. Mater. 174, 334–343.

Wang, L., Jin, Y., Nie, Y., Li, R., 2010b. Recycling of municipal solid waste incineration fly ash for ordinary Portland cement production: A real-scale test. Resour. Conserv. Recycl. 54, 1428–1435.

Wang, P., Hu, Y., Cheng, H., 2019. Municipal solid waste (MSW) incineration fly ash as an important source of heavy metal pollution in China. Environ. Pollut. 252, 461–475. https://doi.org/10.1016/j.envpol.2019.04.082

Wang, P.W., Zhang, L., 1996. Structural role of lead in lead silicate glasses derived from XPS spectra. J. Non. Cryst. Solids 194, 129–134.

Wang, Q., Yan, J.-H., Chi, Y., Li, X.-D., Lu, S.-Y., 2010. Application of thermal plasma to vitrify fly ash from municipal solid waste incinerators. Chemosphere 78, 626–630.

Wang, Qi, Tian, S., Wang, Qunhui, Huang, Q., Yang, J., 2008. Melting characteristics during the vitrification of MSWI fly ash with a pilot-scale diesel oil furnace. J. Hazard. Mater. 160, 376–381.

Wang, Qunhui, Yang, J., Wang, Qi, Wu, T., 2009. Effects of water-washing pretreatment on bioleaching of heavy metals from municipal solid waste incinerator fly ash. J. Hazard. Mater. 162, 812–818.

Wang, S.-D., Pu, X.-C., Scrivener, K.L., Pratt, P.L., 1995. Alkali-activated slag cement and concrete: a review of properties and problems. Adv. Cem. Res. 7, 93–102.

Wang, S.-D., Scrivener, K.L., 2003. 29Si and 27Al NMR study of alkali-activated slag. Cem. Concr. Res. 33, 769–774.

Wang, W., Zhao, Y., Bai, H., Zhang, T., Ibarra-Galvan, V., Song, S., 2018. Methylene blue removal from water using the hydrogel beads of poly(vinyl alcohol)-sodium alginate-chitosan-montmorillonite. Carbohydr. Polym. 198, 518–528. https://doi.org/10.1016/j.carbpol.2018.06.124

Wang, X., Jin, B., Xu, B., Lan, W., Qu, C., 2017. Melting characteristics during the vitrification of MSW incinerator fly ash by swirling melting treatment. J. Mater. Cycles Waste Manag. 19, 483–495.

Wang, Y., Zhang, X., Liao, W., Wu, J., Yang, X., Shui, W., Deng, S., Zhang, Y., Lin, L., Xiao, Y., 2018. Investigating impact of waste reuse on the sustainability of municipal solid waste (MSW) incineration industry using emergy approach: A case study from Sichuan province, China. Waste Manag. 77, 252–267.

Wey, M.-Y., Liu, K.-Y., Tsai, T.-H., Chou, J.-T., 2006. Thermal treatment of the fly ash from municipal solid waste incinerator with rotary kiln. J. Hazard. Mater. 137, 981–989.

Wieker, W., Grimmer, A.R., Winkler, A., Mägi, M., Tarmak, M., Lippmaa, E., 1982. Solid-state high-resolution 29Si NMR spectroscopy of synthetic 14 Å, 11 Å and 9 Å tobermorites. Cem. Concr. Res. 12, 333–339. https://doi.org/10.1016/0008-8846(82)90081-3

Wu, H.-Y., Ting, Y.-P., 2006. Metal extraction from municipal solid waste (MSW) incinerator fly ash—Chemical leaching and fungal bioleaching. Enzyme Microb. Technol. 38, 839–847.

Xin-gang, Z., Gui-wu, J., Ang, L., Yun, L., 2016. Technology, cost, a performance of waste-to-energy incineration industry in China. Renew. Sustain. Energy Rev. 55, 115–130.

Xu, T.-J., Ramanathan, T., Ting, Y.-P., 2014. Bioleaching of incineration fly ash by Aspergillus niger–precipitation of metallic salt crystals and morphological alteration of the fungus. Biotechnol. Reports 3, 8–14.

Xuan, D., Poon, C.S., 2018. Removal of metallic Al and Al/Zn alloys in MSWI bottom ash by alkaline treatment. J. Hazard. Mater. 344, 73–80. https://doi.org/10.1016/j.jhazmat.2017.10.002

Yao, Q., Samad, N.B., Keller, B., Seah, X.S., Huang, L., Lau, R., 2014. Mobility of heavy metals and rare earth elements in incineration bottom ash through particle size reduction. Chem. Eng. Sci. 118, 214–220.

Ye, N., Chen, Y., Yang, J., Liang, S., Hu, Y., Xiao, B., Huang, Q., Shi, Y., Hu, J., Wu, X., 2016a. Co-disposal of MSWI fly ash and Bayer red mud using an one-part geopolymeric system 318, 70–78. https://doi.org/10.1016/j.jhazmat.2016.06.042

Ye, N., Yang, J., Liang, S., Hu, Y., Hu, J., Xiao, B., Huang, Q., 2016b. Synthesis and strength optimization of one-part geopolymer based on red mud. Constr. Build. Mater. 111, 317–325. https://doi.org/10.1016/j.conbuildmat.2016.02.099

Yi, H., Ai, Z., Zhao, Y., Zhang, X., Song, S., 2020. Design of 3D-network montmorillonite nanosheet/stearic acid shape-stabilized phase change materials for solar energy storage. Sol. Energy Mater. Sol. Cells 204, 110233.

Yi, H., Zhan, W., Zhao, Y., Qu, S., Wang, W., Chen, P., Song, S., 2019. A novel core-shell structural montmorillonite nanosheets/stearic acid composite PCM for great promotion of thermal energy storage properties. Sol. Energy Mater. Sol. Cells 192, 57–64. https://doi.org/10.1016/j.solmat.2018.12.015

Yin, K., Ahamed, A., Lisak, G., 2018. Environmental perspectives of recycling various combustion ashes in cement production – A review. Waste Manag. 78, 401–416. https://doi.org/10.1016/j.wasman.2018.06.012

Yip, C.K., Deventer, J.S.J. Van, 2003. Microanalysis of calcium silicate hydrate gel formed within a geopolymeric binder. J. Mater. Sci. 38, 3851–3860.

Yuan, W., Zhang, L., Liu, Y., Fu, P., Huang, Y., Wang, L., Ma, H., Wang, H., 2020. Sulfide removal and water recovery from ethylene plant spent caustic by suspension crystallization and its optimization via response surface methodology. J. Clean. Prod. 242, 118439. https://doi.org/10.1016/j.jclepro.2019.118439

Yue, Y., Zhang, J., Sun, F., Wu, S., Pan, Y., Zhou, J., Qian, G., 2019. Heavy metal leaching and distribution in glass products from the co-melting treatment of electroplating sludge and MSWI fly ash. J. Environ. Manage. 232, 226–235.

Zha, X., Ning, J., Saafi, M., Dong, L., Ye, J., 2019. Effect of supercritical carbonation on the strength and heavy metal retention of cement-solidified fly ash. Cem. Concr. Res. 120, 36–45.

Zhan, X., Hu, C., Gong, J., Xu, T., Li, J., Yang, L., Bai, J., Zhong, S., 2018. Co-disposal of MSWI fly ash and electrolytic manganese residue based on geopolymeric system. Waste Manag. 82, 62–70. https://doi.org/10.1016/j.wasman.2018.10.014

Zhang, C., Zhuang, L., Yuan, W., Wang, J., Bai, J., 2016. Extraction of lead from spent leaded glass in alkaline solution by mechanochemical reduction. Hydrometallurgy 165, 312–317. https://doi.org/10.1016/j.hydromet.2016.01.017

Zhang, J., Liu, J., Li, C., Jin, Y., Nie, Y., Li, J., 2009. Comparison of the fixation effects of heavy metals by cement rotary kiln co-processing and cement based solidification/stabilization. J. Hazard. Mater. 165, 1179–1185.

Zhang, J., Provis, J.L., Feng, D., van Deventer, J.S.J., 2008. Geopolymers for immobilization of Cr6+, Cd2+, and Pb2+. J. Hazard. Mater. 157, 587–598.

Zhang, M., Yang, C., Zhao, M., Yang, K., Shen, R., Zheng, Y., 2017. Immobilization potential of Cr (VI) in sodium hydroxide activated slag pastes. J. Hazard. Mater. 321, 281–289.

Zhang, S., Herbell, J.-D., Gaye-Haake, B., 2004. Biodegradable organic matter in municipal solid waste incineration bottom ash. Waste Manag. 24, 673–679.

Zhang, Y., Cetin, B., Likos, W.J., Edil, T.B., 2016. Impacts of pH on leaching potential of elements from MSW incineration fly ash. Fuel 184, 815–825.

Zhao, P., Ni, G., Jiang, Y., Chen, L., Chen, M., Meng, Y., 2010. Destruction of inorganic municipal solid waste incinerator fly ash in a DC arc plasma furnace. J. Hazard. Mater. 181, 580–585.

Zhao, Y., Kang, S., Qin, L., Wang, W., Zhang, T., Song, S., Komarneni, S., 2020. Self-assembled gels of Fe-chitosan/montmorillonite nanosheets: Dye degradation by the synergistic effect of adsorption and photo-Fenton reaction. Chem. Eng. J. 379, 122322. https://doi.org/10.1016/j.cej.2019.122322

Zheng, L., Wang, C., Wang, W., Shi, Y., Gao, X., 2011. Immobilization of MSWI fly ash through geopolymerization: effects of water-wash. Waste Manag. 31, 311–317.

Zheng, L., Wang, W., Shi, Y., 2010. The effects of alkaline dosage and Si/Al ratio on the immobilization of heavy metals in municipal solid waste incineration fly ash-based geopolymer. Chemosphere 79, 665–671. https://doi.org/10.1016/j.chemosphere.2010.02.018

Zhou, X., Zhou, M., Wu, X., Han, Y., Geng, J., Wang, T., Wan, S., Hou, H., 2017. Reductive solidification/stabilization of chromate in municipal solid waste incineration fly ash by ascorbic acid and blast furnace slag. Chemosphere 182, 76–84. https://doi.org/10.1016/j.chemosphere.2017.04.072

Zhu, W., Chen, X., Struble, L.J., Yang, E., 2018. Characterization of calcium-containing phases in alkali-activated municipal solid waste incineration bottom ash binder through chemical extraction and deconvoluted Fourier transform infrared spectra 192, 782–789. https://doi.org/10.1016/j.jclepro.2018.05.049

Zhu, W., Chen, X., Struble, L.J., Yang, E.H., 2019a. Quantitative characterization of aluminosilicate gels in alkali-activated incineration bottom ash through sequential chemical extractions and deconvoluted nuclear magnetic resonance spectra. Cem. Concr. Compos. 99, 175–180. https://doi.org/10.1016/j.cemconcomp.2019.03.014

Zhu, W., Chen, X., Zhao, A., Struble, L.J., Yang, E.H., 2019b. Synthesis of high strength binders from alkali activation of glass materials from municipal solid waste incineration bottom ash. J. Clean. Prod. 212, 261–269. https://doi.org/10.1016/j.jclepro.2018.11.295

Zou, D., Chi, Y., Fu, C., Dong, J., Wang, F., Ni, M., 2013. Co-destruction of organic pollutants in municipal solid waste leachate and dioxins in fly ash under supercritical water using H2O2 as oxidant. J. Hazard. Mater. 248, 177–184.

APPENDIX

List of Articles Published During the P.h.D Study

1. Articles published in international journals during the P.h.D study

1)**Tian, X.**, Rao, F., León-Patiño, C. A., & Song, S. (2020). Effects of aluminum on the expansion and microstructure of alkali-activated MSWI fly ash-based pastes. *Chemosphere*, 240, 124986.

2) **Tian, X.**, Rao, F., Morales-Estrella, R., & Song, S. (2020). Effects of Aluminum Dosage on Gel Formation and Heavy Metal Immobilization in Alkali-Activated Municipal Solid Waste Incineration Fly Ash. Energy & Fuels, 34(4), 4727-4733.

3) **Tian, X.**, Rao, F., León-Patiño, C. A., & Song, S. (2020). Co-disposal of MSWI fly ash and spent caustic through alkaline-activation: Immobilization of heavy metals and organics. *Cement and Concrete Composites*, 114, 103824.

4) **Tian, X.**, Rao, F., León-Patiño, C. A., & Song, S. (2021). Co-disposal of MSWI fly ash and spent caustic through alkaline-activation consolidation. *Cement and Concrete Composite*s, 116, 103888.

5) **Tian, X.**, Xu, W., Song, S., Rao, F., & Xia, L. (2020). Effects of curing temperature on the compressive strength and microstructure of copper tailing-based geopolymers. *Chemosphere*, 126754.

6) **Tian, X**., Zhang, H., Zhang, T., & Fernández, C. A. (2020). Alkali-activated copper tailings-based pastes: compressive strength and microstructural characterization. *Journal of Materials Research and Technology*, 9(3), 6557-6567.

7）**Tian, X.**, Rao, F., Li, C., Ge, W., Lara, N. O., Song, S., & Xia, L. (2021). Solidification of municipal solid waste incineration fly ash and immobilization of heavy metals using waste glass in alkaline activation system. Chemosphere, 131240.

8）Yang, L., Chen, H., Jia, F., Peng, W., **Tian, X.**, Xia, L., ... & Song, S. (2021). Emerging Hexagonal Mo2C Nanosheet with (002) Facet Exposure and Cu Incorporation for Peroxymonosulfate Activation Toward Antibiotic Degradation. ACS Applied Materials & Interfaces, 13(12), 14342-14354.